Vladislav Slabov

Bioreagents in froth flotation and flocculation of copper, iron and cerium oxides

Doctoral thesis

NTNU

Norwegian University of
Science and Technology

Vladislav Slabov

Bioreagents in froth flotation and flocculation of copper, iron and cerium oxides

Thesis for the Degree of Philosophiae Doctor

Trondheim, January 2024

Norwegian University of Science and Technology
Faculty of Engineering
Department of Geoscience and Petroleum

NTNU
Norwegian University of
Science and Technology

Acknowledgement

"You mean old books?"

"Stories written before space travel but about space travel."

"How could there have been stories about space travel before --"

"The writers," Pris said, "made it up.”

— *Philip K. Dick, Do Androids Dream of Electric Sheep?*

Preface

The separation of valuable minerals from ores has undergone a paradigm shift towards sustainability and environmental responsibility. This shift is in response to the growing concerns about the environmental impact of traditional, chemically intensive separation schemes that rely heavily on petroleum-based reagents.

This thesis is based on the understanding that there is a need to replace petrochemicals and to improve sustainability of mineral processing. A mineral processing operation that most heavily relies on petroleum-based reagents is froth flotation. They are also used in the dewatering of concentrates and tailings. Petroleum-based reagents have many issues, from their dependence on non-renewable sources to their complicated synthesis routes that use hazardous organic solvents. In addition, the by-products generated by these routes pose significant environmental hazards. It is clear that we must seek alternatives that not only mitigate these problems, but also improve separation efficiency itself.

Responding to this urgent need, this thesis aims to explore and promote the use of bioreagents, specifically biosurfactants and biopolymers, in flotation and dewatering. The environmental advantage of bioreagents lies in their low toxicity, biodegradability and sustainable production. In addition, their structural versatility offers the potential for innovative and efficient approaches to the selective separation of valuable minerals.

List of papers

Paper 1. Slabov, Vladislav, Garima Jain, Erik Larsen, Hanumantha Rao Kota, and Irina Chernyshova. 2023. "Eco-Friendly Collectors for Flotation of Fine Hematite and Malachite Particles." Mining, Metallurgy & Exploration. doi: 10.1007/s42461-023-00743-z.

Paper 2. Slabov, Vladislav, Kota, Hanumantha Rao, Irina Chernyshova. Submitted 2023. "The oxidation state of ultrafine ceria controls its flotation with sophorolipids and benzohydroxamic acid as collectors".

Paper 3. Slabov, Vladislav, Garima Jain, Irina Chernyshova, Hanumantha Rao Kota, and Helga Ertesvåg. 2023. "Alginates as Green Flocculants for Metal Oxide Nanoparticles." Transactions of the Indian Institute of Metals. doi: 10.1007/s12666-023-02957-7.

Contents

1. Introduction

This thesis focuses on the development of green reagents for mineral processing. Specifically, it demonstrates a potential of sophorolipid biosurfactants as collectors in the froth flotation of ultrafine metal oxides. In addition, the flocculation properties of three types of alginate biopolymers are studied, which can find application in dewatering.

Flotation and dewatering are the main domains of mineral processing that consume chemical reagents, which are mostly petroleum-based. Challenges associated with these reagents include their high cost due to the complex synthesis pathways, the dependence on non-renewable resources, and the hazardous or even toxic properties. Along with the transition to green industries, mineral processing requires a sustainable approach to its operations, which includes the use of environmentally friendly reagents. Bioreagents can offer a solution as a potential replacement for petrochemicals in froth flotation and dewatering due to their biodegradability, low toxicity and sustainable sourcing. Their structural variety and flexibility can provide an opportunity for the improved separation of valuable minerals.

Further, the gradual consumption of easy-to-extract high-grade ores and the compliance with environmental policies and sustainable resources principles are shifting the focus of the raw materials industry on previously ignored low-grade primary (ores) and secondary (tailings) resources. To liberate valuable minerals, these resources need to be grinded down to ultrafine sizes (smaller than 30 µm), which creates a well-known technical problem of fine particle flotation (Sivamohan 1990). Hence, bioreagents that can help combat the problem of fines would offer not only environmental but also economic benefits.

This study focuses on the fundamental knowledge of the interaction of sophorolipids and alginates with ultrafine metal oxide particles, to assess and elucidate their collecting and flocculating properties, respectively. The experimental studies within this thesis include froth flotation of ultrafine oxide particles and flocculation of metal oxide nanoparticles. By addressing both fundamental principles and practical applications, this research improves knowledge of the interactions between sophorolipids and mineral surfaces, as well as the interactions between alginates and nanoparticles, which contributes to the ongoing shift toward sustainable and efficient mineral processing.

The literature review in this section covers several key aspects. It begins with an explanation of the basic principles of froth flotation and flocculation. It then briefly discusses conventional collectors and flocculants used in these methods. Furthermore, the overview of

the current landscape of green chemistry in these areas is provided. Specifically, the green chemistry concept is described, following by the overview of bioreagents and their interaction with minerals. Through these discussions, we aim to highlight the latest advances, challenges and opportunities in the application of green chemistry principles to froth flotation and dewatering.

1.1. Flotation - general principle and challenges

Froth Flotation is a physicochemical method widely used for separating and upgrading finely liberated valuable minerals from nonvaluable ones(Fuerstenau, Jameson, and Yoon 2007). The method involves the interaction of three phases, including solid (mineral particles), liquid (water and reagents), and gas (air bubbles). The principle is based on the difference in surface hydrophobicity of the mineral particles. This can be achieved by selective adsorption of surfactants or amphiphilic organic ligands (called collectors) onto the target mineral particles. This adsorption process renders these particles hydrophobic, which subsequently facilitates their transfer to the froth zone via air bubbles, as shown in Figure 1 (Fuerstenau, Jameson, and Yoon 2007; Leja 1982). Froth flotation is a complex process that involves a wide range of physicochemical processes, where interfacial processes play a key role (Nagaraj and Farinato 2016).

Achieving selectivity in flotation processes is a complex issue that is influenced by many factors, including ore mineralogy, size and shape distribution of the mineral particles, reagents (collectors, depressants, modifiers, and frothers), pH of the system, pulp/water chemistry, and additional physical parameters such as temperature and flotation time (Arslan and Bulut 2022; Nagaraj and Farinato 2016).

Apart from selectivity, a common problem in froth flotation is the so-called 'problem of fines'. The challenge of separating ultrafine particles (smaller than 10-30 µm) is associated with the gradual depletion of easy-to-mine high-grade sulfide ores, as well as the intrinsic mechanical properties of oxide ores. Environmental policies and sustainable resource principles are shifting the focus of the extractive industries to previously ignored low-grade primary (ore) and secondary (tailings) resources (Abaka-Wood et al. 2022). To recover valuable minerals from these depleted resources, they must be ground to fine sizes, which presents a recognized technological challenge known as fine particle flotation (Sivamohan 1990). Due to their mechanical properties, grinding of non-sulfide iron and copper ores naturally produces a significant amount of ultrafine particles. Furthermore, rare earth minerals

(REM) are often highly dispersed in ores and tailings (Chelgani et al. 2015; Abaka-Wood, Addai-Mensah, and Skinner 2021; Alcalde, Kelm, and Vergara 2018). As a result, these ores must be ground to ultrafine sizes, which has a detrimental effect on selectivity. This is because ultrafine particles exhibit poor floatability under flotation conditions optimized for conventional sizes in the 38-150 µm range (Sivamohan 1990).

Several approaches have been applied to tackle the problem of fines (Farrokhpay, Filippov, and Fornasiero 2020; Subrahmanyam and Forssberg 1990; Hassanzadeh et al. 2022). Most of them present physical modifications of the flotation system, including a reduction of the bubble size, modifications of the flotation cell, ultrasound pretreatment of the pulp, an increase in turbulence (the particle-bubble collision rate), as well as carrier flotation. Chemical approaches consist of enlarging particle size by selective flocculation and coagulation (Subrahmanyam and Forssberg 1990). It generally accepted that these processes are controlled by collectors. For example, sodium oleate promotes hydrophobic flocculation of fine mineral particles, while reducing the bubble size, which improves fine particles flotation (Kulkarni and Somasundaran 1980; Akdemir and Hiçyilmaz 1996; Song and Lu 1994). However, there is no such information for biosurfactants as collectors.

Collectors are the main reagents in froth flotation responsible for the selective separation of specific minerals. The choice of the collector depends on the surface chemistry of the specific mineral. These parameters are discussed in more detail in section 1.3.
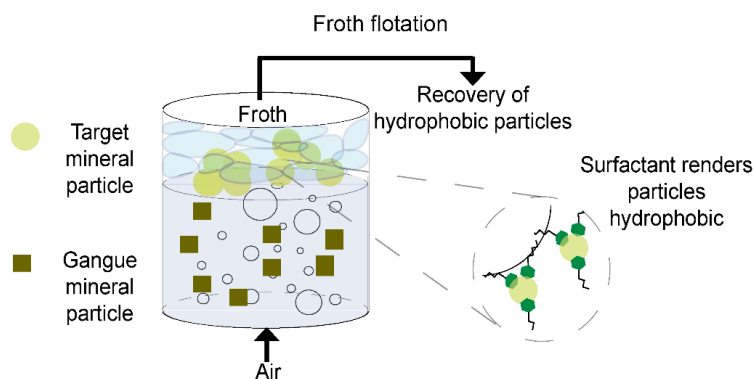

Figure 1 – The schematic representation of froth flotation process.

1.2. Flocculation

1.2.1. Flocculation in dewatering processes

Most mineral separation processes consume significant amounts of water. For example, the water consumption by froth flotation is around 0.72 m^3/ton of ore (Fernando Concha 2014). This results in high water-to-solid ratios in the final concentrate. However, since both concentrate and tailings need to be relatively dry for further processing, transportation or storage, an additional step called dewatering is required (Barry A. Wills and Finch 2015). One of the most common dewatering techniques used in mineral processing is gravity sedimentation or thickening. This method relies on the coagulation or flocculation of fine particles into larger flocs, thereby accelerating their settling process and does not require selectivity.

Coagulation is the modification of the surface charge of particles to cause them to aggregate (Barry A. Wills and Finch 2015). It can be achieved by the use of either inorganic or organic coagulants. Inorganic coagulants typically consist of multivalent metal cations, with common reagents including $Al_2(SO_4)_3$, $Fe_2(SO_4)_3$, $Ca(OH)_2$, and $FeCl_3$ (Barry A. Wills and Finch 2015). Organic coagulants, on the other hand, are low molecular weight cationic polymers, typically ranging from 3000 to 1 million in the chain length. These polymers act as oppositely charged "patches" that facilitate electrostatic attraction between dispersed particles (Barry A. Wills and Finch 2015). Essentially, both types of coagulants work by neutralizing the electrical charges on the particles, causing them to aggregate.

Flocculation is the binding (or "bridging") of the particles by polymers to form flocs (Barry A. Wills and Finch 2015). It typically employs high molecular weight (exceeding 1 million chain length) anionic polymers to bind particles together through polymeric bridges, resulting in the formation of flocs (Figure 2a). In addition, flocculation may involve the simultaneous application of inorganic coagulants such as Ca^{2+}, as shown in the Figure 2b. A key aspect of flocculation is the formation of a chemical bond, commonly referred to as chemisorption, between the polymer and the particle surface (Runkana, Somasundaran, and Kapur 2006).

While the selectivity of flocculation may not be a primary concern, ensuring effective particle binding is critical. This binding process can be adjusted by changing the polymer concentration. An excessive amount of flocculant can paradoxically disperse the particles by the adsorption onto particles in the configuration counteracting the intended aggregation (Figure 2c).
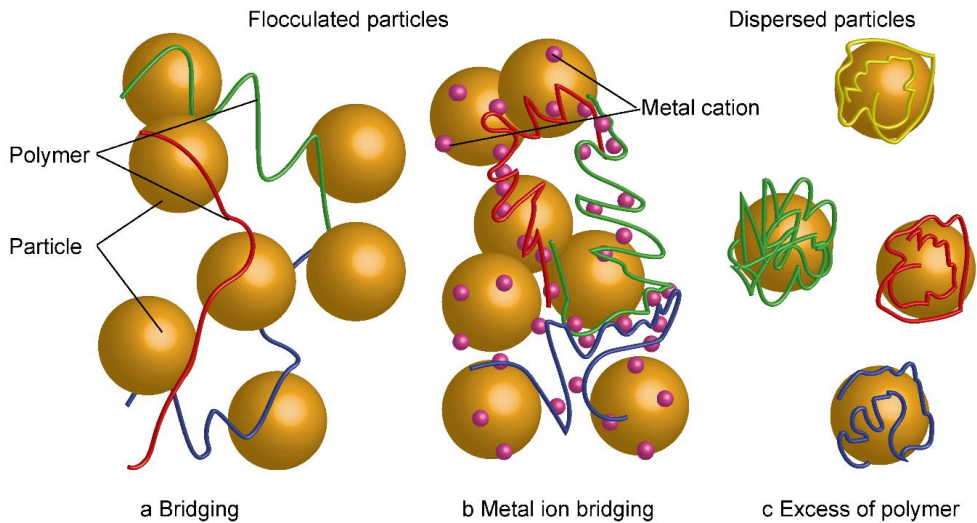
Figure 2 – Flocculation mechanism of fine particle

1.2.2. Flocculation in froth flotation

Flocculation is also utilized in froth flotation of fine particle. By aggregating ultrafine (<10-30 µm) particles, it increases the probability of their collision with bubbles. The methods used for this purpose include selective-polymer flocculation and shear (or hydrophobic) flocculation (Forbes 2011).

Selective-polymer flocculation is similar to the conventional flocculation in dewatering described in section 1.3.3 but, as follows from the method's name, is selective, which is crucial for froth flotation. As an example is the selective flocculation of fine hematite by starch in its reverse flotation from siliceous gangue (Colombo 1980). However, the selectivity remains a big challenge of this method (Forbes 2011).

Shear flocculation, introduced by Warren, relies on the aggregation of hydrophobic ultrafine particles (0.5-10 µm) under a shear field of sufficient magnitude (Forbes 2011; Warren 1975). Notably, the hydrophobicity of these particles can arise naturally or be induced by adsorbed collectors, as was shown for sodium oleate (Warren 1975; Shibata and Fuerstenau 2003). However, the selectivity and nature of shear flocculation is still poorly understood, resulting in the lack of its industrial application (Forbes 2011).

1.3.Reagents in flotation and flocculation processes

Flotation and flocculation processes are the main consumers of chemical reagents in mineral processing. The key parameter controlling the effectiveness of the flotation and flocculation processes is the molecular structure of the collector and flocculant, respectively.

This section discusses the main principles of the reagent selection in froth flotation and flocculation, as well different types of collectors and polymeric flocculants.

1.3.1. Common approach to selecting a collector

The selection of a collector primarily starts with experimental work based on knowledge related to the reagent. Nagaraj and Farinato have identified five distinct historical periods of advances in flotation reagents (Nagaraj and Farinato 2016). In particular, the so-called "targeted design" approach, which was developed in the early 1950s, is based on the hard-soft acid-base (HSAB) principle (Table 1). It has helped increase the selectivity of froth flotation leading to the development of many reagents in the 1980s that are still used commercially today (Nagaraj and Farinato 2016).

Table 1 – Classification of Acids and Bases according to the HSAB principle (Pearson 1963).

Acids	
Hard	Soft
H^+, Li^+, Na^+, K^+, Be^{2+}, Mg^{2+}, Ca^{2+}, Sr^{2+}, Ba^{2+}, Al^{3+}, Sc^{3+}, Ga^{3+}, In^{3+}, La^{3+}, Gd^{3+}, Lu^{3+}, Cr^{3+}, Co^{3+}, Fe^{3+}, As^{3+}, Si^{4+}, Zr^{4+}, Hf^{4+}, Th^{4+}, U^{4+}, Pu^{4+}, Ce^{4+}, Wo^{4+}, Sn^{4+}, UO^{2+}, VO^{2+}, MoO^{3+}	Cu^+, Hg^+, Ag^+, Au^+, Tl^+, Pd^{2+}, Cd^{2+}, Pt^{2+}, Hg^{2+}, CH_3^+Hg, $Co(CN)_5^{2-}$, Pt^{4+}, Te^{4+}, Br^+, I^+
Borderline	
Fe^{2+}, Co^{2+}, Ni^{2+}, Cu^{2+}, Zn^{2+}, Pb^{2+}, Sn^{2+}, Sb^{3+}, Bi^{3+}, Rh^{3+}, Ir^{3+}, $B(CH_3)_3$	
Bases	
Hard	Soft
H_2O, OH^-, F^-, $CH_3CO_2^-$, PO_4^-, SO_4^-, Cl^-, CO_3^{2-}, ClO_4^-, NO_3^-, ROH^-, RO^-, R_2O, NH_3, RNH_2, NH_2NH_2	R_2S, RSH, RS^-, I^-, SCN, $S_2O_3^{2-}$, R_3P, R_3As, $(RO)_3P$, CN^-, RNC, CO, C_2H_4, H^-, R^-
Borderline	
$C_6H_5NH_2$, C_5H_5N, N_3^-, Br^-, NO_2^-, N_2, SO_3^{2-}	

According to the HSAB principle, which was introduced by Pearson (Pearson 1963), hard acids prefer binding to hard bases (Table 1). In particular, oxygen donor (O-donor) ligands have an affinity for hard Lewis acids, while sulfur donors (S-donors) tend to complex soft Lewis acids. The donor-acceptor paradigm has greatly improved the ability to predict

interactions between collectors and metal ions or mineral surfaces. Initially used for simple interactions, it has been extended to explain complex behaviors in competitive adsorption (Nagaraj and Farinato 2016). This approach has led to innovative advancements in collectors and modifiers, focusing on functional groups over attributes like charge. However, the HSAB principle is a conceptual guideline, and there may be exceptions and variations depending on specific cases and the nature of the metal-ligand interactions (Hancock and Martell 2002).

In the mid-1990s, the holistic Flotation Matrix 100TM approach reshaped reagent selection by integrating expert systems, mineralogy and statistics into customizable tools (Figure 3) (Nagaraj 2005). In this approach, only chemical factors are expanded to represent the complex chemical aspect of flotation. It is clearly represented by some of these factors listed in the Table 2 (Nagaraj 2005), where knowledge of the chemistry of water, reagents, and minerals are required for selecting new reagents.

To use this method effectively, we need a fundamental knowledge about the interactions of collectors with minerals under dynamic flotation conditions. In the past, such a knowledge has been developed primarily for petroleum-based collectors and fatty acids (as a representative of green collectors), while very little is known about biosurfactants. It is also essential that this knowledge is extended to ultrafine particles.
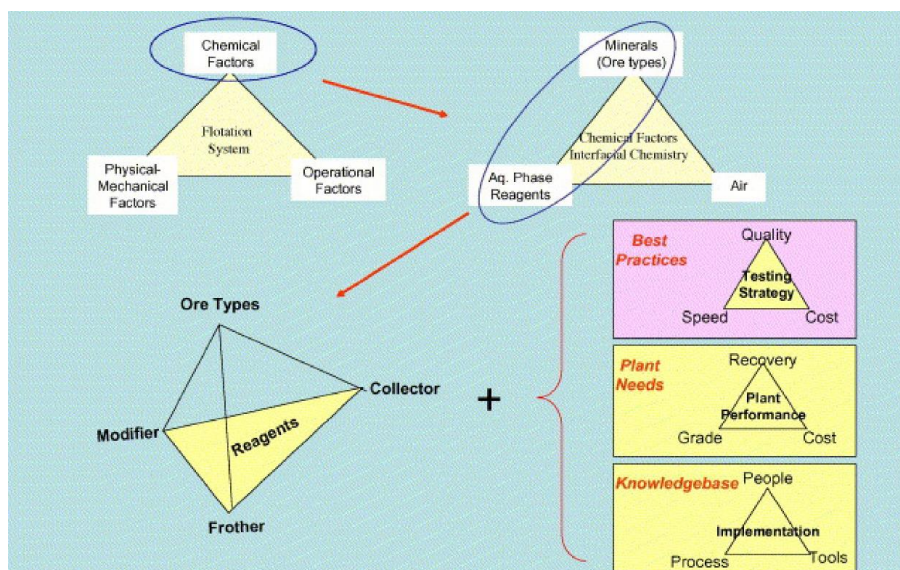

Figure 3 - The holistic view of the flotation system in reagent selection. The chemical factors include mineralogy, reagents and air-water interactions. Triangles at each stage represent necessary complex system trade-offs (Nagaraj 2005).

Table 2 – Selected factors that dictate reagent selection and trade-off (Nagaraj 2005). Copyright © 2004 Elsevier Ltd. All rights reserved.

Technical factors	Constraints
Reagent chemistry	Reagent tox registrations
Ore types, mineralogy and mineral chemistry	Handling
Frothing characteristics	Logistic
Water chemistry	Toxicity and environmental issues
Stability (short and long term)	Odor

1.3.2. Collectors in froth flotation of metal oxides

Over more than a century of flotation history, various types of collectors and general schemes for their interaction with minerals have been developed (Fuerstenau and Pradip 2019; Nagaraj and Farinato 2016; Ramachandra Rao and Leja 2004). Oxhydryl collectors are used in flotation of oxide minerals, as well as in flotation of carbonates and minerals containing sulfo group (Bulatovic 2007). Oxhydryl collectors consist of a limited group of reagents. However, this group represents the largest category of anionic collectors. This category can be further divided into several subcategories, some of which are included in Table 3 (Bulatovic 2007). Among these collectors, fatty alcohol ether sulfates and phosphoric acid esters play a key role in the flotation of tantalite, niobium, and titanium minerals. In industrial mineral practice, collectors based on fatty acids (a subset that falls under the carboxylate category) dominate due to their cost efficiency.

In general, oxhydryl collectors are less selective than their sulfhydryl counterparts (Bulatovic 2007). Their performance depends not only on mineralogy but also pulp chemistry and the type of modifier used, while under the right conditions, selectivity can be significantly improved (Bulatovic 2007).

Table 3 – Various oxhydryl collectors (Bulatovic 2007).

Collector name	Structural general formula	Related compounds
Carboxylate	$R-C(=O)-O^-$	Fatty acids
Phosphonic acid	$R-P(=O)(OH)_2$	Sodium, potassium salts of phosphonic acids. Ammonium salts of phosphonic acid.
Sulfonates	$R-S(=O)_2-O^-$	Alkene sulfonate
Alkyl sulfates	$R-O-S(=O)_2-O^-$	Fatty alcohol ether sulfate
Hydroxamate	$R-C(=O)-N(H)-O^-$	

The adsorption of a collector on a mineral surface is generally determined by several forces such as electrostatic attraction, covalent bonding, hydrogen bonding, hydrophobic bonding, and hydration-dehydration effects (Somasundaran and Huang 2000). The physisorption of ionic collectors is driven by the electrostatic attraction of the oppositely charged collector and the mineral surface, with the mineral surface charge depending on pH of the system. Chemical adsorption (chemisorption), where a polar group of a surfactant forms a chemical bond with the lattice ion on a mineral surface, is limited by a monolayer. Surface precipitation involves the interaction of the ligand with a metal cation that has migrated out of the lattice and is located in the interfacial region. Finally, surface reaction by adsorbed complexes involves the metal ion undergoing hydrolysis reactions, eventually forming intermediate metal-hydroxy complexes on the surface that are critical for subsequent chelation processes.

Surface precipitation is described as one of the mechanism of oleate and hydroxamic acid adsorption in the flotation of oxide, carbonate, and phosphate minerals (Ananthapadmanabhan and Somasundaran 1985) and Ref. in it). Hydroxamate- and

carboxylate-based collectors are the most commonly studied collectors of metal oxides and rare earth minerals, with hydroxamates showing higher selectivity than carboxylate-based collectors (Marion, Li, and Waters 2020). The higher selectivity of hydroxamates is explained by their chelating nature. Hydroxamates can form 5-membered ring chelating complexes with metals, while carboxylic acids can form only a 4-membered ring (Keth, Johann, and Frey 2020). Furthermore, hydroxamic acids are more selective to REM over gangue, such as dolomite. (Espiritu, Naseri, and Waters 2018). According to Pradip (1988), general adsorption mechanisms of chelating agents are chemisorption, surface reaction, and surface reaction through adsorbed metal hydroxy complexes.

The surface precipitation mechanism has also been suggested for the flotation of chrysocolla with potassium octyl hydroxamate, which forms insoluble copper chelate (Peterson et al. 1965). It has been suggested that $Cu(OH)^+$ species are responsible for the complex formation between chrysocolla and hydroxamate. The maximum malachite flotation with hydroxamate is observed at pH 8, where the concentration of $Cu(OH)^+$ is maximal (Marion et al. 2017). As a result, among the benzo-, octyl-, salicyl-, aceto-, and tetradecyl hydroxamates, the first two have the best flotation response. In both the above studies, an increase in the temperature improves the recovery of the copper-bearing minerals. The temperature effect was explained by the endothermic hydrolysis of Cu^{2+} to $Cu(OH)^+$, leading to the formation of surface hydroxide complexes (Peterson et al. 1965).

Even though hydroxamic acids form the most stable complexes with trivalent iron (Figure 4), they are effective as collectors of REE minerals such as bastnaesite and monazite minerals (Zhang, Honaker, and Groppo 2017; Yu et al. 2020; Wanhala et al. 2019). In the flotation of bastnaesite by hydroxamic acids, metal hydroxide species play a critical role. Pradip and Fuerstenau (1983) have suggested that the positive species of cerium and lanthanum ($Ce(OH)_2^+$, $Ce(OH)^{2+}$, $La(OH)_2^+$, $La(OH)^{2+}$) are responsible for the adsorption of hydroxamic acids on the bastnaesite surface. Furthermore, they have suggested that depending on pH and concentration, hydroxamic acids can interact with the mineral surface though chemisorption, surface reaction and surface precipitation. These interaction reactions are driven by the complexation with trivalent species of cerium: Ce^{3+}, $Ce(OH)^{2+}$, $Ce(OH)_2^+$ (Sarvaramini, Azizi, and Larachi 2016; Ren et al. 1997).
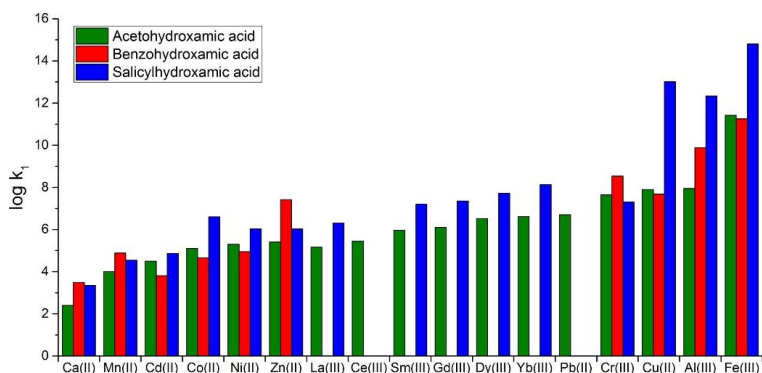
Figure 4 - Stability constants for metal complexes with acetohydroxamic acid, benzohydroxamic acid, and salicylhydroxamic acid (Marion, Li, and Waters 2020). © 2017 Elsevier B.V. All rights reserved.

Hydroxamic acids are available with different structures and hydrophobicity (Marion et al. 2017). Interestingly, with increasing the chain length, alkyl hydroxamic acids show improved collecting properties toward conventional -53 +37 μm and coarse -208 + 100 μm cassiterite SnO_2 particles (Sreenivas and Padmanabhan 2002). The same trend has been observed when octyl hydroxamic acid and oleoyl hydroxamic acid are compared in the flotation of pyrochlore $(Na,Ca)_2Nb_2O_6(OH,F)$ -20 μm and -75+38 μm particles (Liu et al. 2022). However, this approach does not work for improving fine particles flotation. As a result, the collecting performance of octyl hydroxamate and benzohydroxamic acid in the flotation of malachite is adversely affected by fine (-38 μm) particle size, as compared to the coarse (-150 +38 μm) size, indicating the complexity of fine particles flotation (Marion et al. 2017).

1.3.3. Flocculants in mineral processing

Introduced as a flocculant to water treatment in the late 1950s, polyacrylamide (PAM) entered mineral processing in the early 1960s and continued to dominate the flocculant market (Pearse 2003). PAM polymers are most typical flocculants in dewatering. Tailoring of polyacrylamides can address different slurry scenarios, enabling their applications in the solid-liquid separation equipment (Pearse 2003; Wills and Finch 2015). Notably, the current technology has almost reached the upper limit of the average molecular weight for PAM-based flocculants. In general, a longer polymer chain can bind more particles together and increase floc strength. However, in industries such as mineral processing, where traditional linear polymers with higher molecular weights do not necessarily yield optimal results, this shift has prompted the adoption of a molecular architecture approach (Pearse 2003).

The Unique Molecular Architecture® (UMA®) methodology departs from conventional polymer design and incorporates aspects outlined by Pearse et al (Pearse et al. 2001). This novel strategy involves the generation of highly branched and interactive polymer chains, resulting in flocculant solutions containing semi-particulate entities and three-dimensionally linked polymer chains. These structures result in flocs with better characteristics compared to the flocs of conventional flocculants. The former are denser and more stable, while holding less water within their structure than the latter (Pearse 2003).

Depending on the type of co-polymerization, acrylamide-based flocculants can be nonionic, anionic and cationic (Table 4) (Pearse 2003). Low molecular weight organic polymers such as polyDADMAC (diallyldimethyl ammonium chloride) and polyamines can be used as coagulants in combination with PAM flocculants. The primary function of these coagulants is to neutralize the charges on the particles. After charge neutralization, bridging flocculation is initiated by PAM.

Table 4 – Acrylamide monomers used for synthesis of nonionic, anionic and cationic flocculants (Pearse 2003).

Name	Structure
Acrylamide (nonionic)	$-CH_2-CH-$ $C=O$ NH_2
Acrylamide (anionic)	$-CH_2-CH-$ $C=O$ O^- Na^+
Dimethylaminoethyl acrylate (cationic)	$-CH_2-CH-$ $C=O$ O CH_2 CH_2 $H_3C-N^+-CH_3$ CH_3 Cl^-

In shear flocculation, hydrophobic flocs are expected to be formed only by fine particles of the target mineral. Hence, it is essential that the reagents selectively impart hydrophobicity to these particles. Several research studies have shown that achieving the best shear flocculation performance goes beyond simply making the particles hydrophobic. The deposition of insoluble collectors on the particles is equally important ((Forbes 2011) and Ref. in it). The precipitation of colloidal species in solution is known for the collectors with limited solubilization such as dodecyl amine and oleic acid (Laskowski 1993; Castro, Vurdela, and Laskowski 1986). It has been shown that these colloidal precipitates play an important role in the interfacial behavior at the gas-liquid and gas-liquid-solid interfaces (Liu, Pawlik, and Holuszko 2015). Specifically, the colloidal precipitates of an alkyl amine reduce the bubble size. Their migration from the air-water interface to the air-quartz interface leads to hydrophobizing the surface of quartz. However, the exact role of this deposition or precipitation of the collector colloids is still unknown in flotation in general and shear flocculation in particular.

1.4. Environmental impact of synthetic reagents and the concept of green chemistry

Most conventional surfactants employed in flotation and flocculation are synthesized from non-renewable petrochemicals (Nagaraj, Farinato, and Arinaitwe 2019; Eivazihollagh et al. 2019; Chang et al. 2019), which makes them environmentally unsustainable. Moreover, many of them are toxic and/or hazardous due to their chemistry, by-product formation during production, or degradation. For example, xanthates, commonly used in sulfide flotation, produce decomposition products that can be highly irritating to the skin and eyes (1995). Alkyl hydroxamates, used in the froth flotation of rare earth minerals, present occupational and environmental hazards and possess mutagenic properties, making them potentially carcinogenic (Ching Yung 1977; Council 2002). Aliphatic amines, widely used for silicate separation, are known to cause severe skin and eye irritation, and their degradation products are also potentially carcinogenic (Greim et al. 1998). Sodium dodecyl sulfate (SDS), which has widely been used in metal oxide flotation and foam flotation, is toxic to aquatic life (Mariani et al. 2006). PAM-based polymers are the largest category of flocculants in mineral processing (Pearse 2005). However, acrylamide monomers used in PAM-based polymers are toxic (King and Noss 1989). Furthermore, these monomer are usually synthesized from sulfuric acid, acrylonitrile or sodium sulfate, which are also toxic and non-renewable sources. Therefore, replacing toxic or hazardous reagents with less toxic and environmentally friendly bioreagents

in flotation and flocculation processes can reduce health, safety and environment (HSE) risks associated with metal production (Jain et al. 2020).

Replacing petrochemicals in flotation and flocculation by green or eco-friendly reagents requires a knowledge of the functional properties of the latter. The adjective "green", or "eco-friendly" implies that the reagents comply across their life cycle with a set of principles of green chemistry, including production from renewable feedstocks, minimization of hazards, and benign degradation after the use (Höfer and Bigorra 2007; Dhar, Thornhill, et al. 2021). Regarding collectors in mineral processing, it has been suggested that their true "greenness" should be measured over four major life cycle stages (i) manufacturing, (ii) storage and transportation, (iii) usage and processing, and (iv) post-usage and processing (Shen et al. 2016). The latest is still unavailable for most reagents. However, biosurfactants having a low toxicity, good biodegradability and sustainability, could be as a potential alternative to petrochemicals in mineral processing used as collectors.

In addition to the green chemistry aspect, there is a need for the research focused on ultrafine particle separation to address the problems of ore depletion and tailings processing.

1.5. Bioreagent as more sustainable alternatives to chemical reagents in mineral processing

Bio-based materials are derived from renewable resources, and both biosurfactants and biopolymers can be produced by fermenting these resources with bacteria or fungi. They can also be extracted directly from natural sources such as plants and animals (Kashif et al. 2022; Baccile et al. 2021; Nikolova and Gutierrez 2021). These biomolecules are becoming attractive in various applications such as personal care, pharmaceuticals, detergents and cosmetics due to their health and environmental benefits, as well as the growing social demand for sustainability (Jahan et al. 2020). Both biosurfactants and biopolymers have the potential to replace petroleum-based reagents due to their sustainability, low toxicity, and biodegradability, leading to an increase in their research in the raw materials sector (Marchant and Banat 2012). Their structural variation includes mono-, di- and polysaccharides, amino acids, and peptide functional groups, which opens possibilities to find sustainable reagents for efficient separation of metals and minerals.

In this section, we will review different types of biosurfactants and biopolymers. Our primary focus will be on sophorolipid biosurfactants and alginate biopolymers, as they are the main subjects of this dissertation.

1.5.1. Biosurfactants

In coon with synthetic surfactants, biosurfactants are amphiphilic molecules, meaning they have both hydrophilic (water-attracting) and hydrophobic (water-repelling) parts (Lemlich 2012; Mulligan 2005). This amphiphilic nature allows biosurfactants to effectively lower the surface free energy through adsorption at the air-water interface (Lemlich 2012). The ability of biosurfactants to lower surface energy is employed by a wide range of industries, including the pharmaceutical and healthcare sectors. With the increasing trend of sustainability and green transition in various industries, the biosurfactant market is experiencing continuous growth, resulting in the availability of a wider range of biosurfactant structures on the market.

The main classes of low molecular weight biosurfactants are glycolipids, phospholipids and lipopeptides. The feature of phospholipids and lipopeptides is a peptide or phosphorus headgroup attached to the hydrophobic tail, respectively. Lipopeptides are structurally diverse due to many possible peptide compositions. For example, lipopeptide surfactin has a large cyclic headgroup consisting of seven amino acids with two carboxylic residues of amino-acids (Glu1 and Asp5) forming a claw-like structure (Figure 5a). Plant-extracted saponins usually have one or more sugar chains on a triterpene or steroid aglycone backbone, also known as a sapogenin. Fatty acids consist of mixtures of long hydrocarbon chain carboxylic acids, which usually extracted from animal fat or vegetable oils (Pearse 2005). Finally, glycolipids feature a carbohydrate moiety as a headgroup attached to lipids by glycosidic linkages. They are available in the market mostly in the form of rhamnolipids and sophorolipids (Kunal Ahuja 2023).

Rhamnolipids. Mono- and di-rhamnolipids (Figure 5b) are two most studied glycolipids (Abdel-Mawgoud, Lépine, and Déziel 2010). Rhamnolipids are anionic in nature due to the deprotonation of their carboxylic acid moiety above pH 4, which makes them soluble in alkaline solutions (Nitschke, Costa, and Contiero 2005). The structural diversity of rhamnolipids results from factors such as the presence of unsaturated bonds, the length of the alkyl chain and the number of hydrophilic head groups. These variations result in differences in their surfactant properties. Thus, for example rhamnolipids of structures Rha-Rha-C_{10}-C_{10},

Rha-C_{10}-C_{10} , and Rha-Rha-C_{10} show critical micelle concentrations (CMCs) 5 mg/L, 40 mg/L, and 200 mg/L, respectively ((Nitschke, Costa, and Contiero 2005) and Ref. in it). In monorhamnolipids, the rhamnose and carboxyl groups create structural cavities that coordinate with metal ions (McCawley, Maier, and Hogan 2023). It is believed that the selectivity of the ligand is enhanced when the size of the cavity and the metal ion are the same (Hancock and Martell 2002).
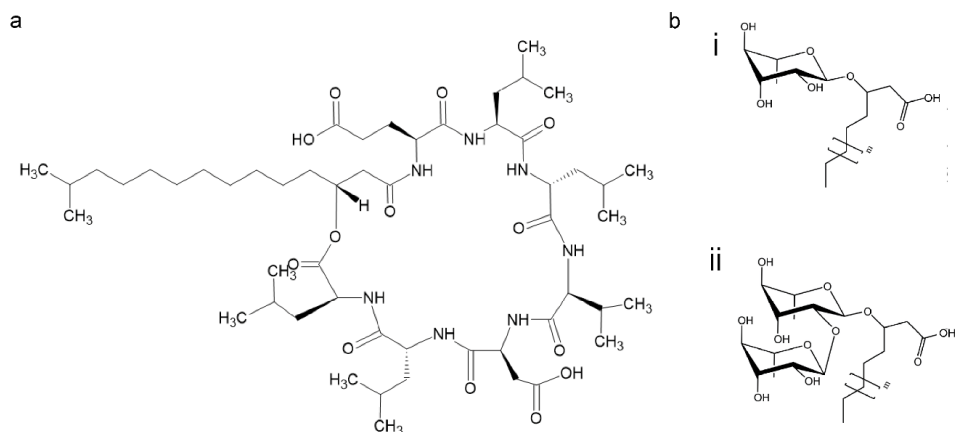

Figure 5 – Structures of most studied microbially-produced biosurfactants: (a) surfactin; (b) (i) mono- and (ii) di-rhamnolipids. Adapted from (Dierickx et al. 2021; Hollenbach et al. 2021).

Sophorolipids. Sophorolipids are glycolipids produced by microorganisms such as *Starmerella* (formerly known as *Candida*) *bombicola* and *Pseudohyphozyma* (Dierickx et al. 2021). These biosurfactants have a wide structural variety and can be easily functionalized further (Figure 6). One of the important benefits of sophorolipids is that they hold the largest share of the biosurfactant market while their production from food waste improves their economic and environmental sustainability (Kunal Ahuja 2023; Hu, Subramanian, Wang, Roelants, To, et al. 2021; Hu, Subramanian, Wang, Roelants, Soetaert, et al. 2021).

Generally, sophorolipids are produced as 80 : 20 acetylated C18:1-cis lactonic (3) : acidic (2) mixture, while the non-acetylated form (1) can be obtained through alkaline hydrolysis (Dierickx et al. 2021). They consist of a hydrophilic sophorose moiety linked by a glycosidic bond to a fatty acid tail (Figure 6). Acidic sophorolipid (ASL) contains a sophorose moiety (β-glucose monomers with 1-2 linkages) at one end of the hydrocarbon chain and a carboxyl group at the other. Lactonic sophorolipid (LSL) can be formed by the lactonization of the carboxyl group and the 4" hydroxyl group of sophorose (Dierickx et al. 2021).
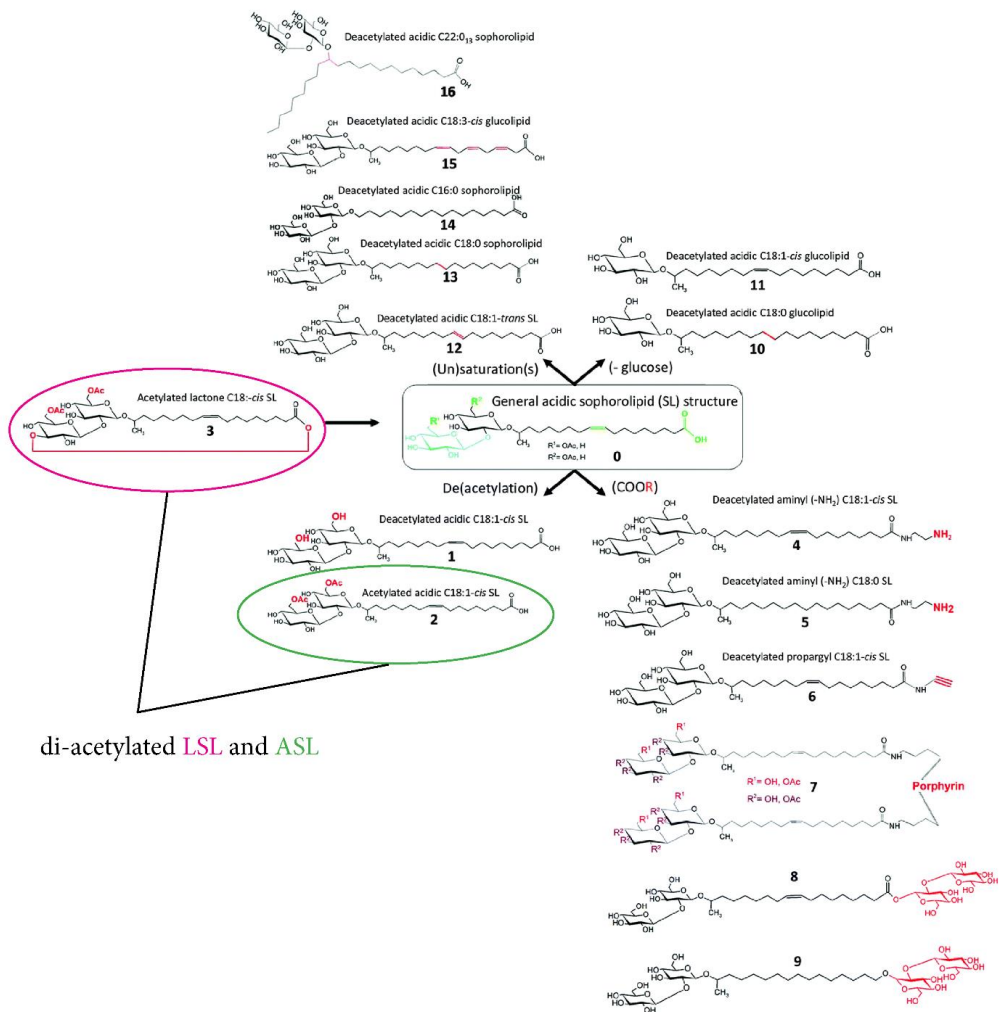
Figure 6 – Structural variation of sophorolipid biosurfactants and their derivatives with different chain length, number of unsaturated bonds, different hydrophilic groups, and their acetylation and de-acetylation. Structures at number 2 and 3 are referred to ASL and LSL biosurfactants studied in the thesis. Adopted from Ref. (Baccile et al. 2021).

Although ASL and LSL share similar structural units (Figure 6), they have different properties due to their anionic and nonionic characters, respectively. ASL is highly soluble and effective in reducing the surface tension of solutions, which makes it a good emulsifier and foamer (Dierickx et al. 2021). LSL has a lower solubility compared to ASL, with acetylated

LSL having a maximum solubility of about 70 mg/L (equivalent to about 100 µM when calculated using a molecular weight of 688) (Otto et al. 1999; Stubenrauch et al. 2010). The greater hydrophobicity of LSL results in its lower surface tension and CMC compared to ASL. Otto et al. have found that CMC of diacetylated and monoacetylated LSL at pH 7.4 and 25 °C are 20 mg/L (29 µM) and 15 mg/L (22 µM), respectively (Otto et al. 1999). Similarly, Li et al. reported a CMC of 15 mg/L at pH 7 and 25 °C for LSL, without specifying the degree of acetylation (Li et al. 2020). In contrast, Hirata et al. reported a CMC of 73 mg/L (120 µM) at pH 8.94 and 20 °C for LSL, again without specifying the degree of acetylation(Zhang, Somasundaran, and Maltesh 1996), a value close to that reported for crude sophorolipids (Li et al. 2020). In comparison, non-acetylated ASL exhibits CMC values of 40 µM and 100 µM at pH 7 and pH 11, respectively (Dhar, Havskjold, et al. 2021).

1.5.2. Biopolymers

Polysaccharides are stereoregular polymers of monosaccharides (sugars) is a large group of biopolymers. These molecules usually can include glucose monomers, mannuronic and guluronic acid unites, galacturonic acid, and amino sugars, such as D-glucosamice linked by α- or β- glycosidic bond with each other. The examples are dextran, pectin, chitosan, cellulose, starch, where the latest is well known in flotation as depressant and flocculant (Crini 2005).

Starch is extensively researched non-ionic polysaccharide composed of two distinct polymers: linear amylose, consisting of D-glucose monomers, and branched amylopectin, which also contains the same monomers (Parker and Ring 2001). Notably, the ratio of amylose to amylopectin, has been found to have a substantial impact on the flocculation properties of starch, where linear chain is more effective as a flocculant (Mierczynska-Vasilev et al. 2013).

In contrast to starch, alginate is anionic biopolymer, which consists of 1-4 linked linear copolymers composed of mannuronic acid (M) and its C5-epimer guluronic acid (G) (Ertesvåg 2015) (Figure 7a). The isoelectric point of alginates is around 3.4-3.7 (Nordgård and Draget 2021), which provides soluble, fully anionic polymers at pH above 4. The distribution of M and G varies between different alginate molecules depending on their source. Hence, alginate chains are described as composed of three block types; G-blocks contain consecutive G residues, M-blocks contain consecutive M residues, and MG-blocks contain alternating M and G residues (Figure 7a,b). The number of residues in any block can vary from two to the length of the chain.
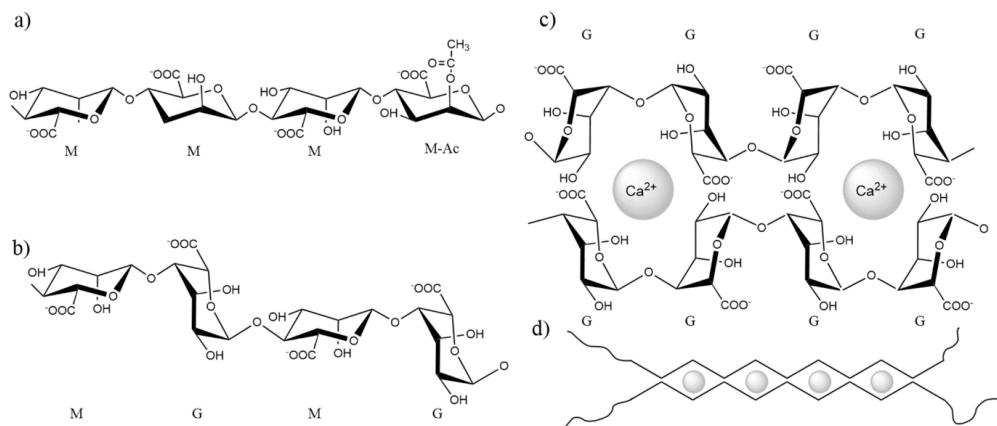
Figure 7 - Alginate structure. a M-block, one residue is O-2-acetylated, b MG-block, c Two G-blocks showing the crosslinking of G-blocks by Ca^{2+}-ions, d Schematic representation of how G-blocks in alginate molecules can be crosslinked by di- or trivalent cations in an eggbox-like structure.

Commercial alginates are manufactured from brown algae, but alginates are also produced by bacteria from the genera *Azotobacter* and *Pseudomonas.* During biosynthesis, the organisms produce mannuronan, and some of the M-residues are then epimerized to G-residues by mannuronan C-5 epimerases acting on the polymer (Haug and Larsen 1969; Ertesvåg 2015). There is a large variation between alginates produced by different species or even under different environmental conditions (Kloareg et al. 2021; Ertesvåg 2015). Given that the two epimers have different structures in the polymer, their relative amounts and distribution within the polymer affect the structure of the alginate and its ability to form gels as recently reviewed (Nordgård and Draget 2021).

Alginates containing G-blocks form gels with divalent metal ions (Nordgård and Draget 2021), where Ca-gels have been most studied. In the junction zones, two G-blocks are crosslinked by Ca^{2+}-ions coordinated by two adjacent G-residues on both chains (Figure 7 c,d). The crosslinking then proceeds, the length of the junction zones is important for the gel strength (Aarstad et al. 2013). It has been found that the crosslinking with MG-blocks might extend these gel junctions (Nordgård and Draget 2021). G-blocks will also bind other alkaline-earth metal ions, the binding strength increasing with the radius (Smidsrød and Haug 1968). Other metal ions also bind alginates, however, for most of them, the composition of alginates does not influence the binding (Lunde, Smidsrød, and Haug 1972; Massana Roquero et al. 2022).

The coordination of individual ions by alginates depends on their size and valency (Agulhon et al. 2012; Menakbi, Quignard, and Mineva 2016; Brus et al. 2017). It has been proposed that the formation of an alginate ionic gel network is needed for flocculation of the dispersed particles (Chen, Mylon, and Elimelech 2006).

1.6. Biosurfactants as collectors in flotation processes
1.6.1.   Carbohydrates and their structural features

Since sugar groups are the key structural units (the hydrophilic moiety) of glycolipids, it is necessary to understand the complexing properties of sugars. The sugar headgroup is a multi-center O-donor and is therefore expected to have an affinity for Lewis acids. The complexation of sugar molecules with metal ions is summarized in two comprehensive reviews (Angyal (1989) Gyurcsik and Nagy (2000)). Early research found that the axial (a) - equatorial (e) - axial (a) (*aea*) sequence (Figure 8) of three hydroxy groups of monosaccharides is preferred for their stable complex formation with metal cations such as Fe, Cu, Mg, La (Angyal 1989). When such a geometrical arrangement forms, oxygen atoms are almost equidistant and able to form strong complexes with large cations, while the complexes with small cations will be weaker (Angyal 1989). Specifically, the *aea* site only coordinates cations with radii > 80 pm. The complexing properties of disaccharides differ, and their ring oxygen is also involved in cation complexation and more than three binding sites are formed (Angyal 1989). Furthermore, the presence of O, N, S, or P anchoring donor groups have significant effect on complex formation with metals and its stability (Angyal 1989).
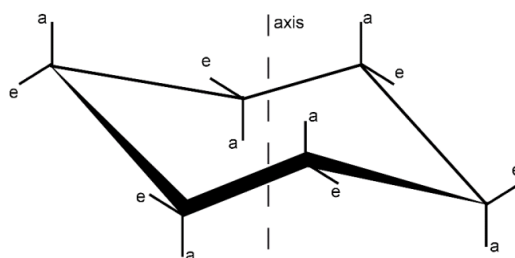

Figure 8 - Equatorial and axial directions of the monosaccharaide hydroxy groups, shown with e and a respectively.

The introduction of additional complexing (anchoring) groups, such as carboxyl, amino, thiol or phosphate, significantly improves the complexing properties of saccharides.

For example, the anchor group such as carboxyl promotes deprotonation of hydroxy groups in a sugar molecule, which can make the complex formation possible even at acidic pH (Gyurcsik and Nagy 2000). Therefore, it is advantageous for metal complex formation to use sugar-based biosurfactants with an additional anchoring group, (e.g. carboxylic group), such as rhamnolipids and sophorolipids.

The carboxyl group also plays a crucial role in promoting the chelating properties of polysaccharides such as alginate (Angyal 1989). Alginate has the ability to chelate multivalent metal cations and can also form a gel network in the presence of certain di- and tri-valent cations (e.g. gelation in the presence of Ca^{2+} and Ce^{3+} but not Na^+ or Mg^{2+}) (Chen, Mylon, and Elimelech 2006; Slabov et al. 2023). The gelation of alginates is not only dependent on specific metal cations (Mørch et al. 2006; Smidsrød 1974; Yang et al. 2013), but also on the structural sequence of G and M acid blocks within the polymer (Kıvılcımdan Moral, Ertesvåg, and Sanin 2016; Smidsrød and Haug 1968). However, polymers are high molecular weight molecules and their complexation with metal cations can be hindered by cross-linking processes (Angyal 1989).

1.6.2. Interaction of biosurfactants and biopolymers with mineral particles

Fatty acids and polysaccharides are two groups of green reagents that are already used in flotation of iron oxides as collectors and depressants, respectively (Zhang et al. 2022; Quast 2021).

Starch is a non-ionic polysaccharide which has extensively been researched in the context of mineral separation. The recent studies using cryo-SEM and high-resolution X-ray computed tomography have shown the ability of starch to flocculate hematite fine particles (Li et al. 2019; Shrimali et al. 2018). Spectroscopic results suggest that starch interacts with hematite via the polysaccharide-metal hydroxide complexation (Moreira et al. 2017), which can explain preferable chemisorption of starch on hematite vs quartz (Rohem Peçanha et al. 2019). In the hematite-starch-oleate system, starch covers almost all free surfaces of hematite and prevents adsorption of oleate (Li et al. 2019), suggesting that it interacts with hematite stronger than oleate. The specific interaction of starch with hematite is behind the dependence of the affinity of the hematite crystallographic planes to starch, which decreases in the order of $(1\ 1\ \bar{2}\ 0) > (1\ \bar{1}\ 0\ 0) > (0\ 0\ 1\ 1)$ (Félix et al. 2022). This dependence has been explained by multisite complexation between starch molecules and oxygen surface sites.

Chemisorption has also been proposed for the adsorption of a nonionic surfactant n-dodecyl-β-d-maltoside (DDM) on hematite, with parallel orientation of the aliphatic chain and two-sugar-ring to the mineral surface (Mielczarski et al. 2004). In contrast, the interaction of hematite with the sugar headgroup of DDM has been interpreted in terms of hydrogen bonding (Zhang, Somasundaran, and Maltesh 1997; Zhang et al. 2002). It has also been found that the surfactant adsorption is proportional to the concentration of hydroxyl groups on the hematite surface (Lu et al. 2007).

Dextran interacts with the surface of ceria CeO_2 through charge transfer, adsorption of hydroxyl groups, and a disproportionation reaction (Ju et al. 2021). The latter leads to the reduction of ceria while adsorbed hydroxyl groups recombine to produce water and an oxygen vacancy. The strength of the adsorption varies with the concentration of dextran, and the structure of the dextran remains unchanged during this interaction.

The flocculation properties of alginates have been studied for a long time; however, mostly algae-derived alginates have been studied (Maruyama, Seki, and Igi 2020; Tripathy, Karmakar, and Singh 2001; Tian et al. 2020; Liu et al. 2020; Chen, Mylon, and Elimelech 2006). The previous research has focused on native or modified alginates and various mono-, di- and trivalent salts (Tripathy and Singh 2000; Rani, Mishra, and Sen 2013; Tian et al. 2020; Liu et al. 2020; Chen et al. 2017; Chen, Mylon, and Elimelech 2006). Still, most of these studies have not addressed the effect of the alginate composition on the flocculation of dispersed particles, although it has been shown that it is important in water treatment (Moral, Ertesvåg, and Sanin 2016).

Alginates can also be used as modifiers and depressants in mineral flotation. In particular, in scheelite flotation alginate selectively depress calcite and fluorite (Chen et al. 2017). In reverse flotation, alginate can support removal of quartz and chlorite from hematite ore (Fu et al. 2018).

Biosurfactants have already been tested at large scales in the remediation of mining sites (Claudia Isabel et al. 2015), while fatty acids are routinely used in froth flotation of salt-type minerals such as oxides, phosphates or carbonates. With fatty acids, iron oxide flotation depends on pH with a maximum at slightly basic pH (Kulkarni and Somasundaran 1980). This maximum can be explained by a mixed adsorption mechanism (physisorption and chemisorption of the fatty acid) and the acid-base properties of the iron oxide (Chernyshova,

Ponnurangam, and Somasundaran 2011). Sodium oleate is also known to be highly effective in the flotation of hematite fines even without a frother (Li, Liu, and Liu 2018).

A surfactin-like biosurfactant obtained from *Bacillus subtilis* floats calcite and magnesite more efficiently than sodium oleate (a conventional collector) (Aytar Çelik, Çakmak, and Öz Aksoy 2023; Öz Derya et al. 2022). In particular, in a single mineral flotation, a 10 times lower amount of surfactin floats 80% of calcite compared to oleate which floats less than 50 % of the mineral. Moreover, the conditioning time with surfactin is three times longer than with oleate. This collecting activity of surfactin can be explained by the coordination activity of its two carboxylate groups.

Rhamnolipids, which have sugar and carboxylic groups, have been used mostly as frothers and depressants in flotation of iron, copper, and phosphate ores, as well as coal (see (Asgari et al. 2022) and references there in).

Another biosurfactant with carboxyl and di-saccharide functional groups is ASL. So far, sophorolipids have been studied in detail in solution and at the air-water interfaces (Baccile et al. 2021), while their interaction with minerals has been addressed only in a handful of works (Baccile, Cuvier, et al. 2013; Dhar, Havskjold, et al. 2021; Castelein et al. 2021; Baccile, Noiville, et al. 2013; Peyre et al. 2017). In particular, ASL renders copper sulfides hydrophobic through the surface precipitation/reaction mechanism that forms hydrophobic Cu-ASL precipitates on the sulfide surface (Dhar, Havskjold, et al. 2021). The hydrophobicity of the precipitates has been explained by a loop-like chelating coordination of both the sophorose and carboxylate headgroups of ASL to Cu(II) cations (Figure 9). This mechanism allows ASL to float copper sulfides from a pyrite-poor copper ore similarly to or even better than conventional thiol collectors (Dhar, Thornhill, et al. 2021). The chelating structure of the Cu-ASL complexes can explain the strong leaching properties of ASL toward Cu from Cu sulfides and metallic Cu (Castelein et al. 2021; Dhar, Havskjold, et al. 2021). In contrast, during the precipitation of iron oxide nanoparticles in ASL solutions, only the carboxylate headgroup of ASL coordinates to iron oxide nanoparticles while the sophorose headgroup is left free, which renders the nanoparticles hydrophilic (Baccile, Noiville, et al. 2013).

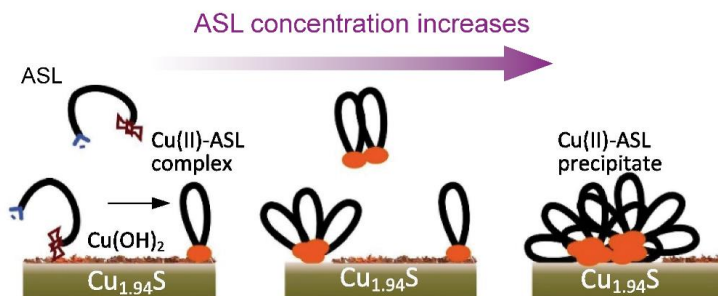At the same time, there is no information on the interaction of LSL with minerals.

Figure – 9 Proposed adsorption mechanisms for de-acetylated ASL on djurleite $Cu_{1.94}S$ (Dhar, Havskjold, et al. 2021). Copyright (2022) Elsevier Ltd. All rights reserved.

2. Aims and scope

Mineral processing is known for its high consumption of water and reagents, while the reagents used are often derived from non-renewable resources such as petrochemicals, which poses both environmental and toxicity risks. Hence, there is a need for basic research to build a library of green (eco-friendly) alternatives the conventional petroleum-based reagents such as collectors in flotation and flocculants in dewatering. Here, promising candidates are biosurfactants and biopolymers. Another persisting problem of mineral processing is the separation of ultrafine particles. The fine and ultrafine size fraction is a significant source of mineral losses in flotation, which hampers the processing of depleted ores and reprocessing of flotation tailings. It remains unclear how this problem can be effectively addressed through the use of appropriate biosurfactants and biopolymers.

The aim of this thesis is to evaluate the performance of sophorolipid biosurfactants and alginate biopolymers in froth flotation and dewatering, respectively. This goal is achieved through answering the following research questions:

1. Can ASL and LSL biosurfactants (Figure 10) selectively float metal oxides? If so, which structure is more effective and why? To answer these questions, we compare the collecting and interfacial properties of these two biosurfactants. They have the same structural units but different ionic characters and interfacial activity. This difference provides an opportunity to bridge their adsorption mechanisms and the effect of their structural differences on the flotation process.

2. What is the effect of the ultrafine particle size on the collecting properties of ASL and LSL in comparison to conventional collectors? To explore this, we compared ASL and LSL with other collectors, including DDM as a model non-ionic alkyl disaccharide surfactant, sodium oleate (NaOl) and benzohydroxamic acid (BHA) as a references.

3. Can the redox state of cerium oxide affect its interaction with the collectors and its separation? For this purpose, ceria particle with different oxidation states were tested in their flotation against hematite and quartz ultrafine particles, using ASL, LSL and BHA as collectors.

4. How does the guluronic acid content of alginates affect their flocculation properties? To answer this question, we used bacterial-derived alginates characterized by different concentrations and sequences of guluronic acid, with and without acetylation, in this

work. This provides a basis for further research in their application in dewatering processes.
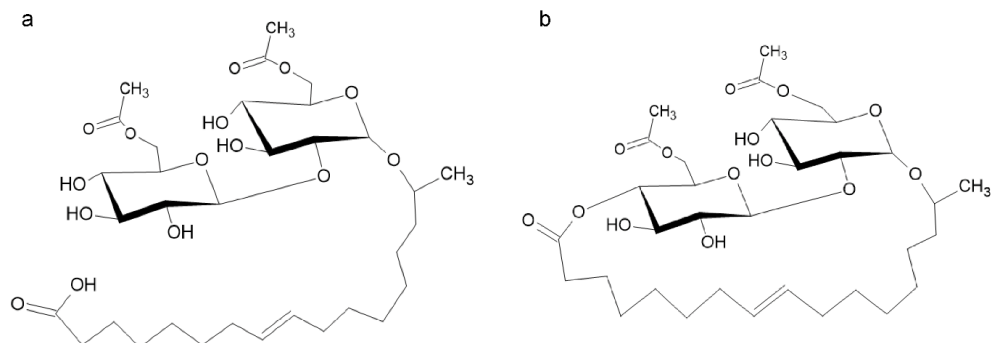

Figure 10 - The scheme of (a) di-acetylated ASL and (b) di-acetylated LSL. In the sophorolipids, an acetylated sophorose moiety is attached to a C18:1 hydrocarbon chain.

3. Summary of results and discussions

The primary goal of Paper 1 and Paper 2 is to improve our understanding of the interactions between sophorolipids and ultrafine particles (<20 µm) of hematite, malachite, cerium oxide, and quartz, which are relevant to their flotation. In Paper 3, the aim is to improve the current understanding of the flocculating properties of alginates.

In Paper 1, ASL and LSL are used as collectors in the flotation of ultrafine particles of hematite, malachite and quartz from their artificial mixtures. The tests are performed at the mini-flotation lab scale. A notable aspect of Paper 1 is that it compares the separation performance of the sophorolipids toward ultrafine (less than 20 µm) and coarser (38-90 µm) size fractions. In addition, the collecting properties of ASL and LSL are compared with those of sodium oleate (NaOl) and DDM.

In Paper 2, ASL and LSL are used as collectors for ultrafine cerium oxide particles, which serve as a model for rare earth mineral particles. This paper explores the interaction between ASL and LSL biosurfactants and ceria particles in single, binary and three mineral flotation configurations with hematite and quartz ultrafine particles. A key feature of this study is the use of the oxidation state of ceria to enhance separation. Specifically, two types of ceria particles were used: fully oxidized CeO_2^{ox} and partially reduced CeO_2^{red}.

In Paper 3, we conducted a comparative study to examine the flocculation properties of three well-characterized alginates with a different guluronic acid content. While research on alginate flocculation has a long history, it has predominantly focused on alginates derived from algae. In contrast, this research takes a unique approach by studying the flocculation capabilities of bacterial-derived alginates that differ in guluronic acid content, guluronic acid distribution, and acetylation levels. The performance of these alginates in flocculating CeO_2 and α-Fe_2O_3 (hematite) nanoparticles is evaluated in this study. These nanoparticles are chosen as model systems to represent cerium (an abundant rare earth element) and iron-bearing slimes, respectively. As the effectiveness of alginates in the flocculation process depends on the type of cross-binding cation used, the comparison is made to evaluate the efficiency of divalent Ca^{2+} and trivalent Ce^{3+} ions in facilitating this process.

4. Conclusions and recommendation for future research

This thesis has conducted an in-depth examination of green reagents in mineral processing operations, with a primary focus on understanding their interactions with metal oxide particles in froth flotation and flocculation.

In the froth flotation part, we studied the collecting properties of ASL and LSL biosurfactants. The key conclusions of this study are as follows.

- ASL and LSL adsorb on ultrafine hematite and malachite but do not adsorb on ultrafine quartz, which makes them selective in the flotation of hematite vs. quartz and malachite vs. quartz binary systems.

- ASL and LSL adsorb on hematite, malachite, and ceria primarily in the anionic form and may involve the surface precipitation of complexes with metal cations. In addition, similar to NaOl, LSL can be deposited on the particle surface at acidic pH as negatively charged colloids. NaOl and LSL exhibit superior collecting properties for ultrafine hematite particles against quartz, outperforming ASL and DDM.

- When LSL is employed as a collector, ultrafine particle size does not negatively impact the selectivity and recovery of hematite and malachite from quartz at pH 5 and pH 6, respectively.

- LSL demonstrates selective agglomeration of ultrafine reduced ceria particles, which makes it a potential candidate for the selective reverse flotation of ultrafine particles of rare earth minerals.

- The fully oxidized state of ceria has an adverse effect on its separation from hematite with ASL, LSL, and BHA.

- The highest grade-recovery figures in the ceria flotation against hematite are achieved by BHA at pH 4. This result suggests that, without employing depressants of gangue minerals, the partial oxidation of Ce-bearing REM can improve their separation with hydroxamic acids by extending their optimum floatability range to acidic pH.

- In a three-mineral flotation system, both ASL and LSL separate reduced ceria and hematite as a group from quartz at pH 10. ASL can separate ultrafine reduced ceria from its mixture with ultrafine hematite and quartz at pH 7. And finally, LSL can achieve hematite separation from reduced ceria and quartz at pH 4.

- An important control of flotation is the frothing properties of biosurfactants in the presence of ultrafine particles. Hematite particles can stabilize the froth of LSL, while ceria particles act as a defoamers due to their hydrophobic agglomeration.

In summary, the findings of Paper 1 and Paper 2 suggest that ASL and LSL hold a potential as green collectors for ultrafine REM, hematite, and malachite. The explanation of the adsorption mechanisms of the biosurfactants is provided using various test methods, including single-mineral flotation, ζ-potential, solubility, and wettability. Additionally, our work highlights the importance of considering the redox state of ceria in improving the separation of REM.

In the flocculation part, we explored the use of bacteria-derived alginate biopolymers in the flocculation of iron and cerium oxide nanoparticles. Providing an alternative to algae-derived alginates, this study explores *P. fluorescens* derived alginates, which are acetylated and de-acetylated, and contain 30 % of guluronic acid and no G-blocks. In addition, these alginates are compared with a commercial alginate, LF10/60 having 50 % of G-blocks. Based on this work, several key conclusions have emerged:

- The three alginates require metal cations for activation of their flocculation properties.
- The G-blocks (or guluronic acid residues) contents plays significant role in flocculation activity of alginates. Specifically, LF 10/60 can be activated with divalent Ca^{2+} and trivalent Ce^{3+} cations. In contrast, the flocculation properties of *P. fluorescens* derived alginates are activated only by trivalent Ce^{3+} cation.
- The acetylation of alginate strongly affects size and geometry of the flocs, which can be potentially used for sedimentation improvements.

In summary, the findings of Paper 3 show the structural importance of the alginate biopolymer for flocculation application. Specifically, the G-blocks are important for the gel formation in alginates when divalent cations are used. Finally, we show that the alginates can be used for the flocculation of stable dispersions of metal oxide nanoparticles if a suitable cation is present to cross-link the alginate molecules.

Altogether, the results of this thesis work revealed a potential of sophorolipids and alginate for mineral processing operations. However, this conclusion needs to be further verified on complex ore systems.

5. References

1995. Sodium Ethyl Xanthate - Priority Existing Chemical No. 5. edited by Australian Government Department of Health.

Aarstad, O., B. L. Strand, L. M. Klepp-Andersen, and G. Skjåk-Bræk. 2013. "Analysis of G-block distributions and their impact on gel properties of in vitro epimerized mannuronan." *Biomacromol.* 14 (10):3409-16. doi: 10.1021/bm400658k.

Abaka-Wood, George Blankson, Jonas Addai-Mensah, and William Skinner. 2021. "The Use of Mining Tailings as Analog of Rare Earth Elements Resources: Part 1 – Characterization and Preliminary Separation." *Mineral Processing and Extractive Metallurgy Review*:1-15. doi: 10.1080/08827508.2021.1920410.

Abaka-Wood, George Blankson, Kathy Ehrig, Jonas Addai-Mensah, and William Skinner. 2022. "Recovery of Rare Earth Elements Minerals from Iron-Oxide-Silicate-Rich Tailings: Research Review." *Eng* 3 (2):259-275.

Abdel-Mawgoud, Ahmad Mohammad, François Lépine, and Eric Déziel. 2010. "Rhamnolipids: diversity of structures, microbial origins and roles." *Applied Microbiology and Biotechnology* 86 (5):1323-1336. doi: 10.1007/s00253-010-2498-2.

Agulhon, Pierre, Velina Markova, Mike Robitzer, Françoise Quignard, and Tzonka Mineva. 2012. "Structure of alginate gels: Interaction of diuronate units with divalent cations from density functional calculations." *Biomacromol.* 13 (6):1899-1907. doi: 10.1021/bm300420z.

Akdemir, Ünal, and Cahit Hiçyilmaz. 1996. "Shear flocculation of chromite fines in sodium oleate solutions." *Colloids and Surfaces A: Physicochemical and Engineering Aspects* 110 (1):87-93. doi: https://doi.org/10.1016/0927-7757(95)03428-5.

Alcalde, J., U. Kelm, and D. Vergara. 2018. "Historical assessment of metal recovery potential from old mine tailings: A study case for porphyry copper tailings, Chile." *Minerals Engineering* 127:334-338. doi: 10.1016/j.mineng.2018.04.022.

Ananthapadmanabhan, K. P., and P. Somasundaran. 1985. "Surface precipitation of inorganics and surfactants and its role in adsorption and flotation." *Colloids and Surfaces* 13:151-167. doi: 10.1016/0166-6622(85)80014-7.

Angyal, Stephen J. 1989. "Complexes of metal cations with carbohydrates in solution." In *Advances in carbohydrate chemistry and biochemistry*, 1-43. Elsevier.

Arslan, Fatma, and Gülay Bulut. 2022. "Ion flotation and its applications on concentration, recovery, and removal of metal ions from solutions." *Physicochemical Problems of Mineral Processing*. doi: 10.37190/ppmp/152061.

Asgari, Kaveh, Qingqing Huang, Hamid Khoshdast, and Ahmad Hassanzadeh. 2022. "A Review on Bioflotation of Coal and Minerals: Classification, Mechanisms, Challenges, and Future Perspectives." *Mineral Processing and Extractive Metallurgy Review*:1-31. doi: 10.1080/08827508.2022.2121919.

Aytar Çelik, Pınar, Hakan Çakmak, and Derya Öz Aksoy. 2023. "Green bioflotation of calcite using surfactin as a collector." *Journal of Dispersion Science and Technology* 44 (6):911-921. doi: 10.1080/01932691.2021.1979999.

Baccile, Niki, Anne-Sophie Cuvier, Claire Valotteau, and Inge N. A. Van Bogaert. 2013. "Practical methods to reduce impurities for gram-scale amounts of acidic sophorolipid biosurfactants." *European Journal of Lipid Science and Technology* 115 (12):1404-1412. doi: 10.1002/ejlt.201300131.

Baccile, Niki, Romain Noiville, Lorenzo Stievano, and Inge Van Bogaert. 2013. "Sophorolipids-functionalized iron oxide nanoparticles." *Phys. Chem. Chem. Phys.* 15 (5):1606-1620. doi: 10.1039/c2cp41977g.

Baccile, Niki, Chloé Seyrig, Alexandre Poirier, Silvia Alonso-de Castro, Sophie L. K. W. Roelants, and Stéphane Abel. 2021. "Self-assembly, interfacial properties, interactions with macromolecules and molecular modelling and simulation of microbial bio-based amphiphiles

(biosurfactants). A tutorial review." *Green Chemistry* 23 (11):3842-3944. doi: 10.1039/D1GC00097G.

Barry A. Wills, and James Finch. 2015. *Wills' Mineral Processing Technology*: Butterworth-Heinemann.

Brus, Jiri, Martina Urbanova, Jiri Czernek, Miroslava Pavelkova, Katerina Kubova, Jakub Vyslouzil, Sabina Abbrent, Rafal Konefal, Jiri Horský, David Vetchy, Jan Vysloužil, and Pavel Kulich. 2017. "Structure and dynamics of alginate gels cross-linked by polyvalent ions probed via solid state NMR spectroscopy." *Biomacromol.* 18 (8):2478-2488. doi: 10.1021/acs.biomac.7b00627.

Bulatovic, Srdjan M. 2007. *Handbook of flotation reagents: chemistry, theory and practice: Volume 1: flotation of sulfide ores*: Elsevier.

Castelein, Martijn, Florian Verbruggen, Lisa Van Renterghem, Jeroen Spooren, Lourdes Yurramendi, Gijs Du Laing, Nico Boon, Wim Soetaert, Tom Hennebel, Sophie Roelants, and Adam J. Williamson. 2021. "Bioleaching of metals from secondary materials using glycolipid biosurfactants." *Minerals Engineering* 163. doi: 10.1016/j.mineng.2020.106665.

Castro, S. H., R. M. Vurdela, and J. S. Laskowski. 1986. "The surface association and precipitation of surfactant species in alkaline dodecylamine hydrochloride solutions." *Colloids and Surfaces* 21:87-100. doi: 10.1016/0166-6622(86)80084-1.

Chang, Luping, Yijun Cao, Guixia Fan, Chao Li, and Weijun Peng. 2019. "A review of the applications of ion floatation: wastewater treatment, mineral beneficiation and hydrometallurgy." *RSC Advances* 9 (35):20226-20239. doi: 10.1039/C9RA02905B.

Chelgani, S. Chehreh, M. Rudolph, T. Leistner, J. Gutzmer, and Urs A. Peuker. 2015. "A review of rare earth minerals flotation: Monazite and xenotime." *International Journal of Mining Science and Technology* 25 (6):877-883. doi: https://doi.org/10.1016/j.ijmst.2015.09.002.

Chen, Kai Loon, Steven E. Mylon, and Menachem Elimelech. 2006. "Aggregation Kinetics of Alginate-Coated Hematite Nanoparticles in Monovalent and Divalent Electrolytes." *Environmental Science & Technology* 40 (5):1516-1523. doi: 10.1021/es0518068.

Chen, W., Q. M. Feng, G. F. Zhang, Q. Yang, and C. Zhang. 2017. "The effect of sodium alginate on the flotation separation of scheelite from calcite and fluorite." *Miner. Eng.* 113:1-7. doi: 10.1016/j.mineng.2017.07.016.

Chernyshova, Irina V., Sathish Ponnurangam, and Ponisseril Somasundaran. 2011. "Adsorption of Fatty Acids on Iron (Hydr)oxides from Aqueous Solutions." *Langmuir* 27 (16):10007-10018. doi: 10.1021/la2017374.

Ching Yung, Wang. 1977. "Mutagenicity of hydroxamic acids for Salmonella typhimurium." *Mutation Research/Fundamental and Molecular Mechanisms of Mutagenesis* 56 (1):7-12. doi: 10.1016/0027-5107(77)90235-4.

Claudia Isabel, Sáenz-Marta, Ballinas-Casarrubias María de Lourdes, E. Rivera-Chavira Blanca, and Nevárez-Moorillón Guadalupe Virginia. 2015. "Biosurfactants as Useful Tools in Bioremediation." In *Advances in Bioremediation of Wastewater and Polluted Soil*, edited by Shiomi Naofumi, Ch. 5. Rijeka: IntechOpen.

Colombo, AF. 1980. "Selective flocculation and flotation of iron-bearing materials." *Fine particles processing* 2:1034-1056.

Council, National Research. 2002. *Evolutionary and Revolutionary Technologies for Mining*. Washington, DC: The National Academies Press.

Crini, Grégorio. 2005. "Recent developments in polysaccharide-based materials used as adsorbents in wastewater treatment." *Progress in Polymer Science* 30 (1):38-70. doi: 10.1016/j.progpolymsci.2004.11.002.

Dhar, Priyanka, Hakon Havskjold, Maria Thornhill, Sophie Roelants, Wim Soetaert, Hanumantha Rao Kota, and Irina Chernyshova. 2021. "Toward green flotation: Interaction of a sophorolipid biosurfactant with a copper sulfide." *Journal of Colloid and Interface Science* 585:386-399. doi: 10.1016/j.jcis.2020.11.079.

Dhar, Priyanka, Maria Thornhill, Sophie Roelants, Wim Soetaert, Irina V. Chernyshova, and Hanumantha Rao Kota. 2021. "Linking molecular structures of yeast-derived biosurfactants with their foaming, interfacial, and flotation properties." *Minerals Engineering* 174:107270. doi: https://doi.org/10.1016/j.mineng.2021.107270.

Dierickx, Sven, Martijn Castelein, Jelle Remmery, Veerle De Clercq, Sofie Lodens, Niki Baccile, Sofie L. De Maeseneire, Sophie L. K. W. Roelants, and Wim K. Soetaert. 2021. "From bumblebee to bioeconomy: Recent developments and perspectives for sophorolipid biosynthesis." *Biotechnology Advances*. doi: 10.1016/j.biotechadv.2021.107788.

Eivazihollagh, A., I. Svanedal, H. Edlund, and M. Norgren. 2019. "On chelating surfactants: Molecular perspectives and application prospects." *Journal of Molecular Liquids* 278:688-705. doi: 10.1016/j.molliq.2019.01.076.

Ertesvåg, Helga. 2015. "Alginate-modifying enzymes: biological roles and biotechnological uses." *Frontiers in microbiology* 6:523.

Espiritu, Eileen Ross L., Shiva Naseri, and Kristian E. Waters. 2018. "Surface chemistry and flotation behavior of dolomite, monazite and bastnäsite in the presence of benzohydroxamate, sodium oleate and phosphoric acid ester collectors." *Colloids and Surfaces A: Physicochemical and Engineering Aspects* 546:254-265. doi: 10.1016/j.colsurfa.2018.03.030.

Farrokhpay, Saeed, Lev Filippov, and Daniel Fornasiero. 2020. "Flotation of Fine Particles: A Review." *Mineral Processing and Extractive Metallurgy Review*:1-11. doi: 10.1080/08827508.2020.1793140.

Félix, Lizbet León, Gabriela F. Moreira, Laurindo S. Leal Filho, and Fernando Stavale. 2022. "Starch adsorption on hematite surfaces: Evidence of the adsorption mechanism dependence on the surface orientation." *Minerals Engineering* 178. doi: 10.1016/j.mineng.2022.107429.

Fernando Concha, A. 2014. *Solid-liquid separation in the mining industry*: Springer.

Forbes, Elizaveta. 2011. "Shear, selective and temperature responsive flocculation: A comparison of fine particle flotation techniques." *International Journal of Mineral Processing* 99 (1-4):1-10. doi: 10.1016/j.minpro.2011.02.001.

Fu, Y. F., W. Z. Yin, B. Yang, C. Li, Z. L. Zhu, and D. Li. 2018. "Effect of sodium alginate on reverse flotation of hematite and its mechanism." *Int. J. Miner. Metall.* 25 (10):1113-1122. doi: 10.1007/s12613-018-1662-z.

Fuerstenau, D. W., and Pradip. 2019. "A Century of Research Leading to Understanding the Scientific Basis of Selective Mineral Flotation and Design of Flotation Collectors." *Mining Metallurgy & Exploration* 36 (1):3-20. doi: 10.1007/s42461-018-0042-6.

Fuerstenau, Maurice C., Graeme J. Jameson, and R. H. Yoon. 2007. "Froth flotation : a century of innovation." In. Littleton, Colo.: Society for Mining, Metallurgy, and Exploration.

Greim, H., D. Bury, H. J. Klimisch, M. Oeben-Negele, and K. Ziegler-Skylakakis. 1998. "Toxicity of aliphatic amines: Structure-activity relationship." *Chemosphere* 36 (2):271-295. doi: 10.1016/s0045-6535(97)00365-2.

Gyurcsik, Béla, and László Nagy. 2000. "Carbohydrates as ligands: coordination equilibria and structure of the metal complexes." *Coordination Chemistry Reviews* 203 (1):81-149. doi: 10.1016/s0010-8545(99)00183-6.

Hancock, Robert D., and Arthur E. Martell. 2002. "Ligand design for selective complexation of metal ions in aqueous solution." *Chemical Reviews* 89 (8):1875-1914. doi: 10.1021/cr00098a011.

Hassanzadeh, Ahmad, Mehdi Safari, Duong H. Hoang, Hamid Khoshdast, Boris Albijanic, and Przemyslaw B. Kowalczuk. 2022. "Technological assessments on recent developments in fine and coarse particle flotation systems." *Minerals Engineering* 180. doi: 10.1016/j.mineng.2022.107509.

Haug, A., and B. Larsen. 1969. "Biosynthesis of alginate. Epimerisation of D-mannuronic to L-guluronic acid residues in the polymer chain." *Biochim. Biophys. Acta* 192 (3):557-559.

Höfer, Rainer, and Joaquím Bigorra. 2007. "Green chemistry—a sustainable solution for industrial specialties applications." *Green Chem.* 9 (3):203-212. doi: 10.1039/b606377b.

Hollenbach, Rebecca, Sophie Oeppling, André Delavault, Annika R. Völp, Norbert Willenbacher, Jens Rudat, Katrin Ochsenreither, and Christoph Syldatk. 2021. "Comparative study on interfacial and foaming properties of glycolipids in relation to the gas applied for foam generation." *RSC Advances* 11 (54):34235-34244. doi: 10.1039/d1ra06190a.

Hu, Xiaomeng, Karpagam Subramanian, Huaimin Wang, Sophie L. K. W. Roelants, Wim Soetaert, Guneet Kaur, Carol Sze Ki Lin, and Shauhrat S. Chopra. 2021. "Bioconversion of Food Waste to produce Industrial-scale Sophorolipid Syrup and Crystals: dynamic Life Cycle Assessment (dLCA) of Emerging Biotechnologies." *Bioresource Technology* 337. doi: 10.1016/j.biortech.2021.125474.

Hu, Xiaomeng, Karpagam Subramanian, Huaimin Wang, Sophie L. K. W. Roelants, Ming Ho To, Wim Soetaert, Guneet Kaur, Carol Sze Ki Lin, and Shauhrat S. Chopra. 2021. "Guiding environmental sustainability of emerging bioconversion technology for waste-derived sophorolipid production by adopting a dynamic life cycle assessment (dLCA) approach." *Environmental Pollution* 269. doi: 10.1016/j.envpol.2020.116101.

Jahan, Ruksana, Andrew M. Bodratti, Marina Tsianou, and Paschalis Alexandridis. 2020. "Biosurfactants, natural alternatives to synthetic surfactants: Physicochemical properties and applications." *Advances in Colloid and Interface Science* 275. doi: 10.1016/j.cis.2019.102061.

Jain, G, H Havskjold, P. Dhar, H Ertesvåg, I Chernyshova, and Hanumantha Rao Kota. 2020. "Green Foam-Based Methods of Mineral and Ion Separation." In *Multidisciplinary Advances in Efficient Separation Processes*, edited by I. Chernyshova, S. Ponnurangam and Q. Liu, 265-301. American Chemical Society.

Ju, Xiaohui, Břetislav Šmíd, Viktor Johánek, Ivan Khalakhan, Yurii Yakovlev, Iva Matolínová, and Vladimír Matolín. 2021. "Investigation of dextran adsorption on polycrystalline cerium oxide surfaces." *Applied Surface Science* 544. doi: 10.1016/j.apsusc.2020.148890.

Kashif, Ayesha, Ramla Rehman, Ahmed Fuwad, Muhammad Kashif Shahid, H. N. P. Dayarathne, Asif Jamal, Muhammad Nauman Aftab, Bandita Mainali, and Younggyun Choi. 2022. "Current advances in the classification, production, properties and applications of microbial biosurfactants – A critical review." *Advances in Colloid and Interface Science* 306. doi: 10.1016/j.cis.2022.102718.

Keth, Jennifer, Tobias Johann, and Holger Frey. 2020. "Hydroxamic Acid: An Underrated Moiety? Marrying Bioinorganic Chemistry and Polymer Science." *Biomacromolecules* 21 (7):2546-2556. doi: 10.1021/acs.biomac.0c00449.

King, Diana J., and Richard R. Noss. 1989. "Toxicity of Polyacrylamide and Acrylamide Monome." *Reviews on Environmental Health* 8 (1-4). doi: 10.1515/reveh-1989-1-403.

Kıvılcımdan Moral, Çiğdem, Helga Ertesvåg, and F. Dilek Sanin. 2016. "Guluronic acid content as a factor affecting turbidity removal potential of alginate." *Environmental Science and Pollution Research* 23 (22):22568-22576. doi: 10.1007/s11356-016-7475-6.

Kloareg, B., Y. Badis, J. M. Cock, and G. Michel. 2021. "Role and evolution of the extracellular matrix in the acquisition of complex multicellularity in eukaryotes: a macroalgal perspective." *Genes (Basel)* 12 (7). doi: 10.3390/genes12071059.

Kulkarni, R. D., and P. Somasundaran. 1980. "Flotation chemistry of hematite/oleate system." *Colloids and Surfaces* 1 (3):387-405. doi: https://doi.org/10.1016/0166-6622(80)80025-4.

Kunal Ahuja, Sarita Bayas. 2023. "Biosurfactants Market." https://www.gminsights.com/industry-analysis/biosurfactants-market-report.

Laskowski, J. S. 1993. "Electrokinetic Measurements in Aqueous Solutions of Weak Electrolyte Type Surfactants." *Journal of Colloid and Interface Science* 159 (2):349-353. doi: 10.1006/jcis.1993.1333.

Leja, J. 1982. *Surface Chemistry of Froth Flotation*. New York: Plenum Press.

Lemlich, Robert. 2012. *Adsorptive bubble separation techniques*: Elsevier.

Li, Guofeng, Xiangyi Yi, Jitao Jiang, Yu Zhang, and Yueli Li. 2020. "Dynamic surface properties and dilational rheology of acidic and lactonic sophorolipids at the air-water interface." *Colloids and Surfaces B: Biointerfaces* 195. doi: 10.1016/j.colsurfb.2020.111248.

Li, Hao, Mingxia Liu, and Qi Liu. 2018. "The effect of non-polar oil on fine hematite flocculation and flotation using sodium oleate or hydroxamic acids as a collector." *Minerals Engineering* 119:105-115. doi: 10.1016/j.mineng.2018.01.004.

Li, Lixia, Chen Zhang, Zhitao Yuan, Xinyang Xu, and Zhenguo Song. 2019. "AFM and DFT study of depression of hematite in oleate-starch-hematite flotation system." *Applied Surface Science* 480:749-758. doi: 10.1016/j.apsusc.2019.02.224.

Liu, Caiyu, Baoyu Gao, Shue Wang, Kangying Guo, Xue Shen, Qinyan Yue, and Xing Xu. 2020. "Synthesis, characterization and flocculation performance of a novel sodium alginate-based flocculant." *Carbohydrate Polymers* 248. doi: 10.1016/j.carbpol.2020.116790.

Liu, Mingxia, Hong Yu, Hanquan Zhang, Kaipeng Wang, Xiaoli Tan, and Qi Liu. 2022. "Roles of the hydrophobic and hydrophilic groups of collectors in the flotation of different-sized mineral particles." *Colloids and Surfaces A: Physicochemical and Engineering Aspects* 637. doi: 10.1016/j.colsurfa.2022.128262.

Liu, Wenying, Marek Pawlik, and Maria Holuszko. 2015. "The role of colloidal precipitates in the interfacial behavior of alkyl amines at gas–liquid and gas–liquid–solid interfaces." *Minerals Engineering* 72:47-56. doi: 10.1016/j.mineng.2014.12.001.

Lu, Shaohua, Yu Bian, Lei Zhang, and Ponisseril Somasundaran. 2007. "pH dependence of adsorption of n-dodecyl-β-d-maltoside on solids." *Journal of Colloid and Interface Science* 316 (2):310-316. doi: 10.1016/j.jcis.2007.08.063.

Lunde, G., O. Smidsrød, and A. Haug. 1972. "Selectivity of polyuronates for lanthanide ions." *Acta Chem. Scand.* 26 (9):3421-3426. doi: DOI 10.3891/acta.chem.scand.26-3421.

Marchant, Roger, and Ibrahim M. Banat. 2012. "Biosurfactants: a sustainable replacement for chemical surfactants?" *Biotechnology Letters* 34 (9):1597-1605. doi: 10.1007/s10529-012-0956-x.

Mariani, Livia, Domenica De Pascale, Olga Faraponova, Andrea Tornambè, Angela Sarni, Silvia Giuliani, Giordano Ruggiero, Fulvio Onorati, and Erika Magaletti. 2006. "The use of a test battery in marine ecotoxicology: The acute toxicity of sodium dodecyl sulfate." *Environmental Toxicology* 21 (4):373-379. doi: https://doi.org/10.1002/tox.20204.

Marion, Christopher, Adam Jordens, Ronghao Li, Martin Rudolph, and Kristian E. Waters. 2017. "An evaluation of hydroxamate collectors for malachite flotation." *Separation and Purification Technology* 183:258-269. doi: https://doi.org/10.1016/j.seppur.2017.02.056.

Marion, Christopher, Ronghao Li, and Kristian E. Waters. 2020. "A review of reagents applied to rare-earth mineral flotation." *Advances in Colloid and Interface Science* 279. doi: 10.1016/j.cis.2020.102142.

Maruyama, Hideo, Hideshi Seki, and Ako Igi. 2020. "Flocculation of quartz and kaolin by alginate-protamine complex." *Biochemical Engineering Journal* 162. doi: 10.1016/j.bej.2020.107713.

Massana Roquero, Daniel, Ali Othman, Artem Melman, and Evgeny Katz. 2022. "Iron(iii)-cross-linked alginate hydrogels: a critical review." *Materi. Adv.* 3 (4):1849-1873. doi: 10.1039/D1MA00959A.

McCawley, Ida A., Raina M. Maier, and David E. Hogan. 2023. "Comparison of synthetic rhamnolipids as chemical precipitants for Pb, La, and Mg." *Journal of Hazardous Materials* 447. doi: 10.1016/j.jhazmat.2023.130801.

Menakbi, Chemseddine, Francoise Quignard, and Tzonka Mineva. 2016. "Complexation of trivalent metal cations to mannuronate type alginate models from a density functional study." *J.Phys. Chemi. B* 120 (15):3615-3623. doi: 10.1021/acs.jpcb.6b00472.

Mielczarski, Ela, Jerzy A. Mielczarski, Lei Zhang, and P. Somasundaran. 2004. "Structure of adsorbed n-dodecyl-β-D-maltoside layers on hematite." *Journal of Colloid and Interface Science* 275 (2):403-409. doi: 10.1016/j.jcis.2004.02.083.

Mierczynska-Vasilev, Agnieszka, Mohammad Kor, Jonas Addai-Mensah, and David A. Beattie. 2013. "The influence of polymer chemistry on adsorption and flocculation of talc suspensions." *Chemical Engineering Journal* 220:375-382. doi: 10.1016/j.cej.2012.12.080.

Moral, Çiğdem Kıvılcımdan, Helga Ertesvåg, and F. Dilek Sanin. 2016. "Guluronic acid content as a factor affecting turbidity removal potential of alginate." *Environ Sci Pollut Res* 1-9. doi: 10.1007/s11356-016-7475-6.

Mørch, Ýrr A., Ivan Donati, Berit L. Strand, and Gudmund Skjåk-Bræk. 2006. "Effect of Ca2+, Ba2+, and Sr2+ on Alginate Microbeads." *Biomacromolecules* 7 (5):1471-1480. doi: 10.1021/bm060010d.

Moreira, Gabriela F., Elaynne R. Peçanha, Marisa B. M. Monte, Laurindo S. Leal Filho, and Fernando Stavale. 2017. "XPS study on the mechanism of starch-hematite surface chemical complexation." *Minerals Engineering* 110:96-103. doi: 10.1016/j.mineng.2017.04.014.

Mulligan, Catherine N. 2005. "Environmental applications for biosurfactants." *Environmental Pollution* 133 (2):183-198. doi: 10.1016/j.envpol.2004.06.009.

Nagaraj, D. R. 2005. "Reagent selection and optimization—the case for a holistic approach." *Minerals Engineering* 18 (2):151-158. doi: 10.1016/j.mineng.2004.10.017.

Nagaraj, D. R., and R. S. Farinato. 2016. "Evolution of flotation chemistry and chemicals: A century of innovations and the lingering challenges." *Minerals Engineering* 96-97:2-14. doi: 10.1016/j.mineng.2016.06.019.

Nagaraj, D.R. , R.S. Farinato, and E Arinaitwe. 2019. "Flotation Chemicals and Chemistry." In *SME Mineral Processing and Extractive Metallurgy Handbook*, edited by R. C. Dunne, K. S. Kawatra and C. A. Young, 967-1010. Englewood, Colorado: Society for Mining, Metallurgy & Exploration.

Nikolova, Christina, and Tony Gutierrez. 2021. "Biosurfactants and Their Applications in the Oil and Gas Industry: Current State of Knowledge and Future Perspectives." *Frontiers in Bioengineering and Biotechnology* 9. doi: 10.3389/fbioe.2021.626639.

Nitschke, Marcia, Siddhartha GVAO Costa, and Jonas Contiero. 2005. "Rhamnolipid surfactants: an update on the general aspects of these remarkable biomolecules." *Biotechnology Progress* 21 (6):1593-1600.

Nordgård, Catherine T., and Kurt Ingar Draget. 2021. "Chapter 26 - Alginates." In *Handbook of Hydrocolloids (Third Edition)*, edited by Glyn O. Phillips and Peter A. Williams, 805-829. Woodhead Publishing.

Otto, R. T., H. J. Daniel, G. Pekin, K. Müller-Decker, G. Fürstenberger, M. Reuss, and C. Syldatk. 1999. "Production of sophorolipids from whey." *Applied Microbiology and Biotechnology* 52 (4):495-501. doi: 10.1007/s002530051551.

Öz Derya, Aksoy, Serhat Özdemİr, Sabiha Koca, Hakan Çakmak, Pınar Aytar Çelik, Ahmet Çabuk, and Hüseyin Koca. 2022. "Modelling of Magnesite Flotations with Two Different Collectors: Biocollector and Oleate." *Eskişehir Osmangazi Üniversitesi Mühendislik ve Mimarlık Fakültesi Dergisi* 30 (1):106-114. doi: 10.31796/ogummf.1000345.

Parker, R., and S. G. Ring. 2001. "Aspects of the Physical Chemistry of Starch." *Journal of Cereal Science* 34 (1):1-17. doi: 10.1006/jcrs.2000.0402.

Pearse, M. J. 2003. "Historical use and future development of chemicals for solid–liquid separation in the mineral processing industry." *Minerals Engineering* 16 (2):103-108. doi: 10.1016/s0892-6875(02)00288-1.

Pearse, M. J. 2005. "An overview of the use of chemical reagents in mineral processing." *Minerals Engineering* 18 (2):139-149. doi: 10.1016/j.mineng.2004.09.015.

Pearse, MJ, S Weir, SJ Adkins, and GM Moody. 2001. "Advances in mineral flocculation." *Minerals Engineering* 14 (11):1505-1511.

Pearson, Ralph G. 1963. "Hard and soft acids and bases." *Journal of the American Chemical society* 85 (22):3533-3539.

Peterson, HD, MC Fuerstenau, RS Rickard, and JD Miller. 1965. "Chrysocolla flotation by the formation of insoluble surface chelates." *Trans. Am. Inst. Min. Eng* 232:388-392.

Peyre, Jessie, Ahmed Hamraoui, Marco Faustini, Vincent Humblot, and Niki Baccile. 2017. "Surface-induced assembly of sophorolipids." *Physical Chemistry Chemical Physics* 19 (23):15227-15238. doi: 10.1039/c7cp01339f.

Pradip. 1988. "Applications of chelating agents in mineral processing." *Mining, Metallurgy & Exploration* 5 (2):80-89. doi: 10.1007/bf03402495.

Pradip, and D. W. Fuerstenau. 1983. "The adsorption of hydroxamate on semi-soluble minerals. Part I: Adsorption on barite, Calcite and Bastnaesite." *Colloids and Surfaces* 8 (2):103-119. doi: 10.1016/0166-6622(83)80079-1.

Quast, Keith. 2021. "Flotation of hematite using 18-carbon fatty acids." *Minerals Engineering* 160. doi: 10.1016/j.mineng.2020.106647.

Ramachandra Rao, S., and Jan Leja. 2004. *Surface chemistry of froth flotation. Vol. 2 Reagents and mechanisms*. 2nd ed. New York: Kluwer.

Rani, Priti, Sumit Mishra, and Gautam Sen. 2013. "Microwave based synthesis of polymethyl methacrylate grafted sodium alginate: its application as flocculant." *Carbohydrate Polymers* 91 (2):686-692. doi: 10.1016/j.carbpol.2012.08.023.

Ren, J., S. Lu, S. Song, and J. Niu. 1997. "A new collector for rare earth mineral flotation." *Minerals Engineering* 10 (12):1395-1404. doi: 10.1016/s0892-6875(97)00129-5.

Rohem Peçanha, Elaynne, Marta Duarte da Fonseca de Albuquerque, Renata Antoun Simão, Laurindo de Salles Leal Filho, and Marisa Bezerra de Mello Monte. 2019. "Interaction forces between colloidal starch and quartz and hematite particles in mineral flotation." *Colloids and Surfaces A: Physicochemical and Engineering Aspects* 562:79-85. doi: 10.1016/j.colsurfa.2018.11.026.

Runkana, Venkataramana, P Somasundaran, and PC Kapur. 2006. "A population balance model for flocculation of colloidal suspensions by polymer bridging." *Chemical Engineering Science* 61 (1):182-191.

Sarvaramini, A., D. Azizi, and F. Larachi. 2016. "Hydroxamic acid interactions with solvated cerium hydroxides in the flotation of monazite and bastnäsite—Experiments and DFT study." *Applied Surface Science* 387:986-995. doi: 10.1016/j.apsusc.2016.07.044.

Shen, Yang, Chi Lo, D. R. Nagaraj, Raymond Farinato, Amy Essenfeld, and P. Somasundaran. 2016. "Development of Greenness Index as an evaluation tool to assess reagents: Evaluation based on SDS (Safety Data Sheet) information." *Minerals Engineering* 94:1-9. doi: 10.1016/j.mineng.2016.04.015.

Shibata, J., and D. W. Fuerstenau. 2003. "Flocculation and flotation characteristics of fine hematite with sodium oleate." *International Journal of Mineral Processing* 72 (1-4):25-32. doi: 10.1016/s0301-7516(03)00085-1.

Shrimali, Kaustubh, Venkata Atluri, Yan Wang, Sanket Bacchuwar, Xuming Wang, and Jan D. Miller. 2018. "The nature of hematite depression with corn starch in the reverse flotation of iron ore." *Journal of Colloid and Interface Science* 524:337-349. doi: 10.1016/j.jcis.2018.04.002.

Sivamohan, R. 1990. "The problem of recovering very fine particles in mineral processing — A review." *International Journal of Mineral Processing* 28 (3-4):247-288. doi: 10.1016/0301-7516(90)90046-2.

Slabov, Vladislav, Garima Jain, Irina Chernyshova, Hanumantha Rao Kota, and Helga Ertesvåg. 2023. "Alginates as Green Flocculants for Metal Oxide Nanoparticles." *Transactions of the Indian Institute of Metals*. doi: 10.1007/s12666-023-02957-7.

Smidsrød, O, and ARNE Haug. 1968. "Dependence upon uronic acid composition of some ion-exchange properties of alginates." *Acta Chem. Scand* 22 (6):1989-1997.

Smidsrød, Olav. 1974. "Molecular basis for some physical properties of alginates in the gel state." *Faraday Discuss. Chem. Soc.* 57 (0):263-274. doi: 10.1039/dc9745700263.

Somasundaran, P., and L. Huang. 2000. "Adsorption/aggregation of surfactants and their mixtures at solid–liquid interfaces." *Advances in Colloid and Interface Science* 88 (1-2):179-208. doi: 10.1016/s0001-8686(00)00044-0.

Song, Shaoxian, and Shouci Lu. 1994. "Hydrophobic Flocculation of Fine Hematite, Siderite, and Rhodochrosite Particles in Aqueous Solution." *Journal of Colloid and Interface Science* 166 (1):35-42. doi: https://doi.org/10.1006/jcis.1994.1268.

Sreenivas, T., and N. P. H. Padmanabhan. 2002. "Surface chemistry and flotation of cassiterite with alkyl hydroxamates." *Colloids and Surfaces A: Physicochemical and Engineering Aspects* 205 (1-2):47-59. doi: 10.1016/s0927-7757(01)01146-3.

Stubenrauch, C., P. M. Claesson, M. Rutland, E. Manev, I. Johansson, J. S. Pedersen, D. Langevin, D. Blunk, and C. D. Bain. 2010. "Mixtures of n-dodecyl-β-d-maltoside and hexaoxyethylene dodecyl ether — Surface properties, bulk properties, foam films, and foams." *Advances in Colloid and Interface Science* 155 (1):5-18. doi: https://doi.org/10.1016/j.cis.2009.12.002.

Subrahmanyam, T. V., and K. S. Eric Forssberg. 1990. "Fine particles processing: shear-flocculation and carrier flotation — a review." *International Journal of Mineral Processing* 30 (3):265-286. doi: https://doi.org/10.1016/0301-7516(90)90019-U.

Tian, Zhenle, Liping Zhang, Xinxin Sang, Gang Shi, and Caihua Ni. 2020. "Preparation and flocculation performance study of a novel amphoteric alginate flocculant." *Journal of Physics and Chemistry of Solids* 141. doi: 10.1016/j.jpcs.2020.109408.

Tripathy, Tridib, N. C. Karmakar, and R. P. Singh. 2001. "Development of novel polymeric flocculant based on grafted sodium alginate for the treatment of coal mine wastewater." *Journal of Applied Polymer Science* 82 (2):375-382. doi: 10.1002/app.1861.

Tripathy, Tridib, and R. P. Singh. 2000. "High performance flocculating agent based on partially hydrolysed sodium alginate–g–polyacrylamide." *European Polymer Journal* 36 (7):1471-1476. doi: 10.1016/s0014-3057(99)00201-3.

Wanhala, Anna K., Benjamin Doughty, Vyacheslav S. Bryantsev, Lili Wu, Shannon M. Mahurin, Santa Jansone-Popova, Michael C. Cheshire, Alexandra Navrotsky, and Andrew G. Stack. 2019. "Adsorption mechanism of alkyl hydroxamic acid onto bastnäsite: Fundamental steps toward rational collector design for rare earth elements." *Journal of Colloid and Interface Science* 553:210-219. doi: 10.1016/j.jcis.2019.06.025.

Warren, Leonard J. 1975. "Shear-flocculation of ultrafine scheelite in sodium oleate solutions." *Journal of Colloid and Interface Science* 50 (2):307-318.

Wills, Barry A, and James Finch. 2015. *Wills' mineral processing technology: an introduction to the practical aspects of ore treatment and mineral recovery*: Butterworth-Heinemann.

Yang, Can Hui, Mei Xiang Wang, Hussain Haider, Jian Hai Yang, Jeong-Yun Sun, Yong Mei Chen, Jinxiong Zhou, and Zhigang Suo. 2013. "Strengthening Alginate/Polyacrylamide Hydrogels Using Various Multivalent Cations." *ACS Applied Materials & Interfaces* 5 (21):10418-10422. doi: 10.1021/am403966x.

Yu, Xinyang, Ruirui Zhang, Siyuan Yang, Cheng Liu, Guichun He, Haolin Wang, and Jingliang Wang. 2020. "A novel decanedioic hydroxamic acid collector for the flotation separation of bastnäsite from calcite." *Minerals Engineering* 151. doi: 10.1016/j.mineng.2020.106306.

Zhang, Jinxia, Chao Yang, Fusheng Niu, and Shuling Gao. 2022. "Molecular dynamics study on selective flotation of hematite with sodium oleate collector and starch-acrylamide flocculant." *Applied Surface Science* 592. doi: 10.1016/j.apsusc.2022.153208.

Zhang, L., P. Somasundaran, J. Mielczarski, and E. Mielczarski. 2002. "Adsorption Mechanism of n-dodecyl-β-D-maltoside on Alumina." *Journal of Colloid and Interface Science* 256 (1):16-22. doi: 10.1006/jcis.2001.7858.

Zhang, Lei, P. Somasundaran, and C. Maltesh. 1996. "Electrolyte Effects on the Surface Tension and Micellization of n-Dodecyl β-d-Maltoside Solutions." *Langmuir* 12 (10):2371-2373. doi: 10.1021/la950670w.

Zhang, Lei, P. Somasundaran, and C. Maltesh. 1997. "Adsorption ofn-Dodecyl-β-d-maltoside on Solids." *Journal of Colloid and Interface Science* 191 (1):202-208. doi: 10.1006/jcis.1997.4923.

Zhang, W., R. Q. Honaker, and J. G. Groppo. 2017. "Flotation of monazite in the presence of calcite part I: Calcium ion effects on the adsorption of hydroxamic acid." *Minerals Engineering* 100:40-48. doi: 10.1016/j.mineng.2016.09.020.

6. Papers

Paper 1

Eco-Friendly Collectors for Flotation of Fine Hematite and Malachite Particles

Vladislav Slabov[1] · Garima Jain[2] · Erik Larsen[1] · Hanumantha Rao Kota[1] · Irina Chernyshova[1]

Abstract

The separation of fine mineral particles, especially using environmentally friendly approaches, is one of the main problems in the processing of low-grade ores and the re-processing of mining tailings. This work assesses the potential of biosurfactants as collectors in the flotation of ultrafine (smaller than 20 μm) particles of hematite and malachite. As biosurfactants, we test acetylated acidic (ac-ASL) and lactonic sophorolipids (ac-LSL). In addition, n-dodecyl-β-D-maltoside (DDM) is used as a model non-ionic alkyl disaccharide surfactant, and sodium oleate (NaOl) is used as a reference. The biosurfactants are characterized using surface tension and foam analysis. The interaction of the minerals with the surfactants is characterized using zeta potential, solubility, and single-mineral flotation. The collecting properties of the surfactants are compared for the ultrafine (-20 μm) and coarser (38–90 μm) particle size in the two-mineral flotation of hematite and malachite against quartz. The ultrafine particle size improves the grade in the oleate flotation of hematite, as well as the grades in the DDM flotation of hematite and malachite, which is explained by the weak interactions of the metal oxides with fatty acids and DDM. At the same time, the flotation with ac-LSL and ac-ASL is highly tolerant to the ultrafine particle size. These results indicate that biosurfactants are an interesting alternative to conventional petroleum-based surfactants in the flotation of Fe and Cu oxides. Moreover, a proper selection of surfactants can help combat the problem of fines.

Keywords Sophorolipids · Iron oxides · Copper oxides · Green collectors · Fine particles flotation · Separation

1 Introduction

The supply risks and the increasing demand for minerals critical for the energy transition have stimulated their domestic production from both primary (ores) and secondary (waste) resources. This economic shift has in turn spurred more efforts toward the development of novel technological solutions to boost resource efficiency and drastically reduce the carbon footprint of flotation.

Flotation is a physicochemical method that has widely been employed for separating minerals from ores for more than a century. Its selectivity is achieved using surfactants (collectors) that make the target mineral particles hydrophobic. During the long history of flotation, tremendous progress has been achieved in developing collectors for different types of minerals, along with a general framework of the collector-mineral interactions [1–4]. However, most conventional collectors originate from non-renewable resources (petrochemicals). In addition, some of them or products of their chemical degradation are hazardous and pose risks to human health and the environment. The quintessential examples are xanthates [5, 6] and amines [7]. Therefore, there is a growing trend to extend the share of green reagents in flotation [8–11]. The adjective "green," or "eco-friendly," implies that the reagents comply across their life cycle with a set of principles of green chemistry, including production from renewable feedstocks, minimization of hazards, and benign degradation after the use [12, 13]. It has been suggested that the true "greenness" of collectors should be measured over four major life cycle stages, (i) manufacturing, (ii) storage and transportation, (iii) usage and processing, and (iv) post-usage and processing, for which most reagents are still unavailable [14].

✉ Irina Chernyshova
   irina.chernyshova@ntnu.no

1   Department of Geoscience and Petroleum, Norwegian
    University of Science and Technology (NTNU),
    NO-7031 Trondheim, Norway

2   Department of Biotechnology and Food Science,
    Norwegian University of Science and Technology (NTNU),
    NO-7491 Trondheim, Norway

Flotation already employs two important classes of green reagents—fatty acids and polysaccharides—which are mainly used as collectors and depressants of iron oxides, respectively [3, 15, 16].

The fatty acid flotation of iron oxides depends on pH, with a maximum being at pH 6–8 [3, 16, 17]. This maximum can be explained by the physisorption-chemisorption model [18, 19]. In this model, fatty acids are chemisorbed via one O atom of their carboxylate groups. The electrostatic repulsion between the co-adsorbed carboxylate groups is screened by co-adsorbed neutral molecules, which improves the packing density and hydrophobicity of the surfactant layer. Chemisorbed fatty acids become more important at pH above the iso-electric point (IEP) of iron oxides, but their concentration rapidly declines due the relatively weak adsorption strength. Fatty acids have also commercially been used in the flotation of oxide copper minerals from siliceous ores, where "copper oxide" is a generic term for non-sulfide copper minerals [20]. In contrast to iron oxides, the adsorption of fatty acids on Cu oxides is typically explained in terms of chemisorption [21, 22], though, to the best of our knowledge, the adsorption mechanism has not been studied thoroughly. However, the application of fatty acids as collectors is limited by their relatively low selectivity [4, 23]. As a result, there is ongoing research to find more selective alternatives, mainly among chelating petroleum-based surfactants [21].

Starch (a natural polysaccharide) is a common depressant of iron oxides. Spectroscopic results suggest that starch interacts with hematite (α-Fe_2O_3) via complexation with the surface Fe-OH groups [24], which can explain the preferable chemisorption of starch on hematite vs quartz [25]. In the hematite-starch-oleate system, starch covers the hematite surface almost fully, thereby preventing the adsorption of oleate [26], which suggests that starch interacts with hematite more strongly than oleate does. The specific interaction of starch with hematite agrees with the dependence of the affinity of hematite to starch on the hematite crystallographic plane, which decreases in the order of $(1\ 1\ \bar{2}\ 0) > (1\ \bar{1}\ 0\ 0) > (0\ 0\ 1\ 1)$ [27]. This dependence has been explained by multisite complexation between starch molecules and oxygen surface sites. In contrast, a non-ionic sugar-based surfactant n-dodecyl-β-d-maltoside (DDM) is physisorbed on hematite through hydrogen bonding with surface hydroxyl groups [28–30], which can be associated with the strong hydration of the maltose headgroup [31]. In contrast, DDM is likely to chemisorb on hematite at a highly alkaline pH [30]. Interestingly, DDM adsorbs on hematite, but very little on silica [28].

At the same time, there is very limited knowledge about the potential of biosurfactants as green collectors, not to mention a general framework that classifies biosurfactants in terms of the minerals that they can float [8, 9, 11, 13, 32].

Biosurfactants are surfactants that are either extracted from plants or produced by biocatalysis (using enzymes) or non-pathogenic microbial processes from renewable biological sources (biomass) [33, 34]. These surfactants are increasingly introduced into personal care, pharma, detergency, and cosmetics due to their non-hazardous nature as well as higher biocompatibility and biodegradability compared to conventional surfactants.

The most studied biosurfactants are glycolipids, which are built of different sugar groups linked to ß-hydroxy fatty acids [34]. Their sugar headgroups and auxiliary chains have multiple O-donor atoms that can coordinate to a metal center. The large hydrophilic sugar groups can improve the solubility of biosurfactants and their complexes with metal ions and hence make biosurfactants more tolerant to higher levels of total dissolved solids compared to conventional surfactants. An example is sophorolipids which can be produced with various molecular structures and easily functionalized [33]. Another important benefit of sophorolipids is that they hold the largest share of the biosurfactant market while their production from food waste improves their economic and environmental sustainability [35, 36].

So far, sophorolipids have been studied in detail only in solutions and at the air–water interfaces [33], while their interaction with minerals has been addressed only in a handful of works [32, 37–40]. In particular, it has been concluded that an asymmetrical bipolar ("bola") acidic sophorolipid (ASL) renders copper sulfides hydrophobic through the dissolution–precipitation mechanism that forms hydrophobic Cu-ASL precipitates on the sulfide surface [32]. The hydrophobicity of the precipitates has been explained by a loop-like chelating coordination of both the sophorose and carboxylate headgroups of ASL to Cu cations. This mechanism allows ASL to float copper sulfides from a pyrite-poor copper ore similarly to or even better than conventional thiol collectors [13]. The chelating structure of the Cu-ASL complexes can explain the strong leaching activity of ASL toward Cu sulfides and metallic Cu [32, 38]. In contrast, only the carboxylate headgroup of ASL coordinates to iron oxide nanoparticles during the precipitation of iron oxide nanoparticles in ASL solutions, while the sophorose headgroup is left free which renders the nanoparticles hydrophilic [39]. The different coordination of ASL to copper sulfides and iron oxides can underpin its selectivity to Cu and Fe oxides. Thus, given that O-donors ("oxyhydrils") are conventional collectors of iron and copper oxides [3, 4, 41, 42], it is of interest to test the performance of sophorolipids in the flotation of these minerals, starting from model synthetic systems.

Apart from selectivity, a common problem in the flotation of iron and copper oxides is the so-called problem of fines, that is, difficulty to float fine (smaller than 38 m) particles using standard schemes. Fine particles are naturally

produced in significant amounts during the grinding of non-sulfide ores due to their mechanical properties. In addition, the gradual depletion of easy-to-extract high-grade ores has steered the mineral processing industry toward low-grade ores and secondary resources such as flotation tailings [43–46]. Due to the complex intergrowth and ultrafine-grained dissemination of mineral phases, these resources need to be ground down to ultrafine sizes to liberate valuable minerals.

The negative impact of fines on flotation is caused by several chemical and physical mechanisms [15, 47, 48]. In particular, fine particles have lower collision rates with bubbles, which results in slower flotation kinetics [15]. Due to their higher specific surface areas, fine particles can consume a higher amount of the collector per unit weight and be more reactive (change its redox state and dissolve faster) compared to the particles with the conventional flotation size (38–150 m) [15, 48]. The entrainment of fine particles in the froth and their heterocoagulation with other minerals can drop selectivity and increase mineral loss [47, 48]. Entrainment is the mechanical (non-selective) mass transfer of suspended particles to the water between bubbles which brings them to the collected flotation froth. This process can involve hydrophilic particles of other minerals and is linked to the amount of water carried in the froth and the foam stability [49]. Fine particles can also be attached to and monopolize the surface of the air bubbles, preventing them from attaching to other minerals [15]. Even though there are technical solutions to the problem of fines [4, 15, 47, 50], flotation chemistry can be a part of these solutions. At the same time, there is limited information on how different collectors respond to the fine particle size.

Herein, we study the effect of particle size on the efficiency of two sophorolipids as collectors of hematite α-Fe$_2$O$_3$ and malachite CuCO$_3$·Cu(OH)$_2$ in synthetic two-mineral systems with quartz with an outlook for their application to real mineral processing systems which are yet to be defined. Hematite is the main resource of iron on Earth [16]. Malachite is the most common copper oxide mineral. It is usually associated with the weathering of copper ores [20, 21]. Quartz is used as a model gangue mineral given its abundance in iron oxide and malachite-containing copper oxide ores [16, 20, 23]. To delineate the effect of particle size, we compare the flotation of ultrafine (−20 m) and larger (+38−90 μm) particles. Even though the larger particles are in the conventional size range of flotation, we call them "coarse" hereafter to distinguish them from the ultrafine particles.

The sophorolipids studied are acetylated acidic sophorolipid (ac-ASL) and acetylated lactonic sophorolipid (ac-LSL). Ac-ASL is an anionic surfactant with an acetylated sophorose headgroup attached to the C17 carbon of oleic acid (Fig. 1a). In contrast, ac-LSL is non-ionic as it has a closed C17 carbon chain with the carboxylate group of oleic acid linked to the sophorose headgroup through the ester bond (Fig. 1b). As a result, ac-LSL has a stiffer geometry and is less soluble in water than ac-ASL. Lactonic sophorolipids have lower surface tension and critical micelle concentration (CMC) and stronger bactericide properties, while acidic sophorolipids are better foamers [51].

For comparison purposes, we included in our study sodium oleate (NaOl) (Fig. 1d) and DDM (Fig. 1c). NaOl is used as both a reference and a model fatty acid given that fatty acids are among the main collectors of iron and copper oxides [3, 16, 17]. Moreover, oleate is a structural unit of both ac-ASL and ac-LSL. Hence, their comparison with NaOl could inform us about the involvement of the carboxylate and sophorose groups into the phenomena studied. DDM (Fig. 1c) is used for comparison with ac-LSL as both are non-ionic disaccharides. However, the longer hydrocarbon chain, its fixed loop-like shape, and acetylation of the sophorose headgroup make ac-LSL more hydrophobic

Fig. 1 Surfactants used in this study: **a** acetylated acidic sophorolipid (ac-ASL); **b** acetylated lactonic sophorolipid (ac-LSL); **c** n-dodecyl-β-D-maltoside (DDM); **d** sodium oleate (NaOl)
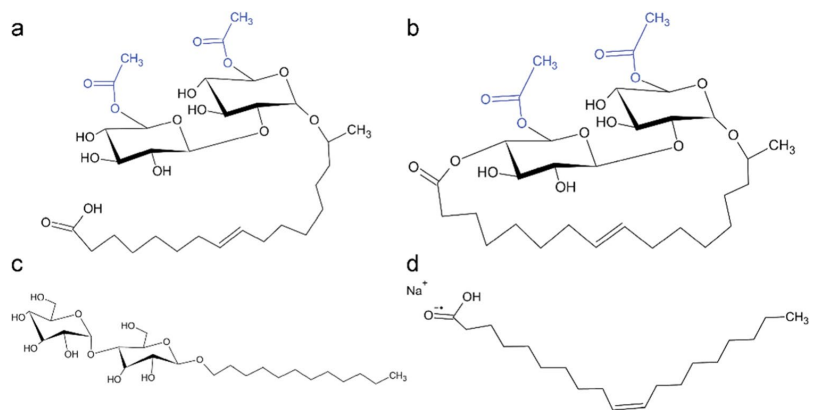
and rigid, which is expected to affect solubility of ac-LSL and its self-assembly at interfaces [31, 52]. The three ester groups can also make ac-LSL chemically reactive. It has been reported that the acetyl groups and ester bonds are irreversibly hydrolyzed during long-term storage at pH values higher than 7.0–7.5 [51]. Finally, the interaction of DDM with hematite has already been studied [28–30, 53], which can help interpret our results. As research methods, we use static surface tension measurements, dynamic foam analysis, ζ-potential, and single- and two-mineral flotation.

2 Materials and Methods

2.1 Materials

Diacetylated ac-LSL and diacetylated ac-ASL were provided by Bio Base Europe Pilot Plant, Ghent, Belgium. The chemical structures of ac-ASL and ac-LSL are confirmed by FTIR as described in the "Supplementary Information" and shown in Fig. S1. Sodium oleate (NaOl) was produced by J. T. Baker and DDM was produced by Avanti Polar Lipids, Alabaster, Alabama. All the surfactants were used without further purification. Milli-Q water was used for all experiments. NaOH and HNO_3 were used for pH adjusting, and $NaNO_3$ and KCl were used as background electrolyte solutions. These reagents were purchased from VWR™.

2.2 Minerals

Hematite was provided by Rana Gruber, Norway. Malachite was purchased from Richard Tayler Minerals, UK. The origin of quartz was Kyshtym, South Ural, Russia.

The minerals were crushed and milled in a planetary mill with a stainless-steel jar and stainless steel 30-mm balls, followed by wet sieving to obtain a − 20-μm fraction. To remove contaminations, − 20-μm hematite and quartz particles were cleaned in a 0.01 M HCl solution followed by washing in Milli-Q water until neutral pH is reached. The cleaning procedure for malachite was eliminated due to the mineral dissolution at acidic pH. The coarse fraction (+ 38 − 90 m) was prepared by dry sieving, followed by the cleaning procedure used for the fine fraction. The samples were split by Retsch mini splitter into three batches—two for flotation (for duplication) and one for analysis.

2.3 Surfactant Solutions

A 1-g/L stock solution of ac-ASL was prepared by dissolving the surfactant in water. The stock solution of ac-ASL had pH 5.6. Ac-LSL was dissolved at a concentration of 0.6 g/L in a 0.002 M NaOH solution to increase its solubility. We limited pH of the stock solution by 9.5 which can cause de-acetylation of ac-LSL.

2.4 Flotation

Flotation tests were conducted using a XFG II flotation machine at surfactant concentrations of 50 μM. These tests were conducted without adding a frother. DowFrother™ 200 at a concentration of 50 μM was used only in single-mineral flotation to create a flotation baseline without surfactants. As NaOl does not generate a measurable froth at 50 μM, we collected the hydrophobic layer of particles on the surface of the flotation cell. In the other cases, we collected the froth.

In the single-mineral flotation of ultrafine particles, 1 g of particles was placed into the 100-mL flotation cell. Then, 90 mL Milli-Q water was added, and the pulp was stirred for 2 min. After 2 min, pH was adjusted to the required value and the surfactant solution at the same pH was added. pH was readjusted after 4 min followed by the flotation in 1 min. The reported pH values were measured under flotation conditions. All these steps were implemented under continuous stirring at 1500 rpm. Flotation time was 2 min at an airflow rate of 100 L/h (approximately 1650 mL/min). Floated and non-floated fractions were collected and filtered using filter paper of a 589/3 grade followed by drying in a heating chamber. The weight of the dried particles was used to determine recoveries. The grade was measured using portable X-ray fluorescence (XRF). Since this method has limited accuracy, each sample was measured three times and the results were averaged. All the flotation tests were repeated twice, and the average values are reported. The same procedure was repeated for mix-mineral flotation. The ratio of minerals was 1:1, where 1 g of each mineral was used for the ultrafine fraction, and 1.5 g of each for the coarse fraction.

2.5 Surface Tension

Static surface tension was measured by Du Nouy's ring method using a Biolin Scientific Sigma 702 instrument. The ring was repeatedly flamed until it glowed red-hot in an ethanol flame and washed with deionized water to ensure the complete removal of impurities. The instrument was first calibrated with water (72 ± 1 mN/m). The stock solutions of ac-LSL or ac-ASL were adjusted to specific pH, and then added to water with the same pH. The pH of the final solution did not drift by more than 0.2 pH. Each reported surface tension data point is an average of 10 measurements in the same solution. Each set of experiments was repeated in two solutions. Differences between the duplicates were insignificant.

2.6 Foaming Properties

Foaming properties were studied by a Kruss Dynamic Foam Analyzer DFA 100. The surfactant solutions were prepared in 0.001 M KCl at pH 5 and pH 10 at a surfactant concentration of 50 µM. KCl was added to provide the solution with the conductivity needed for the analyzer sensors. The volume of each solution sample was 50 mL, and each experiment was repeated twice.

2.7 Solubility

To study the effect of the surfactants on the solubility of ultrafine hematite and malachite, we measured the Fe and Cu concentrations in the supernatant after conditioning 0.5 g of the mineral particles in 50 mL of the 50 M surfactant solutions at pH 5.2 and pH 9.7 for 3 h.

2.8 FTIR Spectroscopy

ATR FTIR spectra of bulk dry surfactants were recorded using a Bruker Vertex 80v FTIR spectrometer. A typical spectrum was an average of 200 scans measured at a 4 cm^{-1} resolution.

2.9 ICP-MS

Metal ions in the surfactant solutions before and after interaction with minerals were analyzed using ICP-HR-MS Element 2 (Thermo) equipped with an auto-sampler SC2 DX dust-covered with a ULPA filter. For these experiments, 0.5 g of ultrafine mineral particles was added to 50 mL of a 50 µM surfactant solution prepared at different pH. pH was readjusted after 30 min, and the dispersions were conditioned for 3 h on a shaking table. The resulting supernatant was filtered through a syringe membrane (0.2 µm), digested by HNO$_3$, and analyzed by ICP-MS. The error was no more than 10% as estimated by duplicating random points.

2.10 Zeta Potential

The zeta (ζ) potential of minerals in water and surfactant solutions was measured using a Malvern ZetaSizer Nano Z (laser Doppler micro-electrophoresis) instrument. Mineral particles were first dispersed in a 0.001 M NaNO$_3$ background solution at 0.1 wt.% by sonication for 15 min. This dispersion was split into five parts to prepare dispersions with the four surfactants and one blank (mineral particles in 0.001 M NaNO$_3$). Then, the prepared samples were split into seven 30-mL samples followed by pH adjustment of each sample. The pH-adjusted samples were equilibrated on a shaking table overnight. Afterward, pH was readjusted with 0.01 M NaOH and HNO$_3$ solutions. Final pH was measured

for each sample before measuring its ζ-potential. As the material settings in ZetaSizer, we used refractive indices of 3.0, 3.6, and 1.5 and absorption of 0.8, 0.7, and 0.2 for hematite, malachite, and quartz respectively. ζ-potential of NaOl and ac-LSL was measured in water using a refractive index of 1.0 and an absorption index of 0.1. Each ζ-potential data point is an average of 3 replicate points where each point was an average of 10 scans each. The ζ-potential uncertainty is ± 2 mV and the pH uncertainty is within 0.1 pH.

2.11 The BET (Brunauer, Emmett, and Teller) Surface Area and Particle Size Distribution

The BET surface areas were measured using a Micromeritics Tristar 3000 Analyzer. All samples were degassed at 250 °C under helium flow for 3 h. The particle size distribution was measured by the dynamic light scattering method using a Mastersizer 3000E.

2.12 XRD

X-ray diffractometry (XRD) was used to determine the phase composition of the minerals. For the quantitative phase analysis, ultrafine particles were additionally ground in ethanol by agate milling rods. Bruker D8 Advance Series 2 XRD equipment was used. The samples were scanned in the θ range of 5–80° under the Co Kα radiation.

2.13 SEM

The morphology analysis of mineral particles was performed using a Hitachi SU6600 field emission SEM. A copper double-sided tape was used as a support. Materials were placed on individual tapes and coated with carbon to eliminate charging.

3 Results and Discussion

3.1 Characterization of Minerals

The XRD analysis shows that malachite and quartz used in our study are mineralogically pure (> 99%) (Fig. 2). However, the hematite diffractogram has a small peak at 31° corresponding to a quartz impurity of about 1%. The particle size distribution of the ultrafine (− 20 µm) fraction is from 0.8 to 24 µm (Table 1). The specific surface area of ultrafine hematite and ultrafine quartz is 1.5 m^2/g, while that of ultrafine malachite is three times larger (Table 1). The specific surface areas of coarse (+ 38 − 90 µm) hematite and malachite particles are 0.31 m^2/g and 0.38 m^2/g, respectively, closer one to another than in the case of ultrafine particles.

Fig. 2 XRD of (black line) ultrafine hematite, (blue line) ultrafine malachite, and (red line) ultrafine quartz. Malachite and quartz have a purity > 99%. Hematite ultrafine particles have ca. 1% quartz impurity
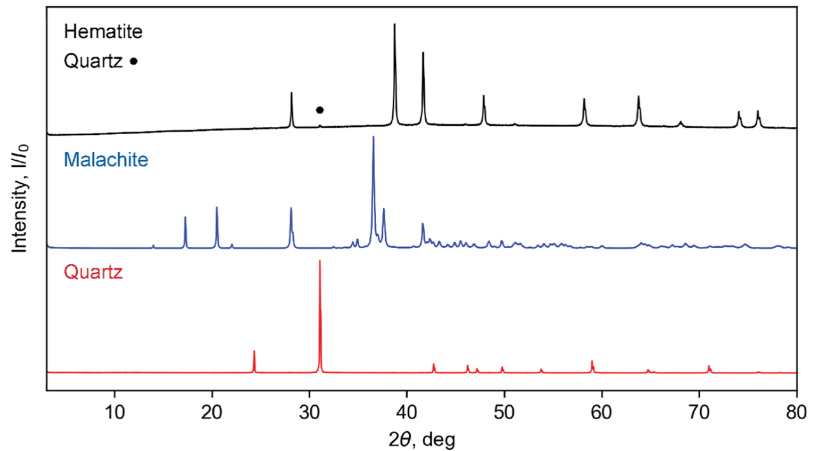

Table 1 BET surface area and particle size distribution of hematite, malachite, and quartz particles

Mineral	BET, m^2/g	Particle size distribution, μm		
		D_{10}	D_{50}	D_{90}
Hematite -20 μm (ultrafine)	1.5 ± 0.1	2.0 ± 0.2	8.4 ± 0.6	23.9 ± 2.1
Hematite $+38-90$ μm ("coarse")	0.31 ± 0.05	8.4 ± 0.3	48.7 ± 0.5	85.0 ± 2.1
Malachite -20 μm (ultrafine)	4.5 ± 0.1	0.8 ± 0.1	6.0 ± 0.9	22.0 ± 1.9
Malachite $+38-90$ μm ("coarse")	0.38 ± 0.07	6.0 ± 0.4	51.0 ± 0.7	89.5 ± 0.5
Quartz -20 μm (ultrafine)	1.5 ± 0.2	2.4 ± 0.2	9.5 ± 1.6	24.3 ± 2.6

Ultrafine hematite particles have irregular morphologies and cleavage surfaces with sharp edges (Fig. 3a), while coarse particles have rounder shapes (Fig. 3b). Both fractions contain submicron particles ("slimes"), the percentage of which is higher for the coarse particles (Table 1). The ultrafine fraction of malachite includes 10–20-μm particles with a fibrous structure and multistep rectangular edges, as well as a large portion of micron and submicron particles with shapes of broken rectangular rods (Fig. 3c). The coarse fraction of malachite contains large particles with interlayered ruptured-plate morphology typical of malachite, which comes along with an admixture of micron and submicron particles (Fig. 3d). Ultrafine quartz particles (Fig. 3e, 3f) have shapes similar to those of the ultrafine hematite particles (Fig. 3a).

3.2 Surface Tension and Foaming Properties

We measured the surface tension of ac-ASL and ac-LSL to characterize their propensity to self-assemble in solution and at the air–water interface. The interfacial properties of DDM and NaOl have been studied earlier [31, 54, 55]. At low ionic strengths, CMC and the minimum surface tension of DDM in water is 0.15–0.18 mM and 35.5 mN/m, respectively [31, 54]. CMC of NaOl (defined as the inflection point of the

surface tension) increases from 17 to 90 M in the pH range from 7 to 12, while the minimum surface tension varies non-monotonically between 26.4 and 30.1 mN/m [55].

The surface tension of ac-ASL depends on pH, while there is no significant effect of pH on the surface tension of ac-LSL (Fig. 4). These results are consistent with the presence of the carboxylate headgroup in the former and the non-ionic character of the latter (Fig. 1a, b). The CMC of ac-ASL of 0.18 mM at pH 6 and pH 10 is higher than that of non-acetylated ASL of 40 μM and 0.10 mM at pH 7 and pH 11, respectively (Table 2) [32]. It follows that acetyl groups hamper the self-assembly of ASL in solution and at the air–water interface. In contrast to CMC of non-acetylated ASL [32], CMC of ac-ASL does not depend on pH (Fig. 4a). This difference suggests that acetyl groups impose steric constraints on the carboxyl group to contact water when ac-ASL is most densely packed at the air–water interface.

Since ac-LSL is more hydrophobic than ac-ASL, it is expected to have lower values of CMC and the minimum surface tension than ac-ASL. In fact, CMC of diacetylated LSL at pH 7.4 and 25 °C has been reported to be 20 mg/L (29 M) [56]. A similar value of 15 mg/L has been obtained at pH 7 and 25 °C for LSL with an unspecified degree of acetylation [52]. In contrast, CMC of another LSL, also with the unknown acetylation degree, is 73 mg/L (0.12 mM)

Fig. 3 SEM images of **a** ultrafine hematite, **b** coarse hematite, **c** ultrafine malachite, **d** coarse malachite, **e**, **f** ultrafine quartz particles. The ultrafine particles are smaller than 20 µm. The coarse particles are in the 38–90-µm size range
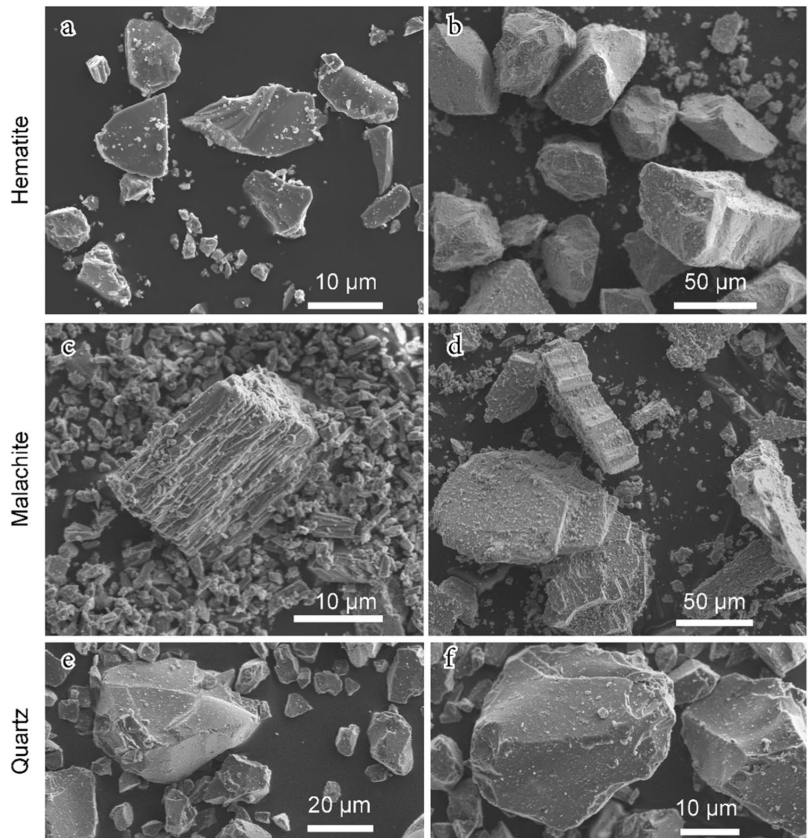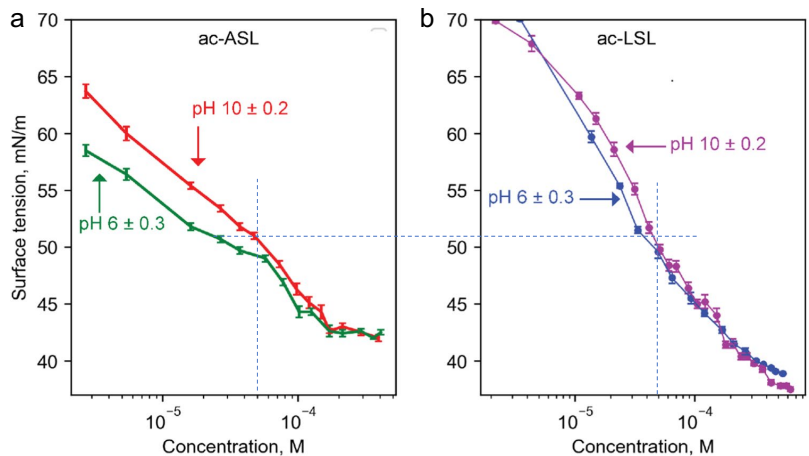

Fig. 4 Surface tension of **a** ac-ASL, and **b** ac-LSL at pH 6 ± 0.3 and 10 ± 0.2. Dashed lines show surface tension at a concentration of 50 µM used in our study

at pH 8.94 and 20 °C [57], which is close to CMC of crude sophorolipids [52]. However, the surface tension curve of the ac-LSL sample used in our study does not reach the

minimum plateau at concentrations up to 0.4–0.6 mM where the solution becomes visually turbid (Fig. 4b). Hence, instead of the classical adsorption/desorption mechanism

Table 2 Air–water interface properties of ac-LSL and ac-ASL

Surfactants	CMC, mM (± 0.02 mM)	Surface tension, mN/m (± 1 mN/m)
ac-LSL pH 6	NA	39
ac-LSL pH 10	NA	38
ac-ASL pH 6	0.18	43
ac-ASL pH 10	0.18	42

at the air–water interface, ac-LSL used in our study is likely to follow the colloidal interfacial adsorption similar to high-molecular-weight biosurfactants [33]. In fact, the formation of a colloidal solution by ac-LSL at 50 µM is detected by ζ-potential measurements (Section 3.3.2). Another reason can be the de-acetylation of ac-LSL stock solution at pH 9.5. At the same time, the lowest surface tension achieved by ac-LSL in our study, which is 39 and 38 mN/m at pH 6 and pH 10, respectively (Fig. 4b), is within the range of 34–41 mN/m reported for LSL [52, 56, 57].

The foaming properties of surfactants are also important for flotation as this process is more effective with less stable wet foams. Foaming properties can affect flotation as they control the attachment of hydrophobic particles to bubbles, the entrainment of the foreign particles with the aqueous solution, and their entrapment between particles attached to air bubbles. Hence, we studied the foaming properties (foamability and foam stability) of ac-ASL, ac-LSL, DDM, and NaOl. The study was performed at the surfactant concentration of 50 µM, which is well below CMC of ac-ASL and DDM but within the CMC range of NaOl (Section 3.2). We also assessed the liquid content and structure of their foams.

NaOl does not produce a stable and measurable foam at a concentration of 50 µM and pH 5 and 10. In contrast, DDM has the strongest foamability and foam stability at pH 10.9 (Fig. 5a and Table 3). Next in the ranking is ac-LSL at pH 5.4. The foaming properties of ac-ASL and ac-LSL at pH 10 are much weaker than at pH 5.3 and cannot be assessed by the foam analyzer under the same foam generation
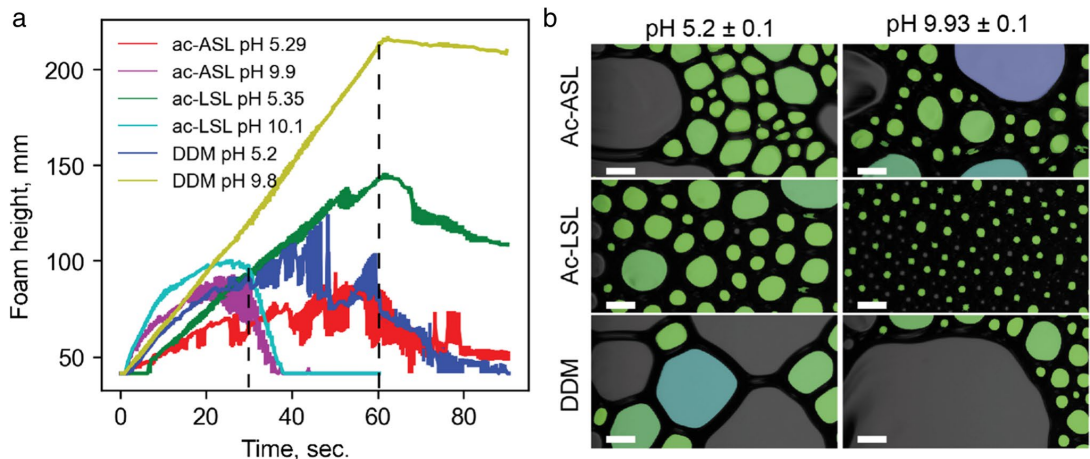
Fig. 5 Foam properties of 50 µM ac-ASL, ac-LSL, and DDM: **a** the foam heights as a function of time (dash lines mark the airflow stop); **b** the structure of the foams when airflow was stopped (30 s for ac-ASL and ac-LSL at pH 10, and 60 s for the rest). The scale bar is 1 mm

Table 3 Conditions of the foam generation and the liquid content of foams

Surfactant	Airflow, L/min	pH ± 0.2	Airflow time (t_0), sec	Air volume, L	Liquid content, %	Error, %
ac-ASL	0.2	5.3	60	0.2	5	0.5
ac-LSL	0.2	5.4	60	0.2	10	2
DDM	0.2	5.2	60	0.2	5	1
ac-ASL*	0.4	9.9	30	0.2	15	1
ac-LSL*	0.4	10.1	30	0.2	35	2
DDM	0.2	9.8	60	0.2	11	1

*Different conditions of the foam production

conditions. Therefore, we measured their foaming properties at pH 10 at a twice as high flow rate and a half interval as compared to the rest surfactants. The purpose of these measurements was to characterize the foam structures, given that a change in the airflow rate did not affect the bubble size distribution of foams generated by rhamnolipids [58].

In terms of the liquid content, foams generated by ac-LSL are wet at both pH, while foams generated by DDM are dry (Table 3). As shown in Fig. 5b, ac-LSL at pH 10.1 generates bubbled water rather than an actual foam, consistent with the poor foam properties of this surfactant. Similarly, the foam produced by ac-ASL at pH 9.9 has a higher liquid content than at pH 5.3 (Fig. 5b). More foam images are reported in Figs. S3 and S4.

3.3 Mineral-Surfactant Interaction

In this section, we study the interaction of ac-ASL, ac-LSL, DDM, and NaOl with ultrafine hematite and malachite particles using their effect on the ζ-potential, solubility, and single-mineral flotation properties of the metal oxides and quartz. This study was performed at a

surfactant concentration of 50 M at which the single-mineral flotation of hematite and malachite with NaOl has a maximum [17, 22, 59, 60].

3.3.1 ζ-Potential

Z-potential is used to determine how the four surfactants affect the surface charge of ultrafine hematite, malachite, and quartz. It is expected that their adsorption will cause a change in surface charge. In addition, ionic surfactants will shift IEP of the minerals. Surface charge controls important physical-chemistry phenomena underpinning flotation, such as the surfactant adsorption on the mineral surface, the heterocoagulation of different types of mineral particles in the pulp, the dispersion-coagulation of ultrafine mineral particles, and the attachment of particles to bubbles [61]. Hence, ζ-potential can help interpret flotation results.

Figure 6a shows the ζ-potential of ultrafine hematite particles in the absence and presence of 50-μM surfactants. In water, IEP of the particles is pH ca. 6, which is below the IEP range of 6.7–9.2 reported for pure hematite [19, 62]. The lower IEP value can be explained by the quartz impurities
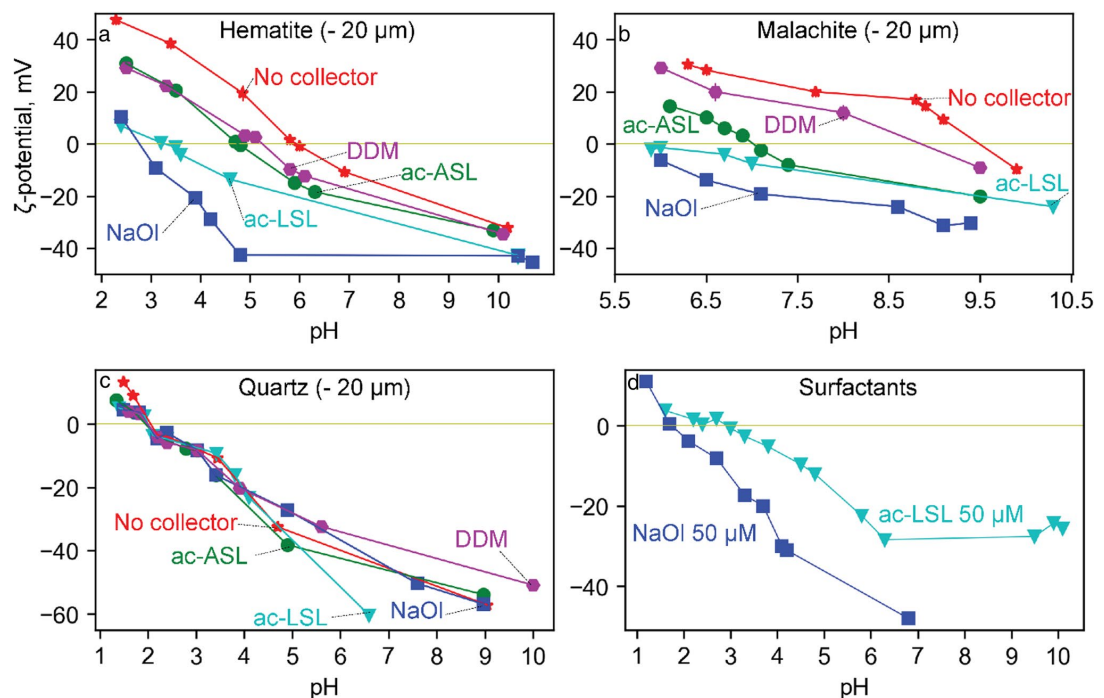
Fig. 6 ζ-potential of ultrafine (− 20 μm) **a** hematite, **b** malachite, and **c** quartz particles in the absence and presence of 50 μM (▼) ac-LSL, (■) ac-ASL, (●) DDM, and (■) NaOl in 0.001 M NaNO₃;

d ζ-potential of surfactant solutions (▼) ac-LSL and (■) NaOl at a concentration of 50 μM. The vertical error bars do not exceed 4 mV and 6 mV for the minerals and the surfactants, respectively

in the hematite used in our study (Fig. 2) [62]. All the surfactants shift IEP of hematite to more acidic pH, which indicates that they adsorb on the positively charged hematite surface. The most pronounced impact is made by NaOl. It renders the hematite surface most negatively charged, shifting IEP to the lowest pH value of 2.7 (Fig. 6a). This IEP is typical of hematite in oleate solutions [63]. Surprisingly, next in the ranking is non-ionic ac-LSL. IEP of hematite in its presence is pH 3.4, while ζ-potential is less negative than in the presence of NaOl (Fig. 6a). Despite their different electrostatic properties, anionic ac-ASL and non-ionic DDM have similarly weak impact on ζ-potential. They shift IEP of hematite to pH ca. 5, while the DDM-adsorbed hematite is somewhat less negatively charged than the ac-ASL counterpart. The effect of all the surfactants on ζ-potential diminishes at pH above 10, which suggests that their surface densities become low when the hematite surface is highly negatively charged.

ζ-potential of malachite was measured at pH above 6 because this mineral becomes increasingly soluble at lower pH [64, 65]. Figure 6b shows that IEP of malachite in water is around 9.5, which is at the upper limit of the reported range of 8.5–9.5 [59, 64, 66, 67]. A shift of IEP to higher pH can be explained by the dissolution of malachite followed by re-adsorption of Cu(II) cations or insufficient equilibration with atmospheric CO_2 [66, 68]. As in the case of hematite, NaOl renders the malachite surface most negatively charged, causing an IEP shift from pH 9.5 to ca. 6.0 (Fig. 6b), which qualitatively agrees with a previous report [59]. Even though ac-LSL causes a similar IEP shift as NaOl, the ζ-potential of malachite at pH above 6.0 is less negative (Fig. 6a). Ac-ASL reduces the positive surface charge of malachite at acidic pH less strongly compared to ac-LSL while the ζ-potential curves of malachite in the solutions of ac-ASL and ac-LSL converge at pH above 7.3. The weakest deviation of the ζ-potential of malachite is caused by DDM. It shifts IEP from 9.5 in water to pH 8.8. Thus, the impact of the four surfactants on the surface charge and IEP of hematite and malachite decreases in the order of NaOl > ac-LSL > /≈ ac-ASL > DDM. We interpret this order below.

The ζ-potential of mineral particles in oleate solutions at pH below 5 is commonly explained following Laskowski et al. by the heterocoagulation of the particles with colloids (droplets) of non-dissolved oleic acid [69]. Only $10^{-7.8}$ M of oleic acid dissolves at pH below 5 (pK_a of oleic acid) reaching 50 M only at pH 9 [69]. At 50 M, IEP of oleic acid colloids is around pH 2.0 (Fig. 6d), which is in good agreement with the reported value of pH 2.5 [69]. Hence, adhered colloids of non-dissolved oleic acid dominate the surface charge of hematite and malachite at pH below 9. The negative surface charge at pH above 9 is consistent with the physisorption-chemisorption model of the fatty acid adsorption on iron (hydr)oxides [18, 19]. The relatively

weak binding strength of a chemisorbed fatty acid results in the steep decline of the absorption densities at pH above IEP [17–19], which explains the convergence of the ζ-potential curves of hematite in the absence and presence of oleate (Fig. 6a).

The adsorption of fatty acids on malachite is currently poorly understood. The effect of NaOl on the ζ-potential of malachite has been explained by chemisorption [59]. The rationale is that malachite is sparingly soluble, while chemisorption is among the mechanisms of the oleate adsorption on salt-type (sparingly soluble) minerals. However, chemisorption does not exclude additional contributions of physisorption and precipitation of the cation-oleate complexes, which also have been proposed for the adsorption of fatty acids on salt-type minerals [70, 71].

The adsorption of non-ionic surfactants is typically interpreted in terms of physisorption [72]. The neutral surfactant layer screens surface charge and shifts the shear plane farther from the Stern plane, which reduces the absolute values of ζ-potential of carbon without significantly affecting IEP of the adsorbent [73]. However, this picture is observed neither for ac-LSL nor DDM. Given the low solubility of ac-LSL, an alternative mechanism can be surface precipitation of the surfactant colloids as in the case of NaOl. To verify this hypothesis, we measured the ζ-potential of colloids in the colloidal solution of 50 M ac-LSL. As shown in Fig. 6d, IEP of these colloids is in the pH 2.5–3.5 range. Hence, these colloids can be deposited at higher pH on the positively charged hematite particles. On this basis, we conclude that the effect of ac-LSL on the ζ-potential of the minerals at acidic pH is dominated by adhered ac-LSL colloids.

In contrast to NaOl and ac-LSL, both ac-ASL and DDM are well soluble in water. Given that DDM is physisorbed on hematite at acidic pH [28, 29], the IEP shift of hematite to pH 5 by adsorbed DDM implies that its maltose group is strongly polarized upon adsorption. At the same time, a similar effect of ac-ASL on the ζ-potential of hematite is likely caused by chemisorption and/or precipitation of ac-ASL complexes as ac-ASL can form complexes with Fe(III) ions (Section 3.3.2). Chemisorption and precipitation are also possible for the adsorption of ac-ASL and DDM on malachite at acidic pH (Section 3.3.2).

Finally, IEP of ultrafine quartz in water is pH 2–3 (Fig. 6c), which is in good agreement with reported values of pH 1.5–4 [74]. The impact of the four surfactants on ζ-potential of quartz is insignificant. Hence, in contrast to hematite and malachite, within the detection limit of ζ-potential, quartz does not adsorb these surfactants. This result agrees with the general notion that negatively charged silicates have a negligible affinity to carboxylate and sugar groups [28, 75].

The ζ-potential dependences show the pH ranges where the metal oxides and quartz have surface charges with the

same sign, which would hamper their heterocoagulation (Fig. 6a–c). This feature offers an opportunity to selectively float the metal oxides from quartz, which we confirm in Section 3.4.

### 3.3.2 Leaching of Ultrafine Hematite and Malachite by Biosurfactants

We studied the effect of ac-ASL, ac-LSL, DDM, and NaOl on the dissolution of ultrafine hematite and malachite to delineate possible contributions of chemisorption and surface precipitation to the surfactant adsorption. Surfactants can enhance dissolution of a mineral by acting as ligands in the ligand-controlled/promoted dissolution mechanism. It starts with the chemisorption of a ligand followed by the detachment of the ligand–metal complexes from the surface [76]. In addition, surfactant-metal complexes can be formed at the mineral-solution interface followed their adsorption or precipitation on the mineral surface. Surface precipitation of surfactant-metal complexes has been observed during the interaction of octyl hydroxamate with hematite, ASL with djurleite, and NaOl with salt-type (sparingly soluble) minerals such as apatite, scheelite, calcite, and fluorite [32, 70, 71, 77]. Hence, if the adsorption of a surfactant is accompanied by an increase in the solubility of the mineral, this surfactant can potentially be chemisorbed and/or its metal complexes can precipitate on the mineral surface.

To study the effect of the surfactants on the solubility of hematite and malachite, we measured the Fe and Cu concentrations in the supernatant after conditioning 0.5 g ultrafine mineral particles in 50 mL of 50 M surfactant solutions at pH 5.2 and pH 9.7 for 3 h. As the baseline, we used the mineral particles stirred in water under the same conditions. The results are reported in Table 4.

Hematite Anhydrous hematite is practically insoluble under oxic conditions in the pH range from 4 to 14 [77, 78]. Accordingly, ultrafine hematite releases in water at

Table 4 Fe and Cu concentration after conditioning of ultrafine hematite and malachite in the absence and presence of 50 μM ac-LSL, ac-ASL, DDM, and NaOl at pH 5.2 and 9.7 for 3 h. The mineral weight and the solution volume are 0.5 g and 50 mL, respectively. The error does not exceed 10%

Solution	Hematite Fe, μg/L		Malachite Cu, μg/L	
	pH 5.2 ± 0.2	pH 9.7 ± 0.2	pH 5.2 ± 0.2	pH 9.7 ± 0.2
H₂O	11	20	800	6.4
Ac-LSL	11	57	1740	15.3
Ac-ASL	17	86	1070	8.6
NaOl	15	26	860	10.2
DDM	10	57	900	5.3

pH 5.2 only 11 g/L Fe (Table 4). The Fe concentration is not affected by non-ionic DDM and ac-LSL. In contrast, anionic ac-ASL and NaOl increase it to 17 g/L and 15 g/L, respectively. The inertness of DDM can be explained by its physisorption on hematite at acidic pH [28–30]. However, the converse is not necessarily true for ac-LSL. The mechanism of its adsorption calls for a separate study. The leaching activity of ac-ASL and NaOl can be attributed to the capacity of their carboxylate groups to form inner-sphere complexes with iron (hydr)oxides [18, 19, 39].

The natural solubility of hematite is almost doubled at pH 9.7 vs. pH 5.2, as follows from the Fe concentration in water of 20 g/L (Table 4). At highly alkaline pH, the FeOOH-like surface layer created by hydration is dissolved by hydroxyl ions [78, 79]:

$$FeOOH + OH^- + H_2O = Fe(OH)_{4-}$$
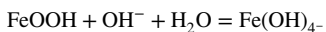
NaOl does not have impact on the Fe concentration due to the low absorption density of oleate on hematite at this pH (Section 3.3.1). In contrast, all three sugar-based surfactants increase the Fe concentration in the order of DDM = ac-LSL < ac-ASL, the Fe concentration in the ac-ASL solution reaching 86 g/L (Table 4). Hence, these surfactants can be chemisorbed and/or precipitated at pH 9.7. This conclusion is in line with the findings that (i) sugars form strong chemical bonds with hydroxylated multivalent metals at basic pH [80, 81], (ii) DDM is chemisorbed on hematite at pH 12 [30], and (iii) starch is chemisorbed on hematite [24, 27]. The stronger leaching properties of ac-ASL compared to as-LSL at pH 9.7 are likely to be caused by two effects. Ac-ASL can form stronger complexes with Fe ions by coordinating both its headgroups as postulated earlier for the ASL complexes with Cu [32]. In addition, due to the carboxylate group, ac-ASL-Fe complexes can be more soluble compared to ac-LSL-Fe complexes.

Malachite Ultrafine malachite is sparingly soluble in water at pH 5.2, releasing 800 g/L Cu (Table 4). The corresponding dissolution reaction reads as [65]

$$^1/_2\,Cu_2(OH)_2CO_3 + 2H^+ \leftrightarrow Cu^{2+} + \,^1/_2\,CO_2 + \,^3/_2\,H_2O$$
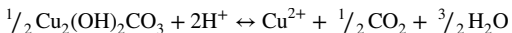
The natural solubility of malachite is explained by the ionic character of its Cu–O bonds, which is also behind the high hydrophilicity of this mineral [21]. The Cu concentration is increased by NaOl, DDM, ac-ASL, and ac-LSL to 860, 900, 1070, and 1740 mg/L, respectively. In contrast, malachite is practically insoluble in water at pH 9.7 (the Cu concentration is only 6.4 g/L). This result agrees with the stability diagram [65] and experimental data [64]. It is explained by increasing natural concentration of (bi) carbonate with increasing pH of air-saturated solutions. The solubility of malachite at pH 9.7 is slightly inhibited

by DDM, the Cu concentration being dropped to 5.3 g/L. The other three surfactants increase it in the order of ac-ASL < NaOl < ac-LSL, the Cu concentration with ac-LSL being 15 g/L.

Thus, the strongest lixiviant of hematite and malachite is ac-ASL and ac-LSL, respectively. The leaching by the sugar-based surfactants at pH 9.7 is consistent with their chemisorption. However, the strongest leaching activity of ac-LSL toward malachite at pH 5.2 is a curious phenomenon given that this non-ionic surfactant is less soluble than ac-ASL and lacks the additional complexing carboxylate group. This result suggests that ac-LSL chemically reacts with malachite also at pH 5.2.

3.3.3 Single-Mineral Flotation of Ultrafine Mineral Particles

Single-mineral flotation (floatability) was used to characterize the hydrophobicity of ultrafine minerals. Mineral particles that adhere to bubbles in flotation (float) are commonly referred to as hydrophobic (water-repelling). Other conventional methods to characterize hydrophobicity include contact angle, water permeation, and partitioning of mineral particles to a non-polar solvent. The advantage of floatability is that it characterizes hydrophobicity in situ under dynamic flotation conditions without affecting the critical properties that affect the amenability of mineral particles to flotation such as the particle size and the aqueous environment [42]. At the same time, it should be kept in mind that the floatability of ultrafine particles can be affected by entrainment [13].

The flotation tests were conducted on ultrafine hematite, malachite, and quartz in 50 μM solutions of ac-ASL, ac-LSL, DDM, and NaOl. The in the pH range for hematite

and quartz was from 2 to 10. The low pH limit for malachite was 6 due to the increased solubility of this mineral at more acidic pH.

Hematite Figure 7a shows that a maximum recovery of 70% can be achieved for hematite with all four surfactants, though at different pH. Specifically, the oleate flotation has a maximum at pH 6, being depressed at pH 2 and 10. This pH dependence is typical of the single-mineral flotation of hematite at low concentrations oleate [16, 17]. It can be explained by the interplay of the chemisorption and physisorption of the fatty acid and acid–base properties of hematite, which impart maximum hydrophobicity to hematite at pH close to its IEP [18, 19]. Non-ionic ac-LSL and DDM achieve the 70% flotation maximum at pH 4–6 and 6–8, respectively. In contrast, the ac-ASL flotation monotonically increases with pH, reaching 70% at pH 10. This increase can be explained by the transition of ac-ASL from the hydrophilic open configuration with the sophorose group dangling in the solution to the hydrophobic closed configuration in which both the headgroups are coordinated to the metal cation (Section 3.3.2). It should be noted that the surface coverages of the surfactants at pH 10 are low as follows from the converging of the ζ-potential curves in the surfactant solutions and water (Fig. 6a). However, these small surface coverages are sufficient for DDM and ac-ASL to float hematite (Fig. 7a).

Malachite The floatability of malachite with NaOl, ac-ASL, and ac-LSL in the pH range from 6 to 10 is higher by 20–30% and much less responsive to pH compared to that of hematite in the same pH range (Fig. 7b). The highest recovery of 98% is achieved by ac-LSL at pH 8. The floatability with NaOl and ac-ASL monotonically increases to 90% at

Fig. 7 Effect of pH on single-mineral flotation of − 20 μm fraction of **a** hematite and **b** malachite with 50 μM of (▼) ac-LSL, (■) ac-ASL, (⬤) DDM, and (⬤) NaOl. The line "no collector" corresponds to flotation using 50 μM DawFroth 200 (a frothing agent)
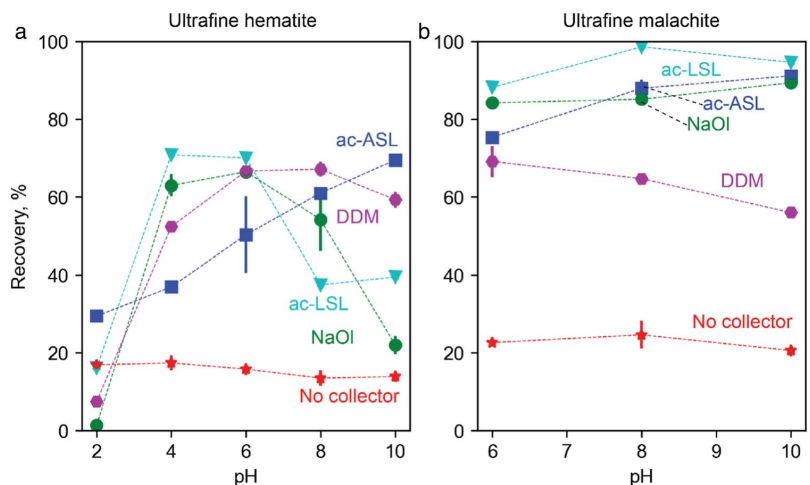
pH 10 from 85 and 75% at pH 6, respectively. A similarly weak pH dependence was reported earlier for the malachite flotation with 50 μM NaOl [60]. The higher hydrophobicity in a wider pH range generally suggests that the mineral interacts with a surfactant more strongly, which results in its higher adsorption density and better packing. We should note this effect is observed even though malachite has the threefold higher BET surface area than hematite (Table 1). In contrast, there is no difference in the floatability of malachite and hematite with DDM.

The trends in the flotation of hematite and malachite do not correlate with the activity of the surfactants at the air–water interface. For example, ac-ASL and ac-LSL float at pH 10 70% and 40% of hematite, respectively (Fig. 7a), while their surface tension at 50 μM and pH 10 is similar (Fig. 4). The collecting power of ac-LSL at pH 6 increases to 70%, while there is no difference in surface tension at pH 6 and 10.

At the same time, there is a correlation between the floatability/hydrophobicity and solubility of the minerals in some systems. In particular, the floatability of hematite at pH 10 increases in the order of NaOl < ac-LSL < DDM < ac-ASL (Fig. 7a), which is similar to NaOl < ac-LSL = DDM < ac-ASL observed for the solubility of hematite at pH 9.7 (Table 4). Also, ac-LSL is both the strongest collector and the strongest lixiviant of malachite at pH 6 and 10, while DDM is both the weakest collector and the weakest lixiviant at pH 10. Hence, the main hydrophobization mechanism these systems is likely to be the chemisorption of the surfactants and/or precipitation of their complexes with metals. The absence of such a correlation at acidic pH indicates the critical role of physisorption. In addition, the flotation at acidic pH can be influenced by entrainment since the foaming properties of the sugar-based surfactants are significantly better at pH 5.2–5.4 than at pH 10–11 (Fig. 5).

Quartz As shown in Fig. 8, all the surfactants do not float ultrafine quartz at pH 5 and 10, which can be explained by their negligible adsorption (Section 3.3.1).

3.4 The Effect of Particle Size on the Flotation of Metal Oxides in Two-Mineral Systems with Quartz

In this section, we study the collecting properties of ac-LSL, ac-ASL, DDM, and NaOl in the flotation of ultrafine ($-20\,\mu m$) and coarse ($+38-90\,\mu m$) hematite and malachite in their binary mixtures with ultrafine ($-20\,\mu m$) quartz. The tests were conducted at pH 5 (hematite) and pH 6 (malachite), as well as pH 10 (both) at a surfactant concentration of 50 μM. This concentration is chosen as in the above studies to keep the same surfactant-metal oxide ratio given that
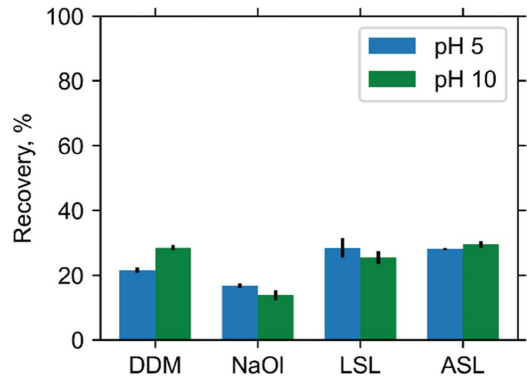
Fig. 8 Recovery of ultrafine ($-20\,\mu m$) quartz particles by 50 μM ac-LSL, ac-ASL, DDM, and NaOl at pH 5 (blue bar) and pH 10 (green bar). The uncertainty of pH is within 0.2 units

the surfactant adsorption on quartz is negligible within the detection level of ζ-potential (Fig. 6c).

3.4.1 Hematite

As seen in Fig. 9, the best collector of ultrafine hematite from quartz at pH 5 and 10 is NaOl. At pH 5, it recovers 91% of hematite at a grade of 87%. NaOl is followed by ac-LSL with a 98% recovery and a 68% grade, and then by ac-ASL with a 93% recovery and a 61% grade (Fig. 9a). The weakest collector at both pH is DDM. It recovers 63% of hematite at a grade of 56%. The decrease in the grade correlates well with ζ-potential of hematite at pH 5, which becomes less negative in the same order of NaOl > ac-LSL > ac-ASL > DDM (Fig. 6a). This correlation suggests that the main reason for the grade loss is the heterocoagulation of hematite with quartz.

The recovery of ultrafine hematite with all four surfactants decreases at pH 10 as compared to pH 5 while there is no significant change in the grade (Fig. 9b and Fig. S5). The same trend is observed in the single-mineral flotation with NaOl, ac-LSL, and DDM (Fig. 7a). However, there is a discrepancy between the trends in the single- and mixed mineral flotation with ac-ASL.

The ranking of the collectors is slightly different for coarse hematite (Fig. 9). Here, the best at both pH is ac-LSL. It recovers 98% of hematite at a grade of 65–68%. The next is NaOl with a 90% recovery at similar grades. DDM is the worst at both pH. At pH 5, it recovers only 24% of coarse hematite at a grade as low as 24%. Such a poor performance of DDM suggests a low surface density of the physisorbed surfactant on coarse hematite. However, the performance of DDM is improved at pH 10, where it recovers 55% of coarse hematite at a grade of 42%.

Taking into accounts the leaching results (Section 3.3.2),
this improvement can be explained by the activation of the
chemical interaction between the maltose headgroup and
the hematite at basic pH.

The comparison of the results for ultrafine and coarse
hematite shows that ac-LSL flotation is tolerant to the
particle size at pH 5 (Fig. 9a). In the case of ac-ASL,
the ultrafine particle size drops the grade by 10% while
increasing the recovery by 25%. In contrast, the ultrafine
particle size significantly improves the collecting proper-
ties of NaOl and DDM. At the same recovery of 90%,
the hematite grade in the oleate flotation at pH 5 is by
22% higher for ultrafine compared to coarse particles.
DDM practically does not float coarse hematite at pH 5
but recovers ultrafine hematite at a recovery of 62% and
a grade of 56%. In the NaOl and DDM flotation at pH
10, the ultrafine particle size improves the grade by 16%
though the recovery is compromised, especially in the
NaOl flotation.

The promoting effect of the ultrafine particle size on
the oleate flotation of hematite can be explained by the
relatively weak (monodentate) coordination of fatty acids
to the crystallographically smooth surfaces of iron (hydr)
oxides [18, 19]. A decrease in the particle size would
increase the adsorption density of fatty acids due to the
associated increase in the concentration of surface defects
(surface energy). A higher adsorption density of an anionic
surfactant would make the hematite particles more nega-
tively charged, thereby enhancing their repulsion from the
negatively charged quartz particles and hence improving
the grade. Surface defects are also expected to improve
the physisorption of DDM on hematite at acidic pH as it
is increased with the surface concentration of OH groups
[28–30]. As a result, the positive charge of the hematite
particles would be screened better.

3.4.2 Malachite

The ranking of the collectors for ultrafine malachite is the
same as for ultrafine hematite (Fig. 10 and Fig. S6). At pH
6, NaOl recovers 75% of malachite at a grade of 80%. Even
though ac-LSL achieves a better recovery of 86% than NaOl,
the corresponding grade is 71%. DDM floats malachite at the
same grade of 61% as ac-ASL but at a lower recovery of 56%
vs. 72%. The principal difference with ultrafine hematite is
that pH 10 improves the recovery of ultrafine malachite vs.
that at pH 6 with all the four surfactants, while the grades
in the NaOl and ac-LSL flotation decrease by 7–10%. This
difference is likely to originate from the difference in the
adsorption mechanisms of these surfactants on hematite and
malachite. These mechanisms remain largely unknown for
all the surfactants on malachite, as well as for ac-LSL on
hematite.

There is a good correlation between the grade and the
impact of the surfactants on the ζ-potential of malachite:
The grade at pH 6 decreases in the same order of NaOl > ac-
LSL > ac-ASL > DDM as the difference between IEP of
malachite in water and in the surfactant solutions (Fig. 6b).
Hence, as in the case of hematite, the main reason for the
loss of selectivity is the heterocoagulation with quartz,
while the contribution of the quartz activation by adsorbed
metal–surfactant complexes is insignificant. In addition,
the recovery of ultrafine malachite in the two-mineral flota-
tion decreases in the same order of ac-LSL > NaOl ≈ ac-
ASL > DDM (Fig. 10 and Fig. S6) as in the single-mineral
flotation (Fig. 7b). This fact suggests that and the non-selec-
tive entrainment of the ultrafine particles to the two-mineral
flotation is insignificant too.

The coarse particle size improves the recovery of mala-
chite in the oleate flotation at pH 6 and 10 by 15–30%
but does not affect the grade (Fig. 10 and Fig. S6). This

Fig. 10 Recovery and grade in the flotation of a 1:1 (wt) mixture of malachite and ultrafine quartz with 50 μM (▼▽) ac-ASL, (▲△) ac-LSL, (●○) DDM, and(■□) at (a) pH 6±0.3 and (b) pH 10±0.3. The filled and empty symbols correspond to ultrafine and coarse malachite particles, respectively. The error of the grade and recovery data points without the error bars is less than 5%. A different representation of the dependencies is shown in Fig. S6
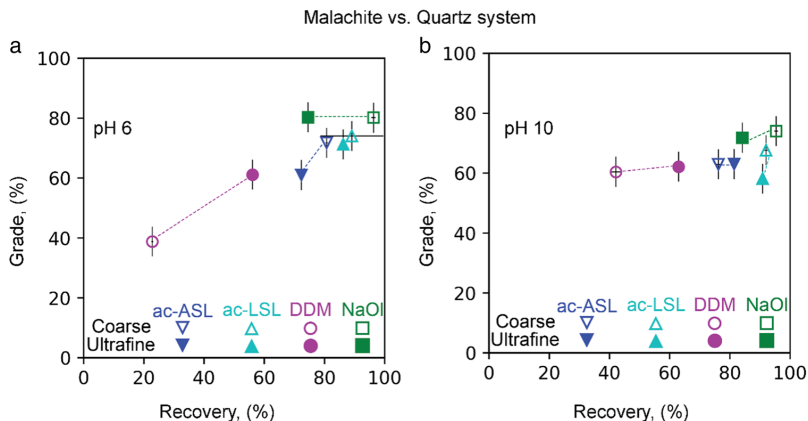
result is different from that observed for hematite, where the coarse size decreases the grade while hardly affecting the recovery (Fig. 9b and Fig. S5). This difference suggests that an increase in the surface density of oleate on the more defective ultrafine malachite particles is not critical for preventing their heterocoagulation with quarts.

As in the case of hematite, ac-LSL and ac-ASL demonstrate good tolerance to the particle size. The difference in the grade and recovery for the two particle sizes is less than a 10% in the ac-LSL flotation at pH 6 and 10, as well as in the ac-ASL flotation at pH 10. Also, the DDM flotation of coarse malachite is inferior to ultrafine malachite, which suggests the promoting role of surface defects (see above).

Finally, it is instructive to compare the performance of the biosurfactants and hydroxamates in the flotation of ultrafine malachite. Hydroxamates are chelating O-donors widely used in oxide flotation as more selective alternatives to fatty acids [41, 66]. Among different hydroxamates tested, benzohydroxamate has demonstrated the best figures of merit (a 95% recovery at a 95% grade) in the flotation of coarse malachite ($-150+38$ μm) against quartz at pH 8 [66]. However, the fine (-38 μm) particle size drops the recovery and the grade to 75% and 35–40%, respectively. To compare, ac-LSL floats the ($+38-90$ μm) fraction of malachite at pH 6 at a 90% recovery and a 75% grade, which remain the same for the ultrafine (-20 μm) fraction (Fig. 10 and Fig. S6). The recovery and grade in the ac-ASL flotation of ultrafine malachite at pH 10 are 82% and 62%, respectively, practically the same as for coarse particles. Hence, hydroxamates lack the tolerance to fines inherent to ac-LSL and ac-ASL. A mechanistic insight into this interesting result could help design collectors for ultrafine particles.

4 Conclusions

This study aimed at extending the knowledge base on biosurfactants as eco-friendly collectors.

Without a frother in synthetic mineral systems, NaOl, ac-LSL, ac-ASL provide similarly high grades in the flotation of coarse hematite against quartz. For coarse malachite, NaOl achieves somewhat higher grades compared to ac-LSL and ac-ASL. DDM is the worst collector of both the metal oxides under the conditions studied.

The ultrafine particle size significantly improves the grade of hematite in the two-mineral flotation against quartz with NaOl and DDM at pH 5 and 10, as well as in the two-mineral flotation of malachite against quartz with DDM at pH 5. In contrast, the ultrafine particle size practically does not affect the high grade of malachite in oleate flotation, as well as the high grades of both the oxides in ac-LSL and ac-ASL flotation. The beneficial effect of the ultrafine particle size on the NaOl and DDM flotation can be explained by the promoting role of surface defects on the adsorption of NaOl and DDM.

There is no direct correlation between the flotation results, the activity of the surfactants at the air–water interface, and their foaming properties. At the same time, the grades of hematite and malachite in the two-mineral flotation against quartz can be explained by the heterocoagulation of the minerals with quartz. The surfactants hydrophobize the minerals at pH 10 through chemisorption and/or precipitation as complexes with metal ions, while there is contribution of physisorption at acidic pH. Malachite adsorbs NaOl, ac-LSL, and ac-ASL more strongly than hematite, while the affinity of these two oxides to DDM is similar. In contrast, quartz does not adsorb all the four surfactants.

Given the low selectivity of fatty acids, the good collecting properties of ac-LSL and ac-ASL along with their tolerance to the ultrafine particle size make these biosurfactants attractive for further studies on natural metal oxide ores in comparison with conventional surfactants. The results of this study can also be used as a benchmark for the development of green collectors for ultrafine mineral particles.

Supplementary Information The online version contains supplementary material available at https://doi.org/10.1007/s42461-023-00743-z.

Data Availability The essential data is available in the main text and in the supplementary file. The additional data is available from the first or corresponding author by reasonable request.

Declarations

Conflict of Interest The authors declare no competing interests.

References

1. Fuerstenau DW (2019) Pradip. A century of research leading to understanding the scientific basis of selective mineral flotation and design of flotation collectors. Min Metall Explor 36(1):3–20. https://doi.org/10.1007/s42461-018-0042-6

2. Nagaraj DR, Farinato RS (2016) Evolution of flotation chemistry and chemicals: a century of innovations and the lingering challenges. Miner Eng 96–97:2–14. https://doi.org/10.1016/j.mineng.2016.06.019

3. Ramachandra Rao S, Leja J (2004) Surface chemistry of froth flotation. Vol. 2 Reagents and mechanisms. 2nd ed. New York: Kluwer

4. Nagaraj DR, Farinato RS, Arinaitwe E (2019) Flotation chemicals and chemistry. In: Dunne RC, Kawatra KS, Young CA (eds) SME Mineral processing and extractive metallurgy handbook. Society for Mining, Metallurgy & Exploration, Englewood, Colorado, pp 967–1010

5. Webb M, Ruber H, Leduc G (1976) The toxicity of various mining flotation reagents to rainbow trout (Salmo gairdneri). Water Res 10(4):303–306. https://doi.org/10.1016/0043-1354(76)90171-8

6. Rocchi L (2018) Xanthates in mining (update). https://www.rshq.qld.gov.au/safety-notices/mines/xanthates-in-mining-update. Accessed

7. Greim H, Bury D, Klimisch HJ, Oeben-Negele M, Ziegler-Skylakakis K (1998) Toxicity of aliphatic amines: Structure-activity relationship. Chemosphere 36(2):271–295. https://doi.org/10.1016/S0045-6535(97)00365-2

8. Jain G, Havskjold H, Dhar P, Ertesvåg H, Chernyshova I, Kota HR (2020) Green Foam-based methods of mineral and ion separation. In: Chernyshova I, Ponnurangam S, Liu Q (eds) Multidisciplinary Advances in Efficient Separation Processes. American Chemical Society, pp 265–301

9. Oulkhir A, Lyamlouli K, Danouche M, Ouazzani J, Benhida R (2022) A critical review on natural surfactants and their potential for sustainable mineral flotation. Rev Environ Sci Bio Technol. https://doi.org/10.1007/s11157-022-09639-8

10. Hartmann R, Beaumont M, Pasquie E, Rosenau T, Serna-Guerrero R (2022) N-Alkylated chitin nanocrystals as a collector in malachite flotation. ACS Sustain Chem Eng 10(32):10570–10578. https://doi.org/10.1021/acssuschemeng.2c01978

11. Asgari K, Huang Q, Khoshdast H, Hassanzadeh A (2022) A review on bioflotation of coal and minerals: classification, mechanisms, challenges, and future perspectives. Mineral Process Ext Metall Rev 1–31. https://doi.org/10.1080/08827508.2022.2121919

12. Höfer R, Bigorra J (2007) Green chemistry—a sustainable solution for industrial specialties applications. Green Chem 9(3):203–212. https://doi.org/10.1039/b606377b

13. Dhar P, Thornhill M, Roelants S, Soetaert W, Chernyshova IV, Rao Kota H (2021) Linking molecular structures of yeast-derived biosurfactants with their foaming, interfacial, and flotation properties. Miner Eng 174:107270. https://doi.org/10.1016/j.mineng.2021.107270

14. Shen Y, Lo C, Nagaraj DR, Farinato R, Essenfeld A, Somasundaran P (2016) Development of Greenness Index as an evaluation tool to assess reagents: Evaluation based on SDS (Safety Data Sheet) information. Miner Eng 94:1–9. https://doi.org/10.1016/j.mineng.2016.04.015

15. Zhang X, Gu X, Han Y, Parra-Álvarez N, Claremboux V, Kawatra SK (2021) Flotation of Iron Ores: A Review. Miner Process Extr Metall Rev 42(3):184–212. https://doi.org/10.1080/08827508.2019.1689494

16. Nakhaei F, Irannajad M (2018) Reagents types in flotation of iron oxide minerals: a review. Miner Process Extr Metall Rev 39(2):89–124. https://doi.org/10.1080/08827508.2017.1391245

17. Kulkarni RD, Somasundaran P (1980) Flotation chemistry of hematite/oleate system. Colloids Surf 1(3):387–405. https://doi.org/10.1016/0166-6622(80)80025-4

18. Chernyshova IV, Ponnurangam S, Somasundaran P (2011) Adsorption of Fatty acids on iron (hydr)oxides from aqueous solutions. Langmuir 27(16):10007–10018. https://doi.org/10.1021/la2017374

19. Ponnurangam S, Chernyshova IV, Somasundaran P (2012) Rational design of interfacial properties of ferric (hydr)oxide nanoparticles by adsorption of fatty acids from aqueous solutions. Langmuir 28(29):10661–10671. https://doi.org/10.1021/la300995g

20. Bulatovic SM (2010) 19 - Flotation of Oxide Copper and Copper Cobalt Ores. In: Bulatovic SM (ed) Handbook of flotation reagents: chemistry, theory and practice. Elsevier, Amsterdam, pp 47–65

21. Feng Q, Yang W, Wen S, Wang H, Zhao W, Han G (2022) Flotation of copper oxide minerals: a review. Int J Min Sci Technol. https://doi.org/10.1016/j.ijmst.2022.09.011

22. Li Z, Rao F, Escudero García R, Li H, Song S (2018) Partial replacement of sodium oleate using alcohols with different chain structures in malachite flotation. Miner Eng 127:185–190. https://doi.org/10.1016/j.mineng.2018.08.022

23. Araujo AC, Viana PRM, Peres AEC (2005) Reagents in iron ores flotation. Miner Eng 18(2):219–224. https://doi.org/10.1016/j.mineng.2004.08.023

24. Moreira GF, Peçanha ER, Monte MBM, Leal Filho LS, Stavale F (2017) XPS study on the mechanism of starch-hematite surface chemical complexation. Miner Eng 110:96–103. https://doi.org/10.1016/j.mineng.2017.04.014

25. RohemPeçanha E, da Fonseca de Albuquerque MD, AntounSimão R, de Salles Leal Filho L, de Mello Monte MB (2019) Interaction forces between colloidal starch and quartz and hematite particles in mineral flotation. Colloids Surf A Physicochem Eng Asp 562:79–85. https://doi.org/10.1016/j.colsurfa.2018.11.026

26. Li L, Zhang C, Yuan Z, Xu X, Song Z (2019) AFM and DFT study of depression of hematite in oleate-starch-hematite flotation system. Appl Surf Sci 480:749–758. https://doi.org/10.1016/j.apsusc.2019.02.224

27. Félix LL, Moreira GF, Filho LSL, Stavale F (2022) Starch adsorption on hematite surfaces: Evidence of the adsorption mechanism dependence on the surface orientation. Miner Eng 178. https://doi.org/10.1016/j.mineng.2022.107429

28. Zhang L, Somasundaran P, Maltesh C (1997) Adsorption ofn-Dodecyl-β-d-maltoside on Solids. J Colloid Interface Sci 191(1):202–208. https://doi.org/10.1006/jcis.1997.4923

29. Zhang L, Somasundaran P, Mielczarski J, Mielczarski E (2002) Adsorption Mechanism of n-dodecyl-β-D-maltoside on Alumina. J Colloid Interface Sci 256(1):16–22. https://doi.org/10.1006/jcis.2001.7858

30. Mielczarski E, Mielczarski JA, Zhang L, Somasundaran P (2004) Structure of adsorbed n-dodecyl-beta-D-maltoside layers on hematite. J Colloid Interface Sci 275(2):403–409. https://doi.org/10.1016/j.jcis.2004.02.083

31. Stubenrauch C, Claesson PM, Rutland M, Manev E, Johansson I, Pedersen JS et al (2010) Mixtures of n-dodecyl-beta-D-maltoside and hexaoxyethylene dodecyl ether - Surface properties, bulk properties, foam films, and foams. Adv Colloid Interface Sci 155(1–2):5–18. https://doi.org/10.1016/j.cis.2009.12.002

32. Dhar P, Havskjold H, Thornhill M, Roelants S, Soetaert W, Kota HR et al (2021) Toward green flotation: Interaction of a sophorolipid biosurfactant with a copper sulfide. J Colloid Interface Sci 585:386–399. https://doi.org/10.1016/j.jcis.2020.11.079

33. Baccile N, Seyrig C, Poirier A, Alonso-de Castro S, Roelants SLKW, Abel S (2021) Self-assembly, interfacial properties, interactions with macromolecules and molecular modelling and simulation of microbial bio-based amphiphiles (biosurfactants). A tutorial review. Green Chemistry 23(11):3842–3944. https://doi.org/10.1039/D1GC00097G

34. Nikolova C, Gutierrez T (2021) Biosurfactants and their applications in the oil and gas industry: current state of knowledge and future perspectives. Front Bioeng Biotechnol 9. https://doi.org/10.3389/fbioe.2021.626639

35. Hu X, Subramanian K, Wang H, Roelants SLKW, To MH, Soetaert W, et al (2021) Guiding environmental sustainability of emerging bioconversion technology for waste-derived sophorolipid production by adopting a dynamic life cycle assessment (dLCA) approach. Environ Pollut 269. https://doi.org/10.1016/j.envpol.2020.116101

36. Hu X, Subramanian K, Wang H, Roelants SLKW, Soetaert W, Kaur G et al (2021) Bioconversion of food waste to produce industrial-scale sophorolipid syrup and crystals: dynamic life

cycle assessment (dLCA) of emerging biotechnologies. Bioresour Technol 337. https://doi.org/10.1016/j.biortech.2021.125474

37. Baccile N, Cuvier A-S, Valotteau C, Van Bogaert INA (2013) Practical methods to reduce impurities for gram-scale amounts of acidic sophorolipid biosurfactants. Eur J Lipid Sci Technol 115(12):1404–1412. https://doi.org/10.1002/ejlt.201300131

38. Castelein M, Verbruggen F, Van Renterghem L, Spooren J, Yurramendi L, Du Laing G et al (2021) Bioleaching of metals from secondary materials using glycolipid biosurfactants. Miner Eng 163. https://doi.org/10.1016/j.mineng.2020.106665

39. Baccile N, Noiville R, Stievano L, Bogaert IV (2013) Sophorolipids-functionalized iron oxide nanoparticles. Phys Chem Chem Phys 15(5):1606–1620. https://doi.org/10.1039/c2cp41977g

40. Peyre J, Hamraoui A, Faustini M, Humblot V, Baccile N (2017) Surface-induced assembly of sophorolipids. Phys Chem Chem Phys 19(23):15227–15238. https://doi.org/10.1039/C7CP01339F

41. Lee JS, Nagaraj DR, Coe JE (1998) Practical aspects of oxide copper recovery with alkyl hydroxamates. Miner Eng 11(10):929–939. https://doi.org/10.1016/S0892-6875(98)00080-6

42. Wills BA, Finch JA (2016) Chapter 12 - Froth Flotation. In: Wills BA, Finch JA (eds) Wills' Mineral Processing Technology, 8th edn. Butterworth-Heinemann, Boston, pp 265–380

43. Abaka-Wood GB, Addai-Mensah J, Skinner W (2021) The use of mining tailings as analog of rare earth elements resources: part 1 – characterization and preliminary separation. Miner Process Extr Metall Rev 1–15. https://doi.org/10.1080/08827508.2021.1920410

44. Ceniceros-Gómez AE, Macías-Macías KY, de la Cruz-Moreno JE, Gutiérrez-Ruiz ME, Martínez-Jardines LG (2018) Characterization of mining tailings in México for the possible recovery of strategic elements. J S Am Earth Sci 88:72–79. https://doi.org/10.1016/j.jsames.2018.08.013

45. Alcalde J, Kelm U, Vergara D (2018) Historical assessment of metal recovery potential from old mine tailings: A study case for porphyry copper tailings. Chile Miner Eng 127:334–338. https://doi.org/10.1016/j.mineng.2018.04.022

46. Tang C, Li K, Ni W, Fan D (2019) Recovering iron from iron ore tailings and preparing concrete composite admixtures. Minerals 9(4). https://doi.org/10.3390/min9040232

47. Farrokhpay S, Filippov L, Fornasiero D (2020) Flotation of fine particles: a review. Miner Process Extr Metall Rev 1–11. https://doi.org/10.1080/08827508.2020.1793140

48. Sivamohan R (1990) The problem of recovering very fine particles in mineral processing — a review. Int J Miner Process 28(3–4):247–288. https://doi.org/10.1016/0301-7516(90)90046-2

49. Melo F, Laskowski JS (2006) Fundamental properties of flotation frothers and their effect on flotation. Miner Eng 19(6):766–773. https://doi.org/10.1016/j.mineng.2005.09.031

50. Hassanzadeh A, Safari M, Hoang DH, Khoshdast H, Albijanic B, Kowalczuk PB (2022) Technological assessments on recent developments in fine and coarse particle flotation systems. Miner Eng 180. https://doi.org/10.1016/j.mineng.2022.107509

51. Van Bogaert INA, Zhang J, Soetaert W (2011) Microbial synthesis of sophorolipids. Process Biochem 46(4):821–833. https://doi.org/10.1016/j.procbio.2011.01.010

52. Li G, Yi X, Jiang J, Zhang Y, Li Y (2020) Dynamic surface properties and dilational rheology of acidic and lactonic sophorolipids at the air-water interface. Colloids Surf B Biointerfaces 195. https://doi.org/10.1016/j.colsurfb.2020.111248

53. Lu S, Bian Y, Zhang L, Somasundaran P (2007) pH dependence of adsorption of n-dodecyl-β-d-maltoside on solids. J Colloid Interface Sci 316(2):310–316. https://doi.org/10.1016/j.jcis.2007.08.063

54. Zhang L, Somasundaran P, Maltesh C (1996) Electrolyte Effects on the Surface Tension and Micellization of n-Dodecyl

β-d-Maltoside Solutions. Langmuir 12(10):2371–2373. https://doi.org/10.1021/la950670w

55. Theander K, Pugh RJ (2001) The influence of ph and temperature on the equilibrium and dynamic surface tension of aqueous solutions of sodium oleate. J Colloid Interface Sci 239(1):209–216. https://doi.org/10.1006/jcis.2000.7543

56. Otto RT, Daniel HJ, Pekin G, Müller-Decker K, Fürstenberger G, Reuss M et al (1999) Production of sophorolipids from whey. Appl Microbiol Biotechnol 52(4):495–501. https://doi.org/10.1007/s002530051551

57. Hirata Y, Ryu M, Oda Y, Igarashi K, Nagatsuka A, Furuta T et al (2009) Novel characteristics of sophorolipids, yeast glycolipid biosurfactants, as biodegradable low-foaming surfactants. J Biosci Bioeng 108(2):142–146. https://doi.org/10.1016/j.jbiosc.2009.03.012

58. Díaz De Rienzo MA, Kamalanathan ID, Martin PJ (2016) Comparative study of the production of rhamnolipid biosurfactants by B. thailandensis E264 and P. aeruginosa ATCC 9027 using foam fractionation. Process Biochem 51(7):820–7. https://doi.org/10.1016/j.procbio.2016.04.007

59. Choi J, Choi SQ, Park K, Han Y, Kim H (2016) Flotation behaviour of malachite in mono- and di-valent salt solutions using sodium oleate as a collector. Int J Miner Process 146:38–45. https://doi.org/10.1016/j.minpro.2015.11.011

60. Li H, Liu M, Liu Q (2018) The effect of non-polar oil on fine hematite flocculation and flotation using sodium oleate or hydroxamic acids as a collector. Miner Eng 119:105–115. https://doi.org/10.1016/j.mineng.2018.01.004

61. Fuerstenau DW (2005) Pradip. Zeta potentials in the flotation of oxide and silicate minerals. Adv Colloid Interface Sci 114–115:9–26. https://doi.org/10.1016/j.cis.2004.08.006

62. Quast K (2006) Flotation of hematite using C6–C18 saturated fatty acids. Miner Eng 19(6–8):582–597. https://doi.org/10.1016/j.mineng.2005.09.010

63. Quast K (2016) The use of zeta potential to investigate the interaction of oleate on hematite. Miner Eng 85:130–137. https://doi.org/10.1016/j.mineng.2015.11.007

64. Li Z, Rao F, Song S, Uribe-Salas A, López-Valdivieso A (2019) Effects of common ions on adsorption and flotation of malachite with salicylaldoxime. Colloids Surf A 577:421–428. https://doi.org/10.1016/j.colsurfa.2019.06.004

65. Preis W, Gamsjäger H (2002) Solid–solute phase equilibria in aqueous solution. XVI. Thermodynamic properties of malachite and azurite—predominance diagrams for the system Cu 2+– H2 O– CO 2. J Chem Thermodyn 34(5):631–50. https://doi.org/10.1006/jcht.2002.0928

66. Marion C, Jordens A, Li R, Rudolph M, Waters KE (2017) An evaluation of hydroxamate collectors for malachite flotation. Sep Purif Technol 183:258–269. https://doi.org/10.1016/j.seppur.2017.02.056

67. Li F, Zhong H, Xu H, Jia H, Liu G (2015) Flotation behavior and adsorption mechanism of α-hydroxyoctyl phosphinic acid to malachite. Miner Eng 71:188–193. https://doi.org/10.1016/j.mineng.2014.11.013

68. Wang H, Wen S, Han G, He Y, Feng Q (2022) Adsorption behavior and mechanism of copper ions in the sulfidization flotation of malachite. Int J Min Sci Technol 32(4):897–906. https://doi.org/10.1016/j.ijmst.2022.06.006

69. Laskowski JS (1993) Electrokinetic measurements in aqueous solutions of weak electrolyte type surfactants. J Colloid Interface Sci 159(2):349–353. https://doi.org/10.1006/jcis.1993.1333

70. Pawlik M (2022) Fundamentals of froth flotation. ChemTexts 8(4):19. https://doi.org/10.1007/s40828-022-00170-5

71. Rao KH, Cases JM, Forssberg KSE (1991) Mechanism of oleate interaction on salt-type minerals: V Adsorption and precipitation reactions in relation to the solid/liquid ratio in the synthetic fluorite—sodium oleate system. J Colloid Interface Sci 145(2):330–48. https://doi.org/10.1016/0021-9797(91)90365-F

72. Chang Z, Chen X, Peng Y (2018) The adsorption behavior of surfactants on mineral surfaces in the presence of electrolytes – a critical review. Miner Eng 121:66–76. https://doi.org/10.1016/j.mineng.2018.03.002

73. Sis H, Birinci M (2009) Effect of nonionic and ionic surfactants on zeta potential and dispersion properties of carbon black powders. Colloids Surf A 341(1):60–67. https://doi.org/10.1016/j.colsurfa.2009.03.039

74. Kosmulski M (2006) pH-dependent surface charging and points of zero charge. J Colloid Interface Sci 298(2):730–741. https://doi.org/10.1016/j.jcis.2006.01.003

75. Feng Q, Wen S, Zhao W, Chen Y (2018) Effect of calcium ions on adsorption of sodium oleate onto cassiterite and quartz surfaces and implications for their flotation separation. Sep Purif Technol 200:300–306. https://doi.org/10.1016/j.seppur.2018.02.048

76. Stumm W, Morgan JJ (1996) Aquatic chemistry, 3rd edn. Wiley, New York

77. Fuerstenau MC, Harper RW, Miller JD (1970) Hydroxamate vs. fatty acid flotation of iron oxide. Transactions SME/AIME 247:69–73

78. Diakonov II, Schott J, Martin F, Harrichourry J-C, Escalier J (1999) Iron(III) solubility and speciation in aqueous solutions. experimental study and modelling: part 1. hematite solubility from 60 to 300°C in NaOH–NaCl solutions and thermodynamic properties of Fe(OH)4−(aq). Geochim Cosmochim Acta 63(15):2247–61. https://doi.org/10.1016/S0016-7037(99)00070-8

79. Jang JH, Dempsey BA, Burgos WD (2007) Solubility of hematite revisited: Effects of hydration. Environ Sci Technol 41(21):7303–7308. https://doi.org/10.1021/es070535t

80. Liu Q, Zhang Y, Laskowski JS (2000) The adsorption of polysaccharides onto mineral surfaces: an acid/base interaction. Int J Miner Process 60(3–4):229–245. https://doi.org/10.1016/S0301-7516(00)00018-1

81. Liu Q, Laskowski JS (1989) The interactions between dextrin and metal hydroxides in aqueous solutions. J Colloid Interface Sci 130(1):101–111. https://doi.org/10.1016/0021-9797(89)90081-7

Eco-friendly collectors for flotation of fine hematite and malachite particles

Vladislav Slabov[1], Garima Jain[2], Erik Larsen[1], Irina Chernyshova*[1] and Hanumantha Rao Kota[1].

[1]Department of Geoscience and Petroleum, Norwegian University of Science and Technology (NTNU), Trondheim, NO-7031, Norway

[2]Department of Biotechnology and Food Science, Norwegian University of Science and Technology (NTNU), Trondheim, NO-7491, Norway

*Corresponding author: irina.chernyshova@ntnu.no

FTIR

ATR FTIR spectra of ac-SLS and ac-ASL in the powder form were recorded using a Bruker Vertex 80v FTIR spectrometer with an ATR accessory. A typical spectrum was an average of 200 scans measured at a 4 cm^{-1} resolution.
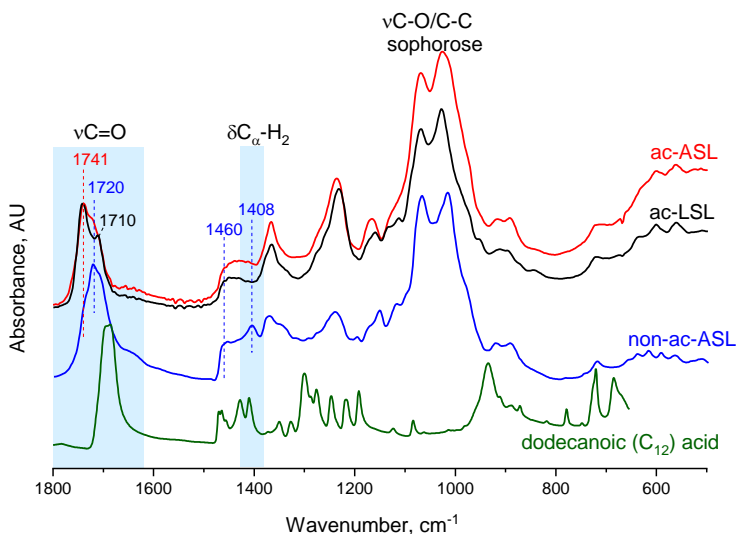
Figure S1 – FTIR spectra of (red) ac-ASL and (black) ac-LSL in comparison with (blue) non-acetylated ASL and (green) dodecanoic acid in the dry form

FTIR spectra show that ac-LSL and ac-ASL are the dominant components of the correspondingly labelled biosurfactants. Specifically, the presence of the sophorose headgroup in their structure follows from the comparison of FTIR spectra of ac-LSL, ac-ASL, and non-acetylated ASL (the latter was characterized by us earlier).[1] As seen from Figure S1, all the three spectra are similar in the fingerprint region of sugar groups (C-C/C-O stretching bands and C-OH bending)[2] at 1000-1100 cm^{-1}.

FTIR spectra of ac-LSL and ac-ASL are consistent with the structures of these biosurfactants. Specifically, the presence of the sophorose headgroup follows from the comparison of FTIR spectra of ac-LSL, ac-ASL, and non-acetylated ASL (the latter was characterized by us earlier).[1] As seen from Figure S1, all the three spectra are similar in the fingerprint region of sugar groups (C-C/C-O stretching bands and C-OH bending)[3] at 1000-1100 cm^{-1}.

Acetylation of both ac-LSL and ac-ASL is evidenced by the main component at 1741 cm-1 observed for the complex broad C=O stretching band at 1700-1740 cm^{-1} (Figure S1). This component is consistent with the νC=O stretching vibration of the carbonyl moiety of the acetyl groups.[3] Accordingly, it is transformed into a weak shoulder in the spectrum of non-acetylated ASL.

The presence of carboxyl groups in ac-ASL follows from a shoulder at 1720 cm^{-1} in the C=O stretching band at 1700-1740 cm^{-1} of this biosurfactant (Figure S1). The position of this shoulder is typical of the C=O stretching vibrations of the carboxyl groups of isolated fatty acids.[3,4] Crystalline linear fatty acids have this band red shifted to ca. 1700 cm^{-1},[4] as seen from the spectrum of dodecanoic acid (Figure 3). This red shift is explained by the formation of solid dimers between the carboxyl groups.[4] The presence of carboxyl groups in ac-ASL is also seen from a shoulder at 1408 cm^{-1}. This shoulder becomes a distinct band in the FTIR spectra of dodecanoic acid and non-acetylated ASL (Figure S1). It is assigned to the bending δC_{α}-H$_2$ vibrations of the methylene group of the hydrocarbon tails (the Cα atom is the closest to the carboxyl group).[4]

Further analysis of the C=O stretching band of ac-LSL at 1700-1740 cm^{-1} shows that this biosurfactant has an admixture of ASL. This conclusion follows from the presence of a distinct component at 1710 cm^{-1} in its νC=O stretching band which is typical of solid dimers of fatty acids.[4] Hence, a fraction of ac-LSL has broken ester linkages between the carboxyl and sophorose headgroups (Figure 1 of the main text).

Additional experimental data
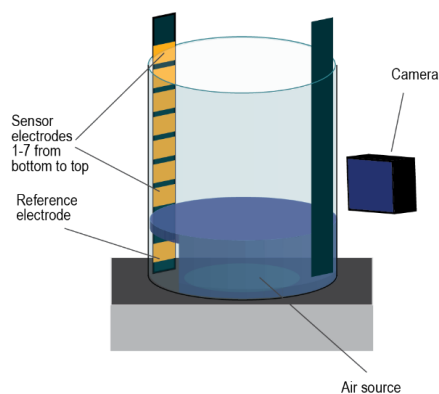
Figure S2 – Scheme of the dynamic foam analyzer.
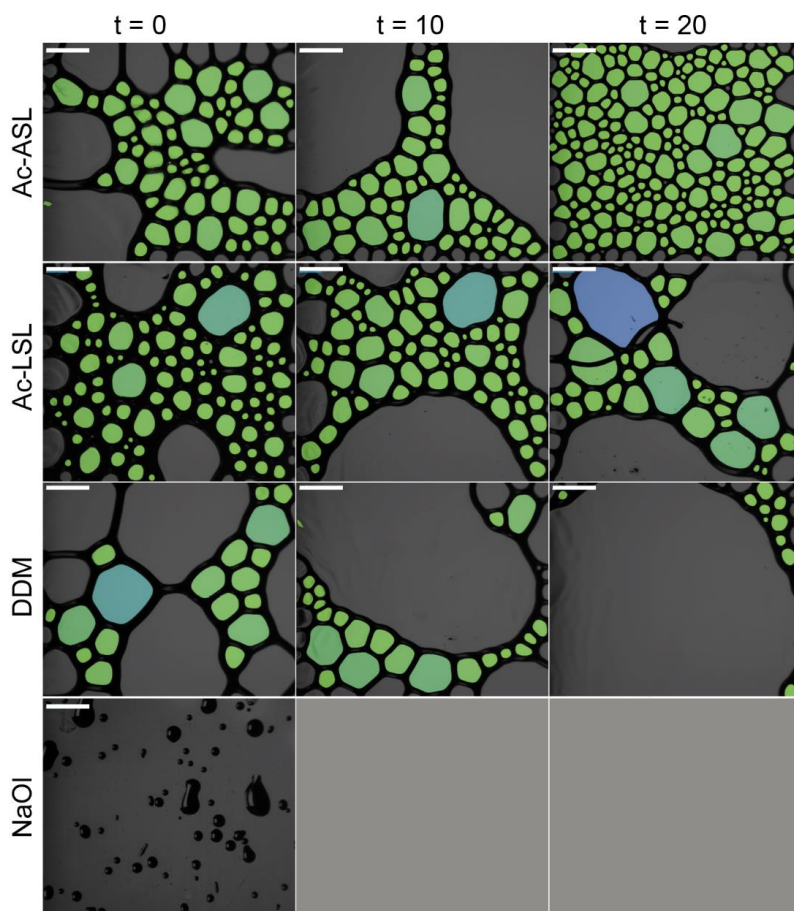
Figure S3 – Time evolution of foams generated by ac-ASL, ac-LSL, DDM and NaOl at pH 5.2 ± 0.1. The time (the top line) was measured after air flow was stopped. Grey squares for NaOl indicate that no foam is registered. The scale bar is 2 mm.
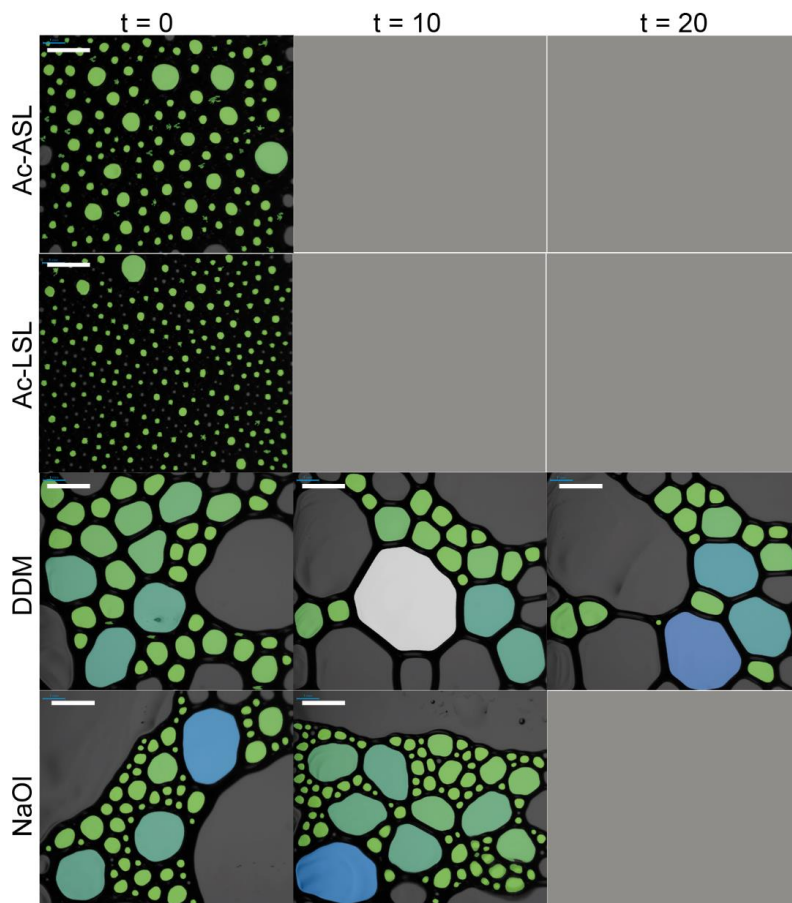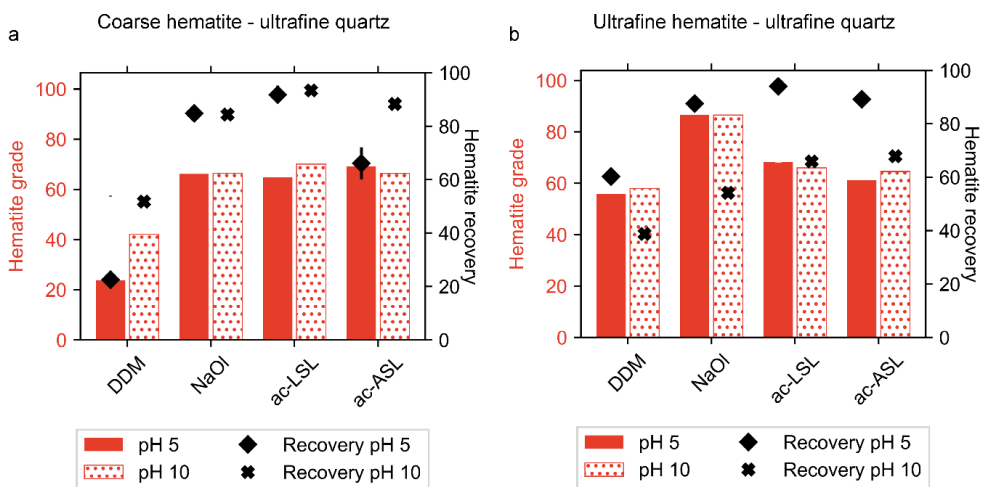
Figure S4 – Time evolution of foams generated by ac-ASL, ac-LSL, DDM and NaOl at pH 5.2 ± 0.1. The time (the top line) was measured after air flow was stopped. Grey squares for NaOl indicate that no foam was registered at this time. The scale bar 2 mm.

Figure S5 - Flotation recovery and grade in a 1:1 (wt) mixture of hematite and quartz in the presence of 50 µM ac-LSL, ac-ASL, DDM, and NaOl at pH 5 ± 0.3 and 10 ± 0.3: (a) coarse (+38 - 90 µm) hematite and fine (-20 µm) quartz; (b) fine (-20 µm) hematite and fine (-20 µm) quartz. Error of the grade and recovery data points without error bars is less than 5 %.
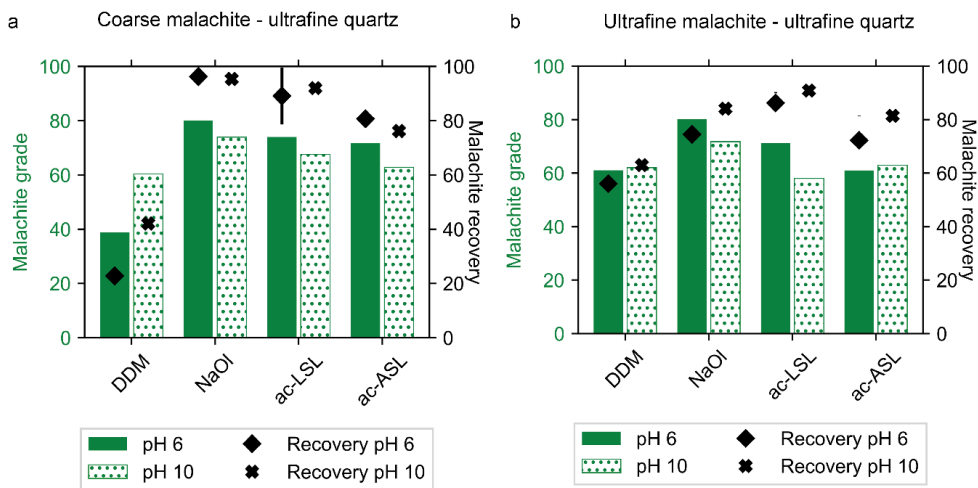
Figure S6 - Flotation recovery and grade in a 1:1 (wt) mixture of malachite and quartz in the presence of 50 µM ac-LSL, ac-ASL, DDM, and NaOl at pH 6 ± 0.3 and 10 ± 0.3: (a) coarse (+38 - 90 µm) malachite and fine (-20 µm) quartz; (b) fine (-20 µm) malachite and fine (-20 µm) quartz. Error of the grade and recovery data points without error bars is less than 5 %.

References

1   Dhar, P. *et al.* Toward green flotation: Interaction of a sophorolipid biosurfactant with a copper sulfide. *Journal of Colloid and Interface Science* **585**, 386-399, doi:10.1016/j.jcis.2020.11.079 (2021).
2   Wiercigroch, E. *et al.* Raman and infrared spectroscopy of carbohydrates: A review. *Spectrochimica Acta Part a-Molecular and Biomolecular Spectroscopy* **185**, 317-335, doi:10.1016/j.saa.2017.05.045 (2017).
3   Socrates, G. *Infrared and Raman Characteristic Group Frequencies: Tables and Charts*. 3rd edn, (Wiley, 2004).
4   Hayashi, S. & Umemura, J. Infrared spectroscopic evidence for coexistence of 2 molecular configurations in crystalline fatty-acids. *Journal of Chemical Physics* **63**, 1732-1740 (1975).

Paper 2

This paper is submitted to minerals engineering journal and is therefore not included.

Paper 3

IIM
Metallurgy
Materials Engineering

Check for updates

ORIGINAL ARTICLE

Alginates as Green Flocculants for Metal Oxide Nanoparticles

Vladislav Slabov[1] · Garima Jain[2] · Irina Chernyshova[1] ·
Hanumantha Rao Kota[1] · Helga Ertesvåg[2]

Abstract Flocculation is used for the removal or separation of colloids, e.g. in water treatment and mineral processing. Alginates are linear, anionic biopolymers composed of mannuronic (M) and guluronic (G) acids. The relative amount and distribution of M and G impact the ion-binding and gel-forming properties of the polymer, but still no one has yet addressed the impact of alginate composition on flocculation of nanoparticles or mineral particles. Our results showed that the distribution of G was important for flocculation, especially when Ca^{2+} was used as activating ion. With Ce^{3+} as activating ion, the shape and size of flocs were affected by alginate acetylation. This work expands the knowledge about the flocculation behavior of alginates and demonstrates that both bacteria- and algae-derived alginates can be potential biodegradable flocculants of ultrafine particles for mineral processing industry.

1 Introduction

The removal or separation of nanoparticles (NPs) and submicron particles dispersed in aqueous media is generally challenging due to the associated disadvantages of the commonly used membrane filtration method [1]. In wastewater treatment and mineral processing, a common method to address this challenge is flocculation, which is used to separate colloids by their sedimentation as large aggregates (flocs). Polymers can assist in forming flocs from destabilized dispersion by acting as flocculants [2].

Polyacrylamide (PAM)-based polymers are the largest category of flocculants in mineral processing [3]. However, acrylamide monomers are toxic [4], but has been found to be one of the main degradation component of cationic PAM [5]. These polymers then need to be replaced by eco-friendly alternatives, for instance bio-based polysaccharides including starch, chitosan, fucoidan and alginate. Several studies have suggested their possible application in mineral processing and wastewater treatment [3, 6–9]. For starch, it has been shown that the linear form is more efficient for flocculation than the branched form, emphasizing the need for using well-characterized polymers when conducting such studies [10].

Alginates are 1–4 linked linear copolymers composed of mannuronic acid (M) and its C5-epimer guluronic acid (G) [11]. The polymer has many uses within industry, pharma and food [12, 13], the current market volume is 44.480 tons (2021) [14]. The isoelectric point of alginates is around 3.4–3.7 [15], which provides soluble, fully anionic polymers at pH above 4. The distribution of M and G vary between different alginate molecules depending on their source. Hence, alginate chains are described as composed of three block types; G-blocks contain consecutive G residues, M-blocks contain consecutive M residues, and MG-blocks
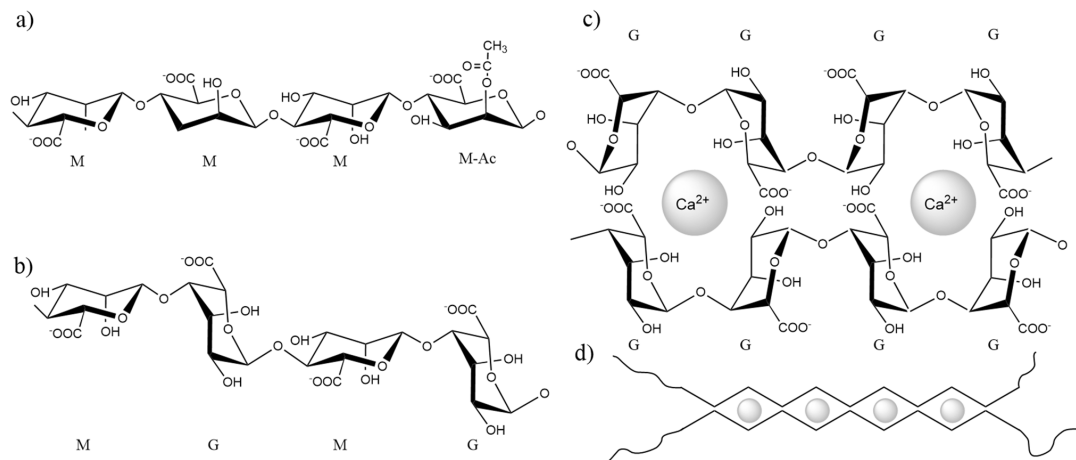
Fig. 1 Alginate structure. **a** M-block, one residue is O-2-acetylated, **b** MG-block, **c** Two G-blocks showing the crosslinking of G-blocks by Ca^{2+}-ions, **d** Schematic representation of how G-blocks in alginate molecules can be crosslinked by di- or trivalent cations in an eggbox-like structure [13]

contain alternating M and G residues (Fig. 1). The number of residues in any block may vary from two to the length of the chain. The average structure of alginate samples is determined by combining ^{1}H-NMR analyses, HPAED-PAD, SEC–MALLS and specific lyases [13].

Commercial alginates are manufactured from brown algae, but alginates are also produced by bacteria from the genera *Azotobacter* and *Pseudomonas.* During biosynthesis, the organisms produce mannuronan, and some of the M-residues are then epimerized to G-residues by mannuronan C-5 epimerases acting on the polymer [11, 16]. Bacterial alginates can also be O-2 or O-3-acetylated [17]. There is a large variation between alginates produced by different species or even under different environmental conditions [11, 18]. Given that the two epimers have different structures in the polymer (Fig. 1), their relative amounts and distribution within the polymer affect the structure of the alginate and its ability to form gels as recently reviewed [15].

Alginates containing G-blocks form gels with divalent metal ions [15], where Ca-gels have been most studied. In the junction zones, two G-blocks are crosslinked by Ca^{2+}-ions coordinated by two adjacent G-residues on both chains (Fig. 1). The crosslinking then proceeds, the length of the junction zones is important for the gel strength [19]. It has been found that crosslinking with MG-blocks might extend these gel junctions [15]. G-blocks will also bind other alkaline-earth metal ions, the binding strength increases with the radius [20]. Other metal ions with higher valencies also bind alginates, however, for most of these, alginate composition does not influence binding [21, 22]. The coordination of individual ions depends on their size and valency [23–25],

however, how trivalent ions bind and crosslink the different block-structures are still not known [22].

The flocculation properties of alginates have been studied for a long time however, mostly algae-derived alginates have been used [8, 26–29] and it has been proposed that the formation of an alginate ionic gel network is needed for flocculation of the dispersed particles [29]. The previous research utilized native or modified alginates and various mono-, di- and trivalent salts [8, 28–32]. Still, most of these studies have not addressed the effect of the alginate composition on flocculation of dispersed particles, although it has been shown that it is important in water treatment [33].

Besides flocculant, alginates can be used as modifiers and depressants in mineral flotation, and as a sorbent for heavy metal removal. In particular, in scheelite flotation, alginate selectively depress calcite and fluorite [32]. In reverse flotation, alginate can support removal of quartz and chlorite from hematite ore [34]. Furthermore, alginate composites and alginate hydrogels effectively adsorb heavy metals (Se(IV), Cr(VI), As(V)) from wastewater [22, 35]. Hence, the interaction of alginates with colloidal mineral particles and multi-valence metal cations has a broad scope.

This work compares the flocculation properties of three well-characterized alginates with different G-content, G-distribution and acetylation, where our main motivation is to explore the effect of alginate composition on their ability to flocculate CeO_2 and α-Fe_2O_3 (hematite) NPs. These NPs serve as model systems for cerium, which is an abundant rare earth element and for iron, which is the most used metal. Since the flocculation performance of alginates depends on the cross-binding cation, we compare the efficiency of

divalent Ca^{2+} and trivalent Ce^{3+} on this process. The ionic radius of Ce^{3+} and Ca^{2+} is 0.102 nm and 0.100 nm, respectively [36], making them good candidates to study the effect of charge on the interaction between metal ions and alginates. We found that trivalent Ce^{3+} activates flocculation properties of alginate independently of its G-block content, while activation by Ca^{2+} requires G-blocks.

2 Material and Methods

2.1 Alginates

Protanal LF 10/60 TM sodium alginate (50% G-blocks, 17% MG-blocks and 33% M-blocks) from *Laminaria hyperborea* was obtained from FMC Biopolymer. Bacterial alginate was isolated from *Pseudomonas fluorescens* Pf201 (no G-blocks, 30% MG blocks, 70% M-blocks, degree of acetylation 0.4), the third was made by deacetylating this alginate [37] [17]. These alginates are specified as LF10/60, PfAc, and PfdeAc, respectively.

2.2 Chemicals

MilliQ water was used in all experiments. NaOH and HCl were used for pH adjustments and $NaNO_3$ as background electrolyte solution (all from VWR). $CaCl_2$ and $Ce(NO_3)_3 \cdot 6 H_2O$ (Merck) (prepared as 18 mM stock solutions) were used as metal cations for flocculation activation.

2.3 NPs

Cerium (IV) oxide (99.9%) 10 nm size was purchased from Meliorum Technology Inc. Hematite (α-Fe(III) oxide) (98%) 30–50 nm (Alfa Aesar 47,044) was purchased from Thermo Fisher Scientific. The initial concentration of CeO_2 and α-Fe_2O_3 NP dispersions in water was 200 and 300 mg/L, respectively. The stability of NPs dispersed in aqua solution is usually explained by a high ζ-potential, which should be >30 mV, but recent work with Fe_3O_4 NPs argues that this is not always the case [38, 39]. In our work we employed two days of ultrasonication to break possible aggregates of CeO_2 and α-Fe_2O_3 NPs [40]. These concentrations were then diluted to 50 and 75 mg/L for CeO_2 and α-Fe_2O_3, respectively, with pH around 5. After four weeks, no sedimentation was observed.

2.4 ζ-potential

The zeta (ζ) potential of NPs in water, alginate solutions or treated with Ca^{2+} and Ce^{3+} was measured using a Malvern ZetaSizer Nano Z (laser Doppler micro-electrophoresis) instrument. NPs were first dispersed in a 0.001 M $NaNO_3$ background solution at 0.1 wt. % by sonication for 20 min. This dispersion was split to prepare dispersions with the three alginate samples and one blank (in 0.001 M $NaNO_3$). Then, the prepared samples were split into 30-mL samples followed by pH adjustment of each sample and equilibration on a shaking table for 5 h. Afterwards, pH was readjusted with 0.01 M NaOH or HCl solutions before measuring its ζ-potential. As material settings in the ZetaSizer, we used refractive indices of 3.0 and 2.2 and absorption of 0.8 and 0.5 for iron and cerium oxide NPs, respectively.

2.5 Flocculation

To observe the flocculation process visually, experiments were conducted in glass vials in the presence and absence of alginate samples. Alginate stock solutions were prepared by dissolving alginates in MilliQ at 400 mg/L. All stock solutions were adjusted to pH 6–7. For the experiments, NPs dispersions with pH 6–7 were split into 10 mL samples and metal cations (Ca^{2+} or Ce^{3+}) were added to each dispersion to a concentration of 3 mM (after addition of alginates). The final concentrations of NPs were 44 mg/L for CeO_2 and 66 mg/L for α-Fe_2O_3. After shaking by hand, alginate stock solutions were slowly added to a final concentration of 50 mg/L over a period of one minute. The dispersions treated with alginate were shaken simultaneously for 5–10 s and then left still for further observation.

2.6 Kinetic Measurement of Flocculation

NP dispersions (10 ml) were conditioned with solutions of either Ca^{2+} or Ce^{3+} for one minute before adding alginates. Final concentrations were as above. The samples were vortexed for 10 s immediately after addition of alginates, moved to cuvettes and the optical density (OD) was recorded at 350 and 450 nm for iron oxide and cerium oxide NPs, respectively. These values were found by preliminary experiments to give good absorbance by the respective NPs. No mixing took place while the cuvette was standing in the spectrophotometer.

2.7 High Speed Camera Analysis of Flocculation

To estimate the shape and size of flocs, a high-speed camera (Chronos 1.4, Kron Technologies Inc.) mounted on an optical microscope (NIKON SMZ45T Stereoscopic Microscope) was used (Supplementary Figure S1). Ten ml NP dispersion pretreated by metal cations was placed into a Petri dish placed on a magnetic stirring (400 rpm), and alginate (50 ppm, ppm is defined as mg/L) was added. After one minute stirring was stopped and video recorded (10 s long, resolution 1280×1024, 1069 frames per second).

2.8 Transmission Electron Microscopy

The NPs were sonicated for 30 min in ethanol to obtain very dilute dispersion, which was drop-cast onto TEM copper grid and dried. TEM images were acquired using a JEOL 2100F electron microscope operated at 200 kV.

2.9 The Brunauer, Emmett, and Teller (BET) Specific Surface Area and Particle Size Distribution

The BET surface areas of NPs were measured using a Micromeritics Tristar 3000 Analyzer. The samples were degassed at 250 °C under helium flow for 3 h. Average values of two duplicate measurements are presented.

3 Results

3.1 *The Morphology of α-Fe₂O₃ and CeO₂ NPs*

One can see from the TEM images (Fig. 2) that α-Fe$_2$O$_3$ NPs have a needle-like shape, while CeO$_2$ NPs have a random, almost cubic shape. The electron diffraction patterns of α-Fe$_2$O$_3$ and CeO$_2$ confirm that the NPs are randomly oriented.

The BET surface area of CeO$_2$ NPs was found to be 72 ± 2 m^2/g, which was two times higher as compared to that of α-Fe$_2$O$_3$, having an area of 36 ± 1 m^2/g. This difference can be explained by the difference in the NP size.

3.2 ζ-potential of Iron and Cerium Oxide NPs in the Presence and Absence of Alginate

The ζ-potential of α-Fe$_2$O$_3$ and CeO$_2$ NPs (Fig. 3a, b) shows that the isoelectric point (IEP) of both NPs was around pH 7. This value is close to the values of 7.8 and 8 previously reported for hematite [41] and cerium oxide [42] NPs.

As expected, the anionic alginates PfAc, PfdeAc and LF 10/60 make the ζ-potential of the NPs negative (Fig. 3a,

b). The decreased charge was observed to be in the pH range from 3 to 10, meaning that at 30 ppm the polymer adsorbs to the NPs even when the ζ-potential of the NPs is negative. Furthermore, the value of ζ-potential became more negative than -30 mV, which could be categorized as a stable colloidal dispersion [43]. As a result, none of the three alginates initiated visible flocculation of NPs (Fig. 4).

3.3 ζ-potential of Iron and Cerium Oxide NPs in the Presence and Absence of Metal Cations

Since we wanted to use Ca^{2+} and Ce^{3+} as flocculation activators, we studied their effect on ζ-potential of the NPs in absence of alginates. Both metal ions should be presented in cationic form in the solution, according to a speciation diagram (Supplementary Figure S2). The result of the ζ-potential measurements (Fig. 3c, d) shows a strong shift of the NPs' IEP indicating adsorption of Ca^{2+} and Ce^{3+} on both NPs. As expected, in the presence of metal cations the ζ-potentials of the NPs increased for all measured pH values and became positive. The increase was significantly higher in the basic pH region when Ce^{3+} ion was added as compared to Ca^{2+}. A positive charge on NPs should enhance their binding with the anionic alginates.

3.4 Flocculation of Cation-Activated NPs

Firstly, the flocculation of NPs activated by cations was tested in glass vials. Dispersed iron oxide or cerium oxide NPs were mixed with Ca^{2+} or Ce^{3+} and then different alginates samples were added. The final concentrations were around 3 mM metal ions and around 50 ppm alginates, while pH was in the range of 6–7.

As was noticed before, the iron oxide NPs did not flocculate in the absence of the cations (Fig. 5a). In the presence of Ca^{2+}, visible flocs were observed only for the LF 10/60
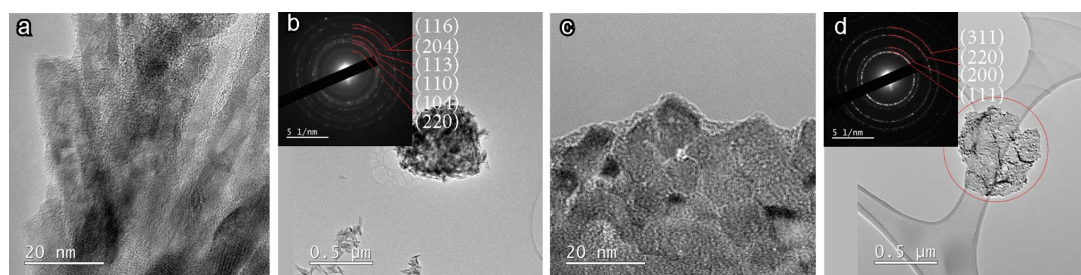

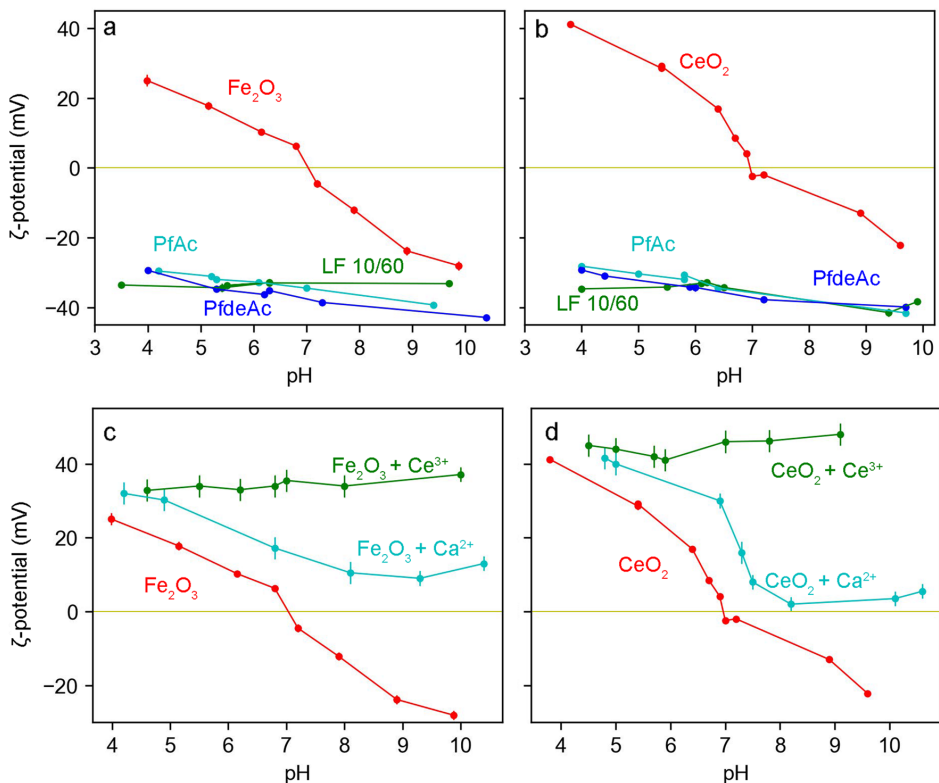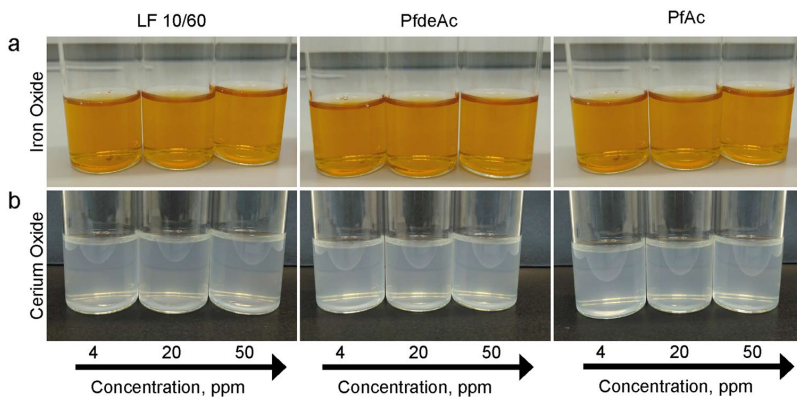**Fig. 2** TEM images of **a**, **b** α-Fe₂O₃ and **c**, **d** CeO₂ NPs

Fig. 3 pH dependence of the ζ-potential of **a** α-Fe₂O₃ and **b** CeO₂ NPs in the absence and presence of 30 ppm concentration of PfAc, PfdeAc and LF 10/60. **c** α-Fe₂O₃ and **d** CeO₂ NPs in the presence and absence of Ca²⁺ and Ce³⁺

Fig. 4 The effect of 4, 20 and 50 ppm concentrations of Lf 10/60, PfdeAc and PfAc on **a** α-Fe₂O₃ and **b** CeO₂ NPs dispersions at pH 6–7

alginate, while the dispersions treated by PfdeAc and PfAc showed no flocculation even after several hours. The same result was obtained for cerium oxide NPs (Fig. 5b). However, when activated by Ce³⁺ any combination of NP and alginate immediately flocculated (Fig. 5).

3.5 Evaluation of Flocculation by Time-Scale Experiments

While the above experiments showed that flocculation took place, changes in optical density (OD) over time were used
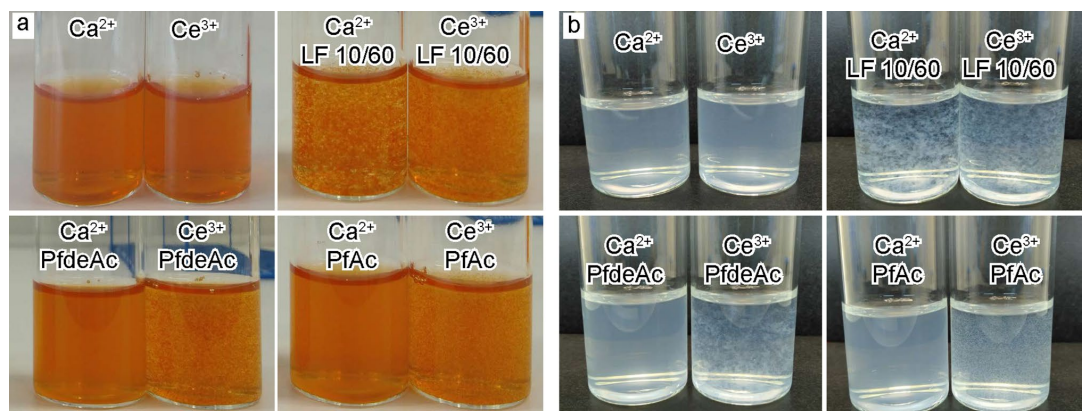
Fig. 5 The effect of 50 ppm of alginates on flocculation of **a** α-Fe_2O_3 and **b** CeO_2 NPs activated by 3 mM Ca^{2+} or 3 mM Ce^{3+}
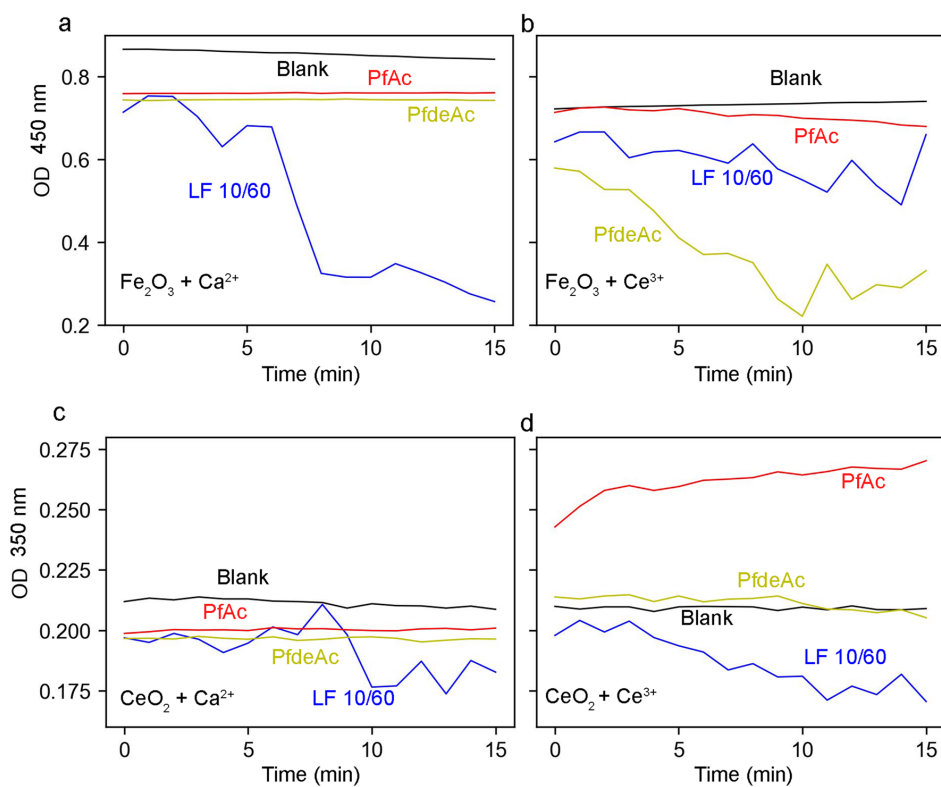
Fig. 6 The influence of NPs flocculation time on the optical density of the dispersions. The final concentrations of metal cations and alginate were 2.4 mM and 43 ppm, respectively. Blank samples contain NP and metal ion but no alginate

to compare the flocculation efficiency of alginates (Fig. 6). The decrease in OD should correlate with the removal of NPs, i.e. sedimentation of flocs. When only metal ions were added to the dispersions, there was a slight shift in initial OD, but no decrease with time (Supplementary Figure S3). These dispersions were used as blank samples in Fig. 6.

The strongest effect on flocculation of iron and cerium oxide NPs activated by Ca^{2+} was observed for the mixture with LF10/60 where the OD decreased from about 0.85 down to 0.3, and from around 0.21 down to around 0.18 for iron and cerium oxide, respectively (Fig. 6 a, c). In contrast, the NPs activated by Ca^{2+} did not flocculate when PfAc and PfdeAc were added; the OD of these systems slightly decreased and remained constant for 15 min (Fig. 6 a, c). These results confirmed the results from the initial flocculation experiments (Fig. 5).

As was expected from the initial experiments, Ce^{3+} affected the OD of the samples more than Ca^{2+}. PfdeAc showed the strongest effect of the three alginates on OD iron oxide NPs activated by Ce^{3+} (Fig. 6b). In contrast, PfAc had the weakest influence on the OD of cerium oxide NPs. When cerium oxide NPs were combined with Ce^{3+} cations, only LF10/60 were able to result in fast sedimentation of flocs (Fig. 6d). The final effect of LF10/60 on cerium oxide OD was similar for systems with Ca^{2+} and Ce^{3+}. However, the shapes of the curves were very different, which could indicate a difference of the formed flocs (Fig. 6c, d).

3.6 Evaluation of the Effect of Alginate Concentration on Flocculation

To study the concentration effect of the alginates on NPs flocculation, we conducted time-scale experiments for

LF 10/60 and PfdeAc at concentrations 5, 15, 30, 44 and 90 ppm. The systems of iron oxide NPs activated by Ca^{2+} and Ce^{3+} were chosen due to the strongest flocculation effect from the previous tests. Figure 7 shows the result of OD changes over 10 min for alginates at different concentrations of alginates. As observed earlier (Fig. 6), the initial OD measurements was influenced by the addition of alginates. Moreover, this effect appears to be dose dependent with an intermediate dose giving the lowest initial OD value. The flocculation seems to start immediately after mixing, since we see a dosage dependent change in OD after only one minute for both LF10/60 (Fig. 7a) and PfdeAc (Fig. 7b).

We observed flocs for all tested concentration of LF 10/60. The flocs at 5 ppm concentration were smaller than the others, and this could have prevented their sedimentation in this experiment. The flocs formed at 15 and 30 ppm were also visibly denser than those formed at the highest alginate concentrations, and sedimented faster (Fig. 7a). According to this, the concentration of 15 ppm of LF 10/60 is the most favorable for the rapid sedimentation of flocs. However, at 10 min the OD is not significantly different for the concentrations in the range of 15–44 ppm, and the observed results could be a result of the short mixing time, the higher concentrations might need more time to reach equilibrium.

For each concentration of PfdeAc in the presence of Ce^{3+}, except 5 ppm, we observed flocs. At 5 ppm, the OD did not change during the 10 min. (Fig. 7b). From Fig. 7b one can see that PfdeAc dosages of 30 and 44 ppm are the most effective ones.

The sedimentation of iron oxide flocs was also tested for the Lf10/60-Ca^{2+} and PfdeAc-Ce^{3+} systems in glass vials, using 44 ppm alginate concentration and 1.5 min mixing time (Fig. 8). Flocs had formed in both systems when the
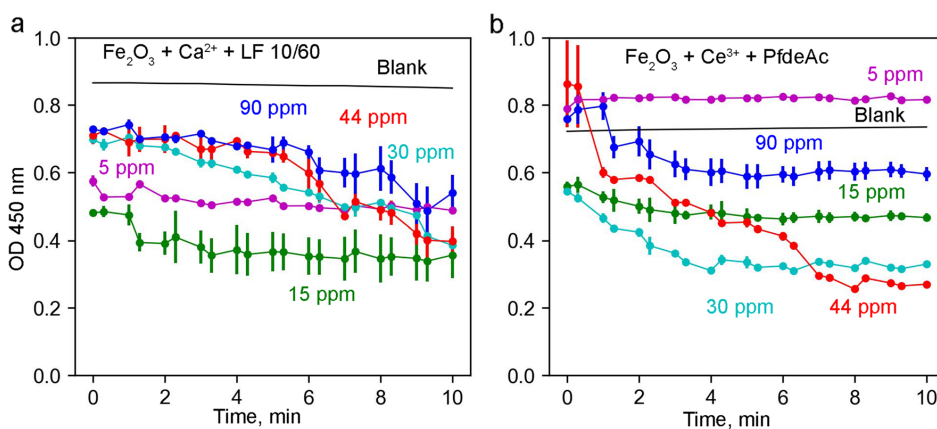

Fig. 7 The flocculation dependence of iron oxide NPs on alginate concentration: **a** LF 10/60 and **b** PfdeAc activated by Ca^{2+} and Ce^{3+}, respectively. Blank samples contain NP and metal ion but no alginate
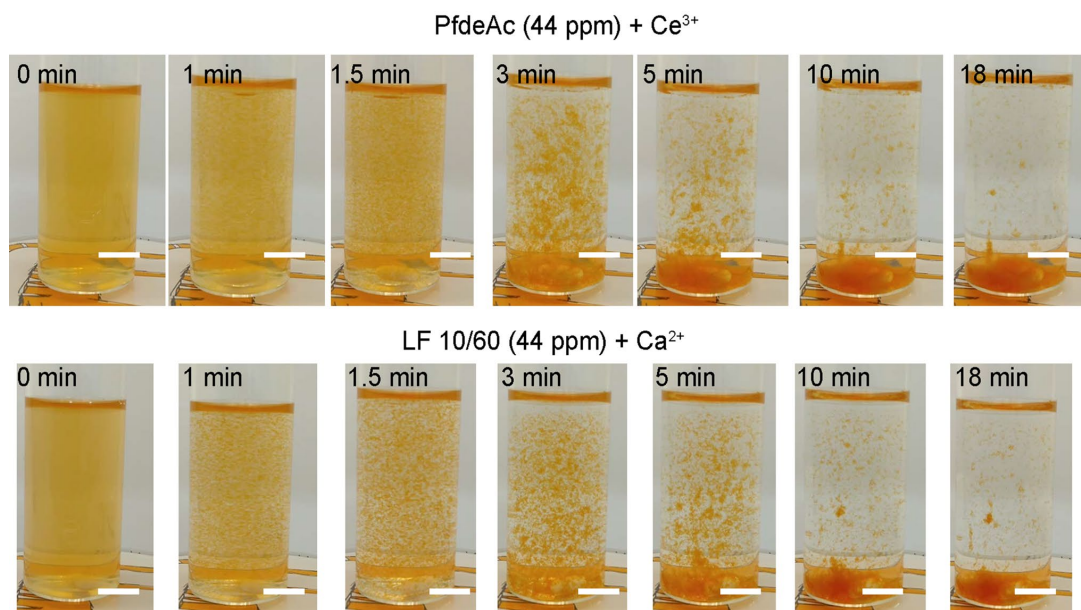
PfdeAc (44 ppm) + Ce^{3+}

LF 10/60 (44 ppm) + Ca^{2+}

Fig. 8 Sedimentation of α-Fe$_2$O$_3$ flocs generated by PfdeAc-Ce^{3+} (*top*) and Lf10/60-Ca^{2+} (*bottom*) alginates. The alginates were added at t = 0 min to NPs dispersions containing 3 mM metal cations that were being stirred at 400 rpm. Stirring was halted at t = 1.5 min, and sedimentation was observed thereafter. Scale bar 1 cm

stirring were stopped, and already after 10 min most of the particles had settled on the bottom, confirming the results obtained from the spectroscopy experiment.

3.7 Floc Shape Depends on Alginate Type and NPs Size

The differences in sedimentation could potentially be caused by differences in the shape or size of flocs. To compare flocs shape, we used a high-speed camera mounted on an optical microscope. The studied NP dispersions in the Petri dish were placed on the magnetic stirrer, and then first the cations and then alginate samples were added. After an interaction time of one minute, stirring was stopped and images were obtained for further analysis (Fig. 9).

The shapes of the iron oxide flocs differed depending on the alginate. The flocs were similar in the LF 10/60 systems activated by Ca^{2+} and Ce^{3+}. However, flocculation of NPs by PfAc and PfdeAc differed according to their shape and size. Thus, iron oxide activated by Ce^{3+} increased in size in the followed sequence of alginate samples: Lf10/60 ≤ PfAc < PfdeAc. These flocs resembled flat flakes and seemed similar in shape. Big flocs should sediment faster, and we can observe the expected stronger effect on OD of PfdeAc (Fig. 7b).

The pale white flocs were less visible than the reddish flocs containing iron NPs, making it harder to compare their size and shape (Fig. 9). As observed for iron oxide NPs, flocs of cerium oxide NPs formed by LF 10/60 and activated by either Ca^{2+} or Ce^{3+} were similar. We can clearly see the formation of fiber-like flocs by PfdeAc, while PfAc forms flocs like those formed by LF 10/60, showing that both G-blocks and acetylation affects the size and shape of cerium oxide NPs flocs. During the experiment, web-like structure was observed in the dispersion, and these did not sediment fast. This could explain the observed weak decrease in OD for the corresponding sample in the OD study (Fig. 6d, PfdeAc).

4 Discussion

Following production and usage of nanomaterials, their migration in waters, soil and atmosphere causes increased environmental issues [44, 45]. Each year the worldwide production of nanomaterials counts tens and hundreds of tons. Specifically, based on 10 years old data, the median worldwide productions of FeO$_x$ and CeO$_x$ is 55 t/year [46]. Moreover, mining and mineral processing generate waste containing NPs, which are difficult to reprocess [47, 48]. Flocculation can be a solution for wastewater treatment or used to reduce the amount of waste in mineral processing industries. Expanding the knowledge of flocculation agents
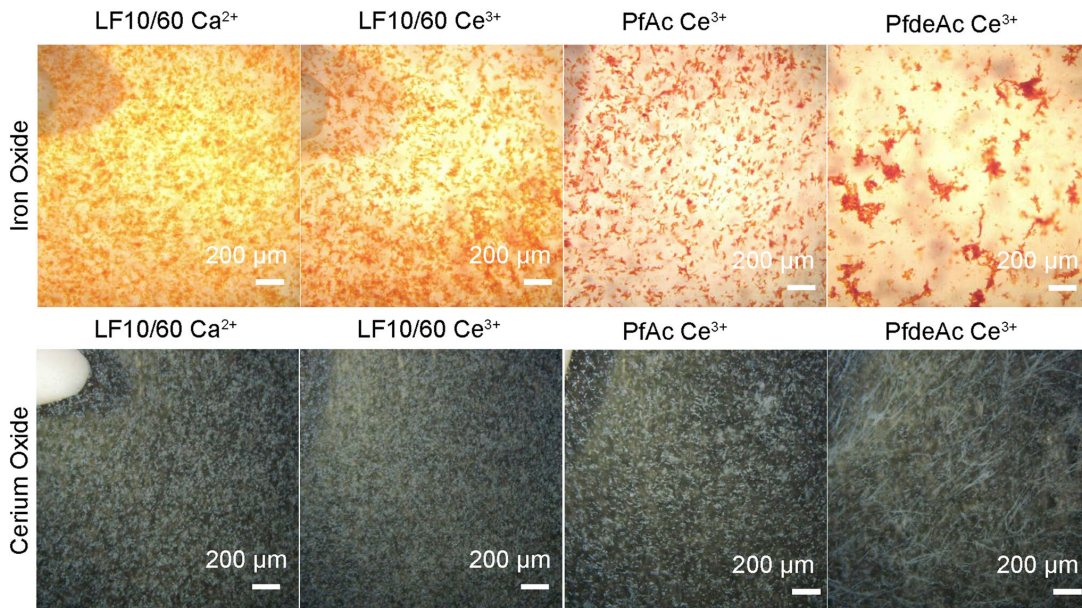
Fig. 9 High speed camera images of flocks taken after 1 min of stirring at 400 rpm. Iron oxide (*top*) and cerium oxide (*bottom*) NPs activated by Ca^{2+} or Ce^{3+}, and flocculated by LF 10/60, PfAc or PfdeAc

will help to reach maximum efficiency in the dewatering processes and find the most sustainable products.

The flocculation process by polymers requires bridging between dispersed particles or their charge neutralization [43]. For bridging to happen, only parts of the polymer should be adsorbed on one particle surface, leaving at least enough polymer length to form a bridge and adsorb to a second particle (Fig. 10a). The ζ-potential results demonstrate adsorption of all studied alginate samples since their IEP is shifted from initial pH (Fig. 3a, b). However, alginate adsorption did not cause any flocculation, in contrast, ζ-potential results show stabilization of NPs dispersions from acidic to basic pH [49, 50]. This is most easily

Fig. 10 Simplified models of possible interactions between NPs (*brown spheres*), alginates (*strands*) and cations (*small purple spheres*). **a** Alginates form bridges between NPs; **b** Each alginate strand envelopes one NP; **c** Alginates are partly crosslinked by cations forming ionic gels. This restricts the parts of the polymer available for binding NPs, and bridging can happen.
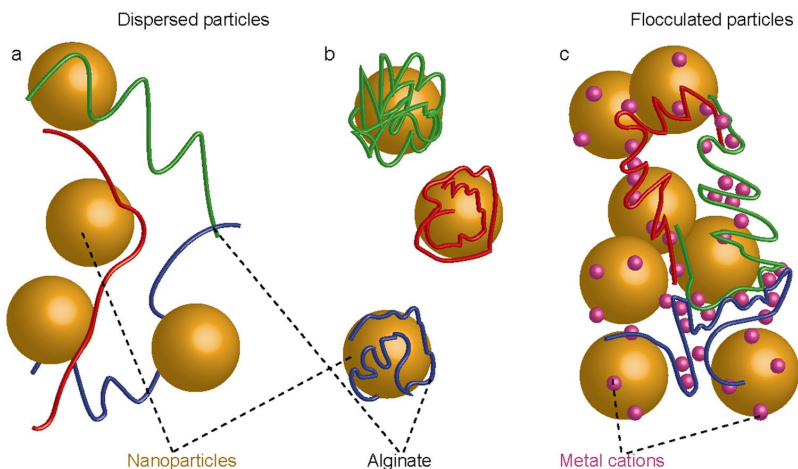
explained by assuming a flat conformation of the adsorbed polymer (Fig. 10b) [35, 51].

If this was the case, then the solution would be to attenuate the binding between the polymer and the NPs, and we tested the use of Ca^{2+} and Ce^{3+} cations for this purpose. It is well known that two G-blocks can crosslink via chelation of Ca^{2+} (Fig. 1), this is the basis for many of the applications of alginate hydrogels [15]. Formation of such junctions start with the exchange of the monovalent counterion attached to the carboxyl groups, in our case Na^+, with divalent or trivalent cations. Binding of cations to the alginate and formation of cross-linking junctions, will diminish the parts of the alginates available for binding to the NPs, and allow the alginate molecules to form bridges between the particles. Cations bound to the particles might participate in the bridging event. Alternatively, the NPs might become entangled in the formed gels. These options are not mutually exclusive and are depicted in Fig. 10c.

In our experiments we clearly see flocculation of both cerium and iron oxide NPs by LF 10/60 in the presence of Ca^{2+} (Fig. 5 and 6a, c), while the bacterial alginates do not seem to make aggregates. These alginates contain no G-blocks, and while Ca^{2+} bind G-blocks well, the binding of MG-blocks are much weaker and no binding to M-blocks is observed [52]. This would explain the absence of flocculation in the systems PfAc and PfdeAc with Ca^{2+}. These data strongly suggest that the formation of a gel network is a necessary factor in the observed flocculation of NPs using Ca^{2+} and G-block-containing alginate [25].

Trivalent cations have been found to crosslink alginate chains by binding to three carboxyl and hydroxyl groups [22, 24, 25], and their selectivity for specific block structures are much less [21] indicating that they are able to crosslink MG blocks or even M-blocks. When we replaced the divalent Ca^{2+} with Ce^{3+}, all three alginates made flocs in the presence of NPs and Ce^{3+}, again indicating that alginate cross-linking is necessary for flocculation. The C-2 oxygen has been implicated in hydrogen binding to trivalent cations [24], explaining why the O-2-acetylated alginate resulted in less flocs. A gel network was also seen by others when studying a mixture of alginate-coated hematite NPs and Ca^{2+} [29].

5 Conclusion

Our study shows that alginates can be used for flocculation of NPs if a suitable cation is present to cross-link the alginate molecules. The efficiency of flocculation is dependent on alginate composition and on the cation used to cross-link alginate molecules. In addition, acetylation of alginate strongly affects size and geometry of the flocks.

As described above, flocculation is used in various industries including the mineral processing industry. To develop alginate for this application, one needs to understand flocculation mechanisms and flocculant behavior in various systems, and a wider range of NPs, cations and characterized alginates should be studied and compared using the methods described in this study. Such studies should also include exploring the possibilities for selective flocculation of different NPs or minerals.

References

1. Obotey Ezugbe E and Rathilal S, *Membranes*, **10** (2020), https://doi.org/10.3390/membranes10050089.
2. Bratby J, *Coagulation and Flocculation in Water and Wastewater Treatment—Third Edition*, IWA Publishing, (2016), https://doi.org/10.2166/9781780407500.
3. Pearse M J, *Miner Eng*, **18** (2005) 139–149, https://doi.org/10.1016/j.mineng.2004.09.015.
4. King D J and Noss R R, *Rev Environ Health*, 8 (1989), https://doi.org/10.1515/reveh-1989-1-403.
5. Wang D, Liu X, Zeng G, Zhao J and Yang Q, *Water Res*, **130** (2018) 281–290, https://doi.org/10.1016/j.watres.2017.12.007.
6. Félix LL, Moreira GF, Filho LSL and Stavale F, *Miner Eng*, **178** (2022), https://doi.org/10.1016/j.mineng.2022.107429.
7. Matusiak J, Grządka E and Bastrzyk A, *Chem Eng J*, **423** (2021), https://doi.org/10.1016/j.cej.2021.130264.
8. Tian Z, Zhang L, Sang X, Shi G and Ni C, *J Phys Chem Solids*, **141** (2020) https://doi.org/10.1016/j.jpcs.2020.109408.
9. Sun Y, Shah KJ, Sun W and Zheng H, *Sep Purif Technol*, **215** (2019) 208, https://doi.org/10.1016/j.seppur.2019.01.017.
10. Mierczynska-Vasilev A, Kor M, Addai-Mensah J and Beattie D A, *Chem Eng J*, **220** (2013) 375, https://doi.org/10.1016/j.cej.2012.12.080.
11. Ertesvåg H, *Front Microbiol.* **6** (2015) 523. https://doi.org/10.3389/fmicb.2015.00523
12. Onsøyen E, *Carbohydr Europe* **14** (1996) 26.

13. Skjåk-Bræk G, Donati I, and Paoletti S, in *Matricardi P*, (eds) Alhaique F, and Coviello T, Characterization and Biomedical Applications, Pan Stanford Publishing Pte Ltd, Polysaccharide Hydrogels (2016), p 449.

14. Grand View Research, Alginate Market Size, Share and Trends Analysis Report By Type (High M, High G), By Product (Sodium, Propylene Glycol), By Application (Pharmaceutical, Industrial), By Region, And Segment Forecasts, 2021−2028, (2021), https://www.grandviewresearch.com/industry-analysis/alginate-market#, Accessed March 8th 2023

15. Nordgård C T and Draget K I, Chapter 26—Alginates, in: Phillips GO, Williams PA (Eds.) Handbook of Hydrocolloids (Third Edition), Woodhead Publishing (2021), pp. 805, https://doi.org/10.1016/B978-0-12-820104-6.00007-3.

16. Haug A and Larsen B, Biosynthesis of alginate. Epimerisation of D-mannuronic to L-guluronic acid residues in the polymer chain, *Biochim Biophys Acta*, 192 (1969) 557

17. Skjåk-Bræk G, Grasdalen H, and Larsen B, *Carbohydr. Res.* **154** (1986) 239.

18. Kloareg B, Badis Y, Cock J M and Michel G, *Genes (Basel)*, **12** (2021), https://doi.org/10.3390/genes12071059.

19. Aarstad O, Strand B L, Klepp-Andersen L M and Skjåk-Bræk G, *Biomacromol*, **14** (2013) 3409, https://doi.org/10.1021/bm400658k.

20. Smidsrød O, and Haug A, *Acta Chem Scand* 22 (1968) 1989.

21. Lunde G, Smidsrød O and Haug A, *Acta Chem Scand*, **26** (1972) 3421, https://doi.org/10.3891/acta.chem.scand.26-3421.

22. Massana Roquero D, Othman A, Melman A and Katz E, *Materi Adv*, **3** (2022) 1849, https://doi.org/10.1039/D1MA00959A.

23. Agulhon P, Markova V, Robitzer M, Quignard F and Mineva T, *Biomacromol*, **13** (2012) 1899, https://doi.org/10.1021/bm300420z.

24. Menakbi C, Quignard F and Mineva T, *J Phys Chemi B*, **120** (2016) 3615, https://doi.org/10.1021/acs.jpcb.6b00472.

25. Brus J, Urbanova M, Czernek J, Pavelkova M and Kulich P, *Biomacromol*, **18** (2017) 2478, https://doi.org/10.1021/acs.biomac.7b00627.

26. Maruyama H, Seki H and Igi A, *Biochem Eng J*, **162** (2020), https://doi.org/10.1016/j.bej.2020.107713.

27. Tripathy T, Karmakar N C and Singh R P, Development of novel polymeric flocculant based on grafted sodium alginate for the treatment of coal mine wastewater, *J Appl Pol Sci*, **82** (2001) 375, https://doi.org/10.1002/app.1861.

28. Liu C, Gao B, Wang S, Guo K and Xu X, *Carbohydr Polym*, **248** (2020), https://doi.org/10.1016/j.carbpol.2020.116790.

29. Chen KL, Mylon S E and Elimelech M, *Environ Sci Technol*, **40** (2006) 1516, https://doi.org/10.1021/es0518068.

30. Tripathy T & Singh RP, *Eurn Polym J*, **36** (2000) 1471, https://doi.org/10.1016/s0014-3057(99)00201-3.

31. Rani P, Mishra S and Sen G, *Carbohydr Polym*, **91** (2013) 686, https://doi.org/10.1016/j.carbpol.2012.08.023.

32. Chen W, Feng Q M, Zhang G F, Yang Q and Zhang C, *Miner Eng*, **113** (2017) 1, https://doi.org/10.1016/j.mineng.2017.07.016.

33. Moral Ç K, Ertesvåg H and Sanin F D, *Environ Sci Pollut Res* (2016) 1, https://doi.org/10.1007/s11356-016-7475-6.

34. Fu Y F, Yin W Z, Yang B, Li C and Li D, *Int J Miner Metall*, **25** (2018) 1113, https://doi.org/10.1007/s12613-018-1662-z.

35. Vajihinejad V, Gumfekar S P, Bazoubandi B, Rostami Najafabadi Z and Soares J B P, *Macromol Mater Eng*, **304** (2019) 1800526, https://doi.org/10.1002/mame.201800526.

36. Greenwood NN & Earnshaw A, *Chemistry of the Elements*, 2 ed., Elsevier, (2012).

37. *Gimmestad M, Sletta H, Karunakaran K P, Bakkevig K, Ertesvåg H, Ellingsen T, Skjåk-Bræk G, Valla S, inventors; FMC Biopolymer AS assignee, New Mutant Strains of Pseudomonas Fluorescens and Variants Thereof, Methods of Their Production, and Uses Thereof in Alginate Production*. WO2004/011628, (2002).

38. Riddick T M and Zeta-Meter I, *Control of Colloid Stability Through Zeta Potential: With a Closing Chapter on Its Relationship to Cardiovascular Disease*, Zeta-Meter, Incorporated, (1968).

39. Pochapski D J, Carvalho Dos Santos C, Leite G W, Pulcinelli S H and Santilli C V, *Langmuir*, **37** (2021) 13379, https://doi.org/10.1021/acs.langmuir.1c02056.

40. Zhang Y, Chen Y, Westerhoff P, Hristovski K and Crittenden J C, *Water Res*, **42** (2008) 2204, https://doi.org/10.1016/j.watres.2007.11.036.

41. He Y T, Wan J and Tokunaga T, *J Nanopart Res*, **10** (2007) 321, https://doi.org/10.1007/s11051-007-9255-1.

42. Baalousha M, Ju-Nam Y, Cole P A, Hriljac J A and Lead J R, *Environ Toxicol Chem*, **31** (2012) 994, https://doi.org/10.1002/etc.1786.

43. Shchukin E D A V P, Amelina E A, and Zelenev AS, *Colloid and Surface Chemistry*, Elsevier Science, (2001).

44. Pietroiusti A, Stockmann-Juvala H, Lucaroni F and Savolainen K, *WIREs NanomedNanobiotechnol*, **10** (2018), https://doi.org/10.1002/wnan.1513.

45. Wigginton N S, Haus K L and Hochella Jr M F, *J Environ Monit*, **9** (2007), https://doi.org/10.1039/b712709j.

46. Piccinno F, Gottschalk F, Seeger S and Nowack B, *J Nanopart Res*, **14** (2012), https://doi.org/10.1007/s11051-012-1109-9.

47. Mohapatra D P and Kirpalani D M, *Nanotechnol Environ Eng*, **2** (2016), https://doi.org/10.1007/s41204-016-0011-6.

48. Almeida V O D, Pereira T C B, Teodoro L D S, Escobar M and Schneider I A H, *Sci Total Environ*, **759** (2021), https://doi.org/10.1016/j.scitotenv.2020.143456.

49. Cosgrove T, *Colloid Science: Principles, Methods and Applications*, John Wiley & Sons, (2010).

50. Ostolska I and Wiśniewska M, *Colloid Polym Sci*, **292** (2014) 2453, https://doi.org/10.1007/s00396-014-3276-y.

51. Gregory J, *Colloids Surf*, **31** (1988) 231, https://doi.org/10.1016/0166-6622(88)80196-3.

52. Mørch Ý A, Donati I, Strand B L and Skjåk-Bræk G, *Biomacromol*, **7** (2006) 1471, https://doi.org/10.1021/bm060010d.

Supplementary material

Alginates as green flocculants for metal oxide nanoparticles.

Vladislav Slabov[1], Garima Jain[2], Irina Chernyshova[1], Hanumantha Rao Kota[1] and Helga Ertesvåg*[2]

[1]Department of Geoscience and Petroleum, Norwegian University of Science and Technology (NTNU), Trondheim, Norway

[2]Department of Biotechnology and Food science, Norwegian University of Science and Technology (NTNU), Trondheim, Norway

*) corresponding author. email: helga.ertesvag@ntnu.no

(a)   (b)   (c)
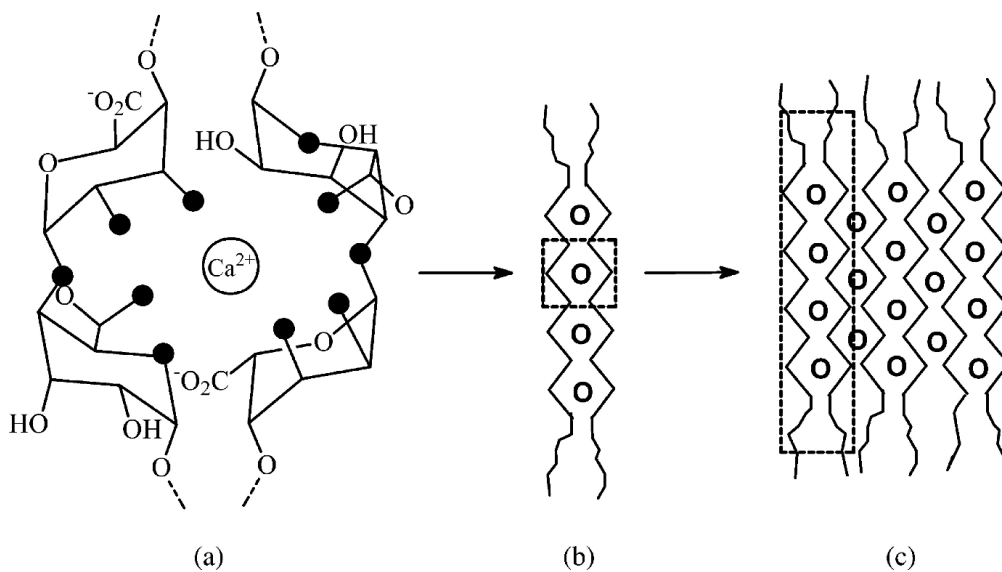
Supplementary Figure S1. Cross binding of two G-blocks by Ca^{2+}. Ca^{2+} fits into the pocket formed by two adjacent G residues and binds strongly to the two carboxyl residues. Reprinted with permission from [50]. Copyright 2007, American Chemical Society.
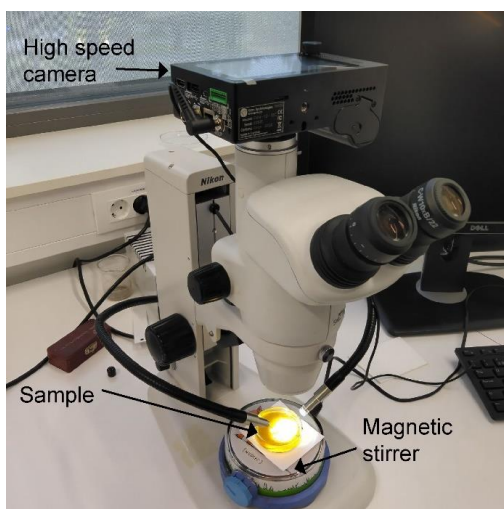
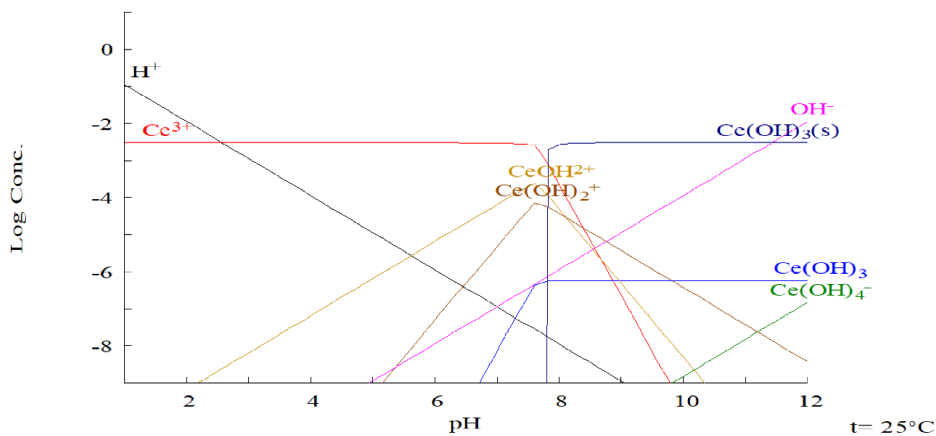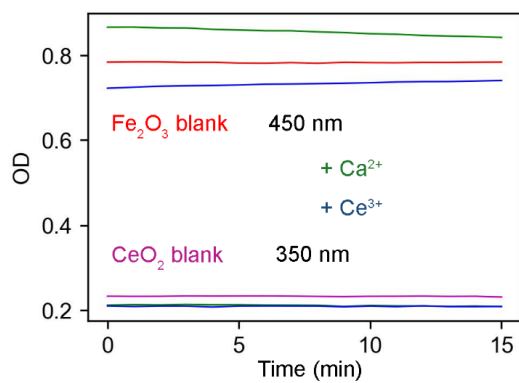Supplementary Figure S2. Setup for high-speed camera analysis
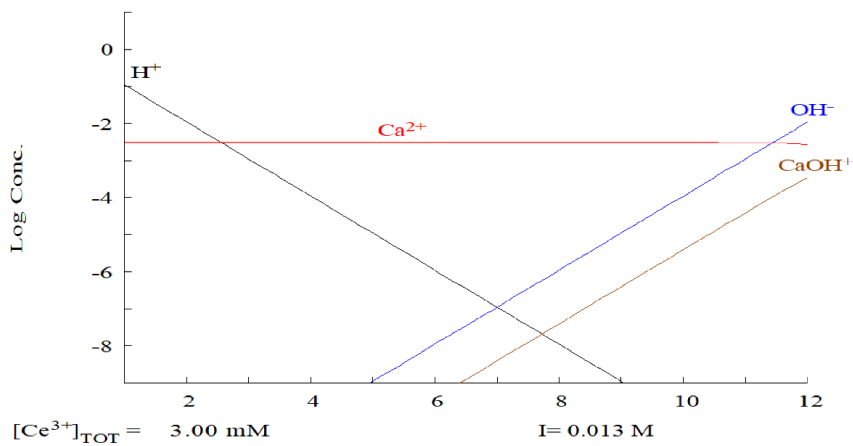
Figure S3 – Speciation diagram of Ca^{2+} and Ce^{3+} calculated by Medusa software.

Supplementary Figure S4. Influence of metal cations on optical density of iron and cerium oxides dispersions.

NTNU
Norwegian University of
Science and Technology